Journal Pre-proofs

The Interpretation of Small Molecule Diffusion Coefficients: Quantitative Use of Diffusion-Ordered NMR Spectroscopy

Robert Evans

PII: S0079-6565(19)30058-5
DOI: https://doi.org/10.1016/j.pnmrs.2019.11.002
Reference: JPNMRS 1492

To appear in: *Progress in Nuclear Magnetic Resonance Spectroscopy*

Received Date: 21 September 2019
Accepted Date: 20 November 2019

Please cite this article as: R. Evans, The Interpretation of Small Molecule Diffusion Coefficients: Quantitative Use of Diffusion-Ordered NMR Spectroscopy, *Progress in Nuclear Magnetic Resonance Spectroscopy* (2019), doi: https://doi.org/10.1016/j.pnmrs.2019.11.002

The Interpretation of Small Molecule Diffusion Coefficients: Quantitative Use of Diffusion-Ordered NMR Spectroscopy

*Robert Evans**

Aston Institute of Materials Research, School of Engineering and Applied Science, Aston University, Birmingham, B4 7ET, United Kingdom

** To whom correspondence should be addressed:*

Telephone: +44 0121 204 5382

Email: r.evans2@aston.ac.uk

Keywords: Diffusion NMR, DOSY, Molecular weight, Stokes-Einstein equation

Contents

Abstract

Measuring accurate molecular self-diffusion coefficients, *D*, by nuclear magnetic resonance (NMR) techniques has become routine as hardware, software and experimental methodologies have all improved. However, the quantitative interpretation of such data remains difficult, particularly for small molecules. This review article first provides a description of, and explanation for, the failure of the Stokes-Einstein equation to accurately predict small molecule diffusion coefficients, before moving on to three broadly complementary methods for their quantitative interpretation. Two are based on power laws, but differ in the nature of the reference molecules used. The third addresses the uncertainties in the Stokes-Einstein equation directly. For all three methods, a wide range of examples are used to show the range of chemistry to which diffusion NMR can be applied, and how best to implement the different methods to obtain quantitative information from the chemical systems studied.

1. Introduction

Translational diffusion is a fundamental form of mass transport and underpins almost all chemical processes. Self-diffusion arises from the random translational movement of molecules driven by thermal energy and can be characterised by the (self-)diffusion coefficient, D, of a species. Diffusion coefficients give information on the size and shape of molecular species. NMR spectroscopy offers a neat, practical method for the measurement of diffusion coefficients in solution. With the advent of pulsed field gradients (PFGs) and the development of ever more robust, versatile and reliable diffusion NMR pulse sequences, particularly since the early 1990s, NMR has increasingly been used to measure diffusion coefficients of chemical systems. These data are typically presented and interpreted in a qualitative manner. Quantitative interpretation of the measured diffusion coefficients is more of a challenge. While there is in principle a simple inverse relationship between hydrodynamic radius and diffusion coefficient - the larger a species is, the more slowly it will move through solution -in practice the detailed relationship between size and diffusion coefficient is more complex. A further challenge is to interpret diffusion coefficients in terms of molecular weight, MW, since this is the parameter of most interest to the chemist.

Section 2 covers the essentials of diffusion NMR methodology and some vital experimental considerations. While advances in instrumentation and techniques have made it easier to measure reliable and meaningful self-diffusion coefficients in NMR experiments, there are a number of experimental problems that can lead to the acquisition of incorrect data and hence misleading diffusion coefficients. These problems are addressed, with particular focus on the highly deleterious effects on data quality of sample convection, and potential solutions are discussed. Section 3 reviews the Stokes-Einstein equation and illustrates its intrinsic assumptions. The Stokes-Einstein equation is the starting point for understanding the relationships between diffusion coefficient and physical parameters such as hydrodynamic

radius. However, as demonstrated in Section 3, it performs poorly at predicting small molecule diffusion coefficients on the basis of their molecular weight. To understand how and why the Stokes-Einstein equation fails, the assumptions implicit in the equation, and where they fail, are discussed and reviewed.

Methods for the estimation of molecular weight from diffusion coefficients fall into two broad categories. Section 4 introduces power laws for rationalising diffusion coefficients. The diffusion behaviour of macromolecules such as proteins and polymers is well described by power laws of the form $D = K\,MW^{\alpha}$. By appropriate parameterisation of the law for a given set of macromolecules, molecular weights of species of similar structure can be estimated from their measured diffusion coefficients. This can be successfully extended to small molecules. The approach needs experimental calibration data to be fitted to the power law to obtain values for the two parameters K and α. Power law methods have been further categorised here into two distinct subsets. Internal calibration methods use three or more compounds, measured in the same sample, to determine the power law parameters. External calibration methods use a calibration curve derived from a larger number of separate measurements on individual compounds in a given solvent; the molecular weight of an unknown is then determined using a measurement on a sample containing the unknown and a single reference calibrant. In these experiments, a relative diffusion coefficient or diffusivity is often used for the estimation of molecular weight. Section 5 returns to the Stokes-Einstein equation, showing how the problems posed by each of the assumptions inherent in its derivation can be addressed, either by well-defined analytical solutions or by appropriate estimation. This gives a third, much more general, approach to molecular weight estimation for small molecules. For each of the three types of method, a small number of key references will be discussed in detail. Sections 6 and 7 compare the different methods and discuss some related issues, before concluding the review.

The aim of this article is not only to review the various approaches for relating diffusion coefficients to molecular weight, but also both to give illustrative examples of their successful application to a wide range of different areas of chemistry, and to give the reader enough information to use the techniques themselves.

2. Experimental Measurement of Diffusion Coefficients

Self-diffusion is one of the fundamental modes of mass transport. It arises from the random translational motion of particles in a liquid, driven by the thermal energy of the system, and the random collisions between particles as they move through the fluid. In the absence of flow, the average displacement of a given molecule over time should be zero. This is not true of the mean square displacement. The root mean square distance, z_{rms}, a particle is displaced by in a time *t* in *n* dimensions is given by Eq. (1).

$$z_{\mathrm{rms}} = (2nDt)^{1/2} \tag{1}$$

The constant here, *D*, is the self-diffusion coefficient, a measure of the rate of displacement of a particle. The study of molecular diffusion in solution, through measurement of self-diffusion coefficients, offers insights into a range of physical properties of molecules, including molecular size and shape [1] as well as aggregation, encapsulation, complexation and hydrogen bonding [2-4]. In contrast to spin relaxation times, diffusion coefficients are (in the absence of intermolecular exchange) the same for all nuclei in a molecule. While relaxation times do depend on the rates of molecular motions, they can be quite different for different nuclei in the same molecule, being determined by local structure and motion.

Diffusion NMR data are often presented in a two-dimensional format known as diffusion-ordered spectroscopy (DOSY) [5-7]. This is a highly visual format and easy to interpret qualitatively, as shown in Fig. 1 where the signals of different components of a mixture containing quinine, geraniol and camphene in methanol-d_4 can be identified. One

dimension contains the chemical shift information, the other depicts the diffusion coefficients of the species. Species' signals are thus separated out by size, rather as in a chromatogram. DOSY spectra act as both a graphical overview and a summary of a set of diffusion results.

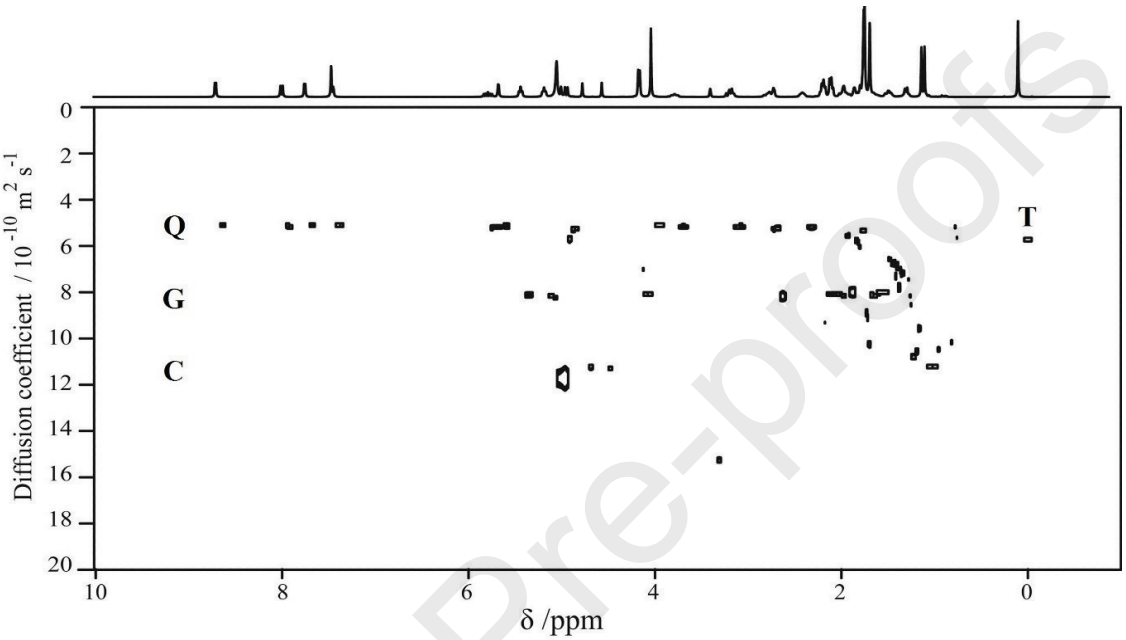

Figure 1: 2D DOSY spectrum of a mixture of quinine (Q), geraniol (G), and camphene (C) in methanol-d_4, with TSP (T) as a reference, acquired on a Varian INOVA 400 MHz spectrometer. The DOSY spectrum was produced using HR-DOSY fitting, with compensation for the effects of non-uniform field gradients [8]. Reproduced with permission from Colbourne et al., *J. Am. Chem. Soc.* **133** (2011) 7640-7643. Copyright (2011) American Chemical Society.

2.1 Pulsed Field Gradient (PFG) NMR

Measurements of diffusion by NMR date back to the earliest pulsed NMR experiments [9, 10], but only became widely used with the introduction of pulsed field gradients [11]. In most NMR experiments, the magnetic field around the sample is kept as homogeneous as possible, in order to obtain narrow, high-resolution signals in the NMR

spectrum. The Larmor equation (Eq. (2)) gives the resonant frequency of a spin ω as the product of the nuclear gyromagnetic ratio γ and the local magnetic field strength B. Where the field B is homogeneous, there will be a single, well-defined, resonant frequency for each spin observed.

$$\omega = -\gamma B \tag{2}$$

The application of a magnetic field gradient, g_z, along the z-axis causes the magnetic field to vary along the z-axis of the sample. This adds a gradient term to B in the Larmor equation above to give Eq. (3).

$$\omega_z = \gamma(B + zg_z) = \omega + \gamma z g_z \tag{3}$$

Applying the gradient for a short pulse, of duration δ, introduces an additional evolution of the phases of the signals, $\Phi = (\delta\gamma z g_z)$. When the field gradient is switched off, the spins revert to their original precession frequencies. The effect of the linear field gradient pulse is to label the spins in the sample with phase angles that depend linearly on their height in the sample tube. This phase labelling is the basis of most diffusion NMR pulse sequences.

While there have been many advances in the design of PFG-based diffusion NMR pulse sequences, they all share a number of common features. An initial 90° radiofrequency (RF) pulse is used to excite the spins. Spins are now in the *xy*-plane and relax according to the transverse relaxation time T_2. A series of RF and magnetic field gradient pulses are applied to the sample that wind the magnetisation into a helix, encoding the positions of the spins within the sample into their phases. All diffusion NMR pulse sequences then include a delay, typically labelled Δ, during which the species move by Brownian motion. A second series of RF pulses and PFGs serve to refocus the magnetisation helix prior to spectrum acquisition. This refocusing is achieved by ensuring that the second gradient pulse has an effective area equal and opposite to that of the first pulse. Any species that have moved during the delay period will therefore experience a difference between the encoding and

decoding effects of the gradient pulses and their magnetisation will not be completely refocused. Hence, the signals from the sample are attenuated to an extent governed by the net displacement of the species responsible over the delay period.

While the first pulsed field gradient diffusion NMR experiments date back to the 1960s [11], it is only since the 1990s that advances in the design and manufacture of NMR spectrometers and hardware have made such techniques routinely accessible. The simplest diffusion NMR pulse sequence is the PFG spin echo experiment (Fig. 2(a)). In this case, the delay Δ contains a single 180° pulse to refocus the precession of the magnetisation and ensure that the second gradient pulse has an equal but opposite effect on the spins in the sample. After the 90° pulse, the signal suffers from losses due to transverse relaxation. As delays of *ca*. 0.1 – 0.5 s are needed for most small to medium sized molecules, these losses due to relaxation can significantly reduce the intensities of the peaks observed. A further complication is evolution of coupling, or *J*-modulation, again when the magnetisation is transverse. This leads to signal phase distortions and, when DOSY processing is used, can cause peaks to be displaced in the diffusion dimension [12].

Most modern diffusion NMR pulse sequences are based on the PFG stimulated echo experiment (Fig. 2(b)) [13]. Here, the single 180° pulse is replaced by a pair of 90° pulses. The second 90° pulse, applied shortly after the first diffusion-encoding gradient pulse, ensures that magnetisation is transverse only for relatively short periods, remaining longitudinal for most of the diffusion period Δ. For small molecules, T_1 is almost always equal to or longer than T_2. Signals therefore decay mostly according to the potentially slower longitudinal (T_1) relaxation rates, and relaxation losses are reduced compared to the spin echo. By minimising the time for which magnetization is transverse, the stimulated echo also reduces both *J*-modulation and the susceptibility to any disturbances in the magnetic field. Following the diffusion period, the magnetisation is returned to the transverse plane by a

third 90° pulse for refocusing and subsequent detection. While the stimulated echo necessarily throws away half of the signal intensity compared with the spin echo, overall it has better performance, for the reasons discussed, and most pulse sequences in current use (see Figs. 2(c) and following) are derived from stimulated echoes.

In order to obtain good quality diffusion data, it is important to minimise gradient-dependent spectral distortions, particularly in signal phase or lineshape. One of the common problems with the hardware used for early diffusion NMR experiments was the presence of eddy currents in the probe and magnet bore and their effects on the acquired diffusion NMR data. When a magnetic field changes, e.g. when a field gradient is switched on or off, eddy currents will be induced in any local conductor and create their own magnetic fields. These can have a number of effects on the NMR experiment, the most obvious of which is disturbance of the field-frequency lock, commonly seen as brief dips in the lock signal level following gradient pulses. Eddy currents cause both the magnitude of the main field B_0 and its shape to be time-dependent. Free induction decays therefore show time-dependent phase shifts and accelerated decay. This leads to distinctive effects on the lineshapes of the signals, which are typically broadened, slightly displaced, and show a negative dip to one side. While changes in pulse sequence, such as the addition of a z-filter just before acquisition of signals [14], can reduce the deleterious effects of eddy currents, these are of limited efficacy. Modern NMR hardware minimises eddy currents at source, by using actively shielded gradient coils and, if necessary, using appropriately shaped gradient pulses to limit the rate of change of magnetic field.

It is also possible to incorporate specific design elements into pulse sequences to further minimise lineshape distortions. Bipolar paired pulse gradients are pairs of gradient pulses, separated by a 180° RF pulse, which replace a single gradient pulse but have half its duration and opposing signs. The two equal but opposite gradient pulses have a net dephasing

effect for all spins refocused by the 180° pulse. The use of paired pulses generates weaker eddy currents as those induced by the first gradient are partially cancelled by those induced by the second. In addition to this, as the RF pulse has no effect on the lock signal, the effect of the first gradient pulse on the lock channel is almost immediately refocused by the second. In contrast a single gradient pulse dephases the lock signal, which then takes hundreds of milliseconds to return to its initial level. Fig. 2(c) depicts a stimulated echo pulse sequence with bipolar paired pulsed gradients [15]. An important extra consideration here is the need for phase cycling; as the number of RF pulses in the experiment increases, so does the length of phase cycle [16] required to enforce the desired coherence transfer pathway through the pulse sequence. One way to reduce the need for phase cycling is to add a single "spoil" or "purge" gradient pulse to the diffusion delay, when the desired magnetisation is longitudinal. Adding a single pulse in this way can cause problems: first, it will dephase the lock signal, and second, it may inadvertently refocus unwanted coherences which will then interfere with the observed peak intensities and lead to inaccurate measurement of diffusion coefficients.

By using asymmetric bipolar paired PFGs and additional balancing pulses, the Oneshot sequence [17] (Fig. 2(d)) sidesteps the requirement for extensive phase cycling. The diffusion-encoding and decoding bipolar pulse pairs are unbalanced, with an intensity ratio of $1+\alpha:1-\alpha$, dephasing any magnetisation that has not been refocused by the 180° pulse. To balance this bipolar pulsed pair and mitigate any effects on the lock signal, an additional pair of gradient pulses, each of relative intensity 2α, is added within the diffusion period. Similarly, to ensure that all gradient pulses are balanced and that the total gradient area of the pulse sequence is zero, an additional gradient pulse is added to the relaxation delay at the start of the experiment to balance the spoil pulse in the diffusion delay. A final refinement is that a further pair of gradient pulses, decremented in strength as the diffusion-encoding pulse pairs are incremented, can be added before the relaxation delay. This keeps the net energy

supplied to the gradient coil by the sequence for a single transient constant, avoiding any effects of changes in gradient coil temperature as the diffusion-encoding gradient amplitude is changed.

Fig. 2 shows a selection of diffusion NMR experiments, all described in the preceding text, starting with the spin echo and gradually incorporating more features to ensure cleaner, less distorted spectra. Note that this is far from a complete list. The four pulse sequences described in this section are just the tip of the iceberg and many others exist. Of particular note are pulse sequences that also include solvent suppression [18, 19] and those based on the perfect echo [20]; the latter can minimise the influence of chemical exchange on the final diffusion data [21]. The acquisition of good quality diffusion NMR data does not end with pulse sequence selection. Section 2.2 will describe and discuss a number of additional experimental factors to be considered when acquiring diffusion NMR data.

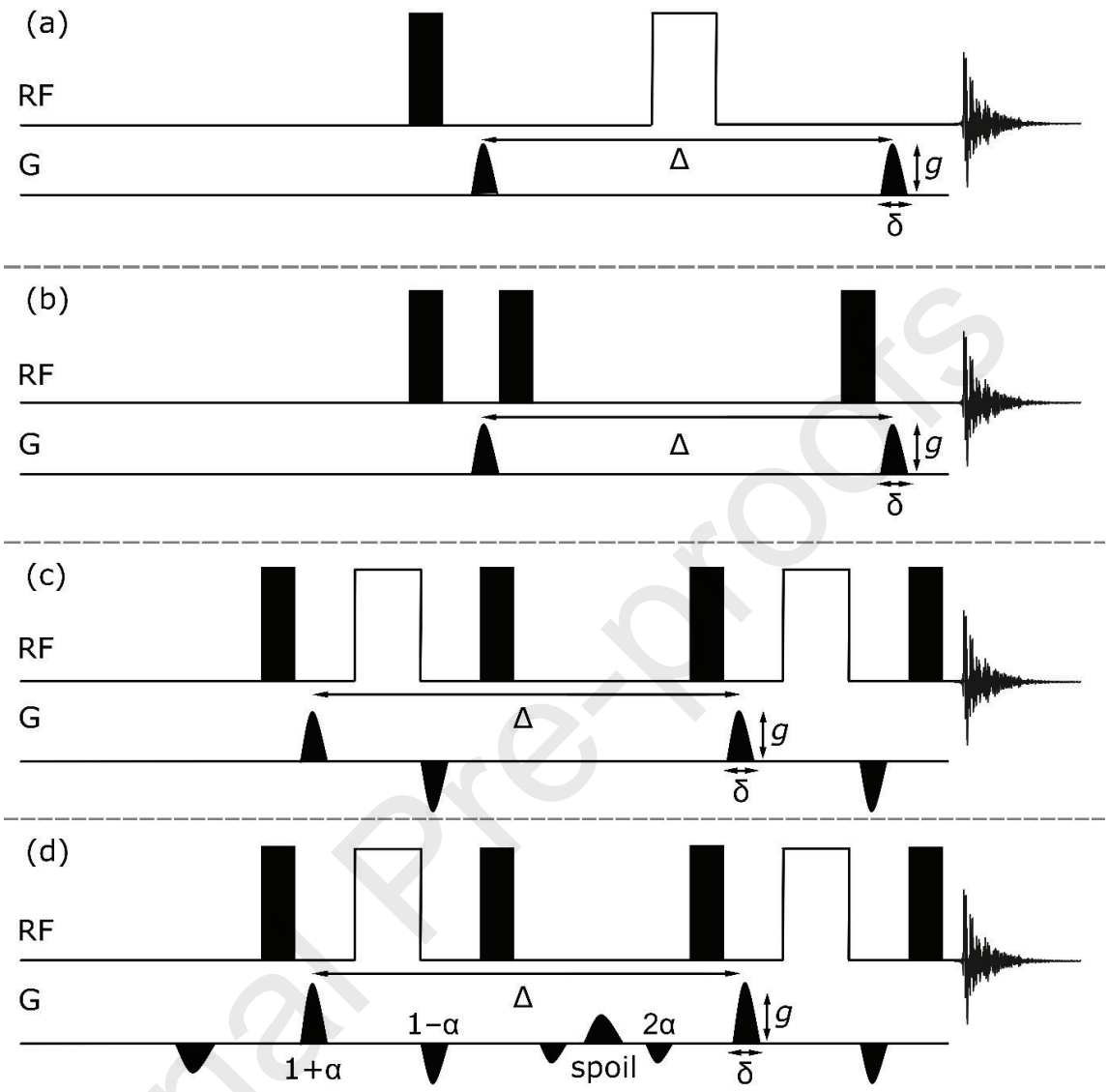

Figure 2: Pulse sequence timing diagrams for PFG diffusion NMR experiments. (a) The PFG spin echo experiment (PFGSE). (b) The PFG stimulated echo experiment (PFGSTE). (c) The stimulated echo experiment with bipolar paired PFGs. (d) The Oneshot experiment. Closed rectangles represent 90° pulses and open rectangles represent 180° pulses.

Obtaining a set of diffusion NMR data is then a case of performing a series of experiments using increasing gradient strength, *g*, with an appropriate PFG NMR pulse sequence. It is also possible to run experiments varying diffusion delays, Δ, or pulsed field

gradient durations, δ, rather than gradient amplitudes, but this approach leads to variable attenuation from relaxation losses. Processing of such data needs to take this attenuation into account.

A full treatment of the evolution of the magnetisation during pulsed field gradient experiments requires the use of the Bloch-Torrey equations [22]. This set of three-dimensional partial differential equations describes how magnetization evolves over time under the effects of chemical shift, the inhomogeneous magnetic field along the z-axis, relaxation, unrestricted diffusion, and translation. Fortunately, full expressions for diffusional attenuation can be derived analytically for a given pulse sequence. A representative example is the Stejskal–Tanner equation (Eq. (4)) [11], which relates the signal, S, measured in a pulsed field gradient experiment to the signal measured with zero gradient, S_0, the gyromagnetic ratio, γ, of the spins being observed, key experimental parameters of the pulse sequence used, δ and Δ', the strength of the magnetic field gradient pulses, g, and the diffusion coefficient of the species of interest, D. The effective diffusion time, Δ', which allows for the effects of diffusion during the gradient pulses, depends on the pulse sequence used; values have been calculated for a number of widely used sequences [23].

$$S = S_0 e^{-D(\delta\gamma g_z)^2\Delta'} \quad (4)$$

Deriving diffusion coefficients from diffusion NMR data in principle requires the use of an inverse Laplace transform, a classic ill-posed problem [24]. The simplest and most widely used approach to DOSY, and that used to generate the 2D spectrum in Fig. 1, is the high resolution approximation (HR-DOSY) [6]. This method fits a single exponential to the decay of each peak in a spectrum. The diffusion coefficient for each peak is estimated by least-squares fitting of the peak height decay, and a DOSY spectrum is constructed in which a peak is centred at the fitted diffusion coefficient with a width determined by the error estimated in the fit. A number of peaks in the proton spectrum of quinine, geraniol and

camphene overlap, violating the high resolution approximation. Where peaks from different species overlap, their net amplitudes will decay multiexponentially and fitting with a single exponential will give an intermediate diffusion coefficient. This leads to misplaced peaks in the DOSY spectrum, such those observed between 1 and 2 ppm in Fig. 1. The overlap of resonances from different components of a mixture may render interpretation of the signals difficult, but it will certainly make quantitative interpretation of their diffusion coefficients impossible. While it is possible to use biexponential fitting [25], this requires very high signal-to-noise ratio data it is much better to use isolated, well-resolved peaks to determine diffusion coefficients. The increased availability and use of 3D DOSY sequences may help, as peaks in such spectra are spread out in a 3rd frequency dimension, with a commensurate improvement in their resolution [26].

A number of alternative methods are available for the processing of diffusion NMR data. It is possible to obtain an estimate of a distribution of diffusion coefficients through the use of constrained, or Tikhonov, regularisation [27, 28], to approximate the numerical Laplace transform. As the result tends to take the form of broad peaks and distributions, constrained regularisation typically finds wider use in the analysis of diffusion NMR data of polydisperse systems such as polymers [29, 30]. The methods discussed so far (monoexponential and multiexponential fitting, and constrained inversion) have been univariate: each signal in a spectrum is analysed individually. Multivariate methods analyse the entire data set as a whole. A defined number of sets of signals with similar attenuation behaviour from across the spectrum are identified and grouped as distinct chemical components. While the data can be presented as a 2D DOSY spectrum, this is potentially misleading. Results are usually presented as a decomposition of the experimental data into a set of 1D spectra, each of which represents an individual chemical component of the original mixture, and is associated with a single diffusion coefficient. Multivariate methods for

processing diffusion data include COmponent-REsolved NMR spectroscopy (CORE) [31-33] and improved algorithms (e.g. SCORE and OUTSCORE) [34, 35], maximum entropy [36], the Direct Exponential Curve Resolution Algorithm (DECRA) [37-39], and blind source separation (BSS) [40]. LOcal Covariance Order DOSY (LOCODOSY) [41] and filter diagonalization [42] may considered as hybrid methods: multivariate techniques applied to spectra which have been broken up into smaller, more manageable chunks of spectrum each containing only signals from a few distinct chemical components. A near-complete set of methods has been implemented in both the free Matlab-based DOSY Toolbox software [43], and its recent successor, GNAT [44].

This introductory section is intended to give an overview of the underlying theory, and some practical aspects, of diffusion NMR. A number of important reviews, papers and book chapters have been referenced earlier in the Section but a full review of diffusion NMR experiments, the Stejskal–Tanner equation, and processing of diffusion NMR data is somewhat beyond its scope. Accurate determination of small molecule diffusion coefficients is vital: if the original experimental data are flawed, then any interpretation of them will necessarily suffer.

2.2 Experimental considerations

Key to the successful interpretation of diffusion data is the acquisition of good quality data in the first place. The experimental data acquired can be vulnerable to a number of different influences. Some, such as the calibration and spatial non-uniformity of the pulsed field gradients, relate directly to the NMR hardware. These systematic errors can be removed by appropriate calibration. Others, such as the presence of eddy currents and the effect of pulsed field gradients on the field-frequency lock, result from the interaction of pulsed field gradients with the experimental hardware and the NMR spectrometer itself. As discussed in

the previous section, advances in spectrometer and pulse sequence design can reduce the effects of both greatly. The remaining, typically minor, deviations from ideal spectrometer behaviour, such as lineshape errors and inconsistencies in RF pulse phase and amplitude, can often be corrected for by the use of reference deconvolution [45].

A final source of errors comes from the sample itself. Diffusion coefficients are very sensitive to temperature. More detrimentally, temperature gradients in a sample lead to convection currents and hence an additional source of motion, and thus of signal attenuation, in the sample. The following section will discuss some of the more important factors for the acquisition of good quality experimental diffusion NMR data, with a particular focus on convection. While severe convection in a sample is readily noticeable, mild convection is much more common than might be expected and leads to higher apparent diffusion coefficients. This, in turn, makes the successful interpretation of such data difficult.

2.2.1 Temperature control

There are two ways in which temperature directly affects diffusion coefficients. First, in the numerator of the Stokes−Einstein equation, the thermal energy driving diffusion is given by $k_B T$. The higher the temperature, the more energy the solute and solvent molecules have and the faster they move through the solution. Second, and much more importantly, in the denominator, the solvent viscosity η depends strongly on temperature. Over the range of temperatures likely to be encountered in NMR diffusion measurements, this temperature dependence is well represented by an Arrhenius-like equation [46], which can be fitted with two parameters.

It follows that accurate and precise knowledge of the temperature of the sample is vitally important for quantitative interpretation of the diffusion coefficients acquired. Temperature control in NMR experiments is typically achieved by the flow of gas, either air

or nitrogen, past a heating element and then around the sample tube. The gas is thermostatted using a thermocouple temperature sensor that is typically placed as close to the sample as possible. This does not give a direct measurement of the true temperature of the sample; that requires an NMR thermometer. NMR thermometers are samples that have a known, calibrated temperature dependence of chemical shift or chemical shift difference, often arising from the temperature dependence of intermolecular hydrogen bonding. Such thermometers can be used to determine the actual temperature of the active sample region. Neat ethylene glycol [47] and neat methanol [48] have found use as standard NMR thermometers, often being supplied as standard samples by spectrometer manufacturers. There are some problems with these samples. The very strong nuclear magnetization in pure liquids can produce broad and/or shifted peaks, degrading accuracy of temperature measurement. Low-viscosity liquids may be limited in the temperature range they can used over due to convection. One effective NMR thermometer is a sample of methanol-d_4 in a thick-walled tube. This sample has a well-defined quadratic relationship between the temperature and the chemical shift difference between the signals of residual CHD_2OD and CD_3OH, and has been shown to measure temperatures accurately from at least 280 K up to 320 K, the temperature range spanned limited here by the probe used in the original study [49].

Once the sample temperature has been calibrated, its stability and uniformity are still important parameters to control or, at least, to account for. This can be troublesome. Most laboratory-scale air conditioning units oscillate in temperature over a range of 1 - 2 K and, particularly for aqueous systems, this can have detrimental effects on individual spectra. Spectra acquired at even slightly different temperatures will show small differences in chemical shift. As the ambient room temperature slowly fluctuates over the duration of an experiment, the effects can be observed as “wiggles” in the raw diffusion data [50]. The best

solution is to minimise temperature gradients by careful temperature control of the spectrometer itself and of its air or nitrogen supply.

2.2.2 Gradient calibration

Key to the acquisition of reliable diffusion coefficients is the accurate calibration of the magnetic field gradients used in the diffusion NMR pulse sequences. Rather than controlling a pulsed field gradient strength directly, the NMR hardware will control a current passing through the gradient coils. The actual gradient strength produced depends on the probe, the gradient coil contained within it, and the gradient amplifier. Each gradient probe will have its own, different, characteristic gradient strength for a given current value. Calibration of the gradient strength for a given probe is therefore vital for acquiring accurate diffusion coefficients.

Several approaches to gradient calibration exist. One is based on obtaining a 1D image (i.e. a signal profile) of a sample containing an NMR phantom of known dimensions. This is typically a small disk of plastic, such as teflon, positioned in the centre of the RF coils. There is no NMR signal from the disk in the 1D image, and the gradient strength can then be calculated by comparing the frequency width of the gap in the image with the known dimensions of the disk. While this method is potentially an absolute calibration of the gradients, there will be distortions of the spectral profile caused by magnetic susceptibility discontinuities at the boundaries of the disk, and the thickness and orientation of the disk need very tight control. A second, more commonly used, method is to deduce the gradient strength from measurements of a standard with a known diffusion coefficient. A number of standards have been suggested, with e.g. the residual HDO in a "pure" D_2O sample giving an expected diffusion coefficient of 1.902×10^{-9} m^2 s^{-1} at 298 K [51, 52]. It is also possible to use pure solvents, such as cyclohexane and DMSO, which also have well-characterised

temperature-dependent diffusion coefficients [53], but these can give problems with radiation damping. A larger collection of accurately known diffusion coefficients for a range of molecular liquids has been provided by Weingartner and Holz [52]; this also includes calibrants for nuclei other than ^{1}H. By using a wider range of compounds, a wider range of diffusion coefficients are included and the calibration no longer depends on a single measurement of diffusion coefficient. While straightforward, the method does require that the spectrometer's temperature control is well-calibrated first.

Neither of these two methods accounts adequately for a significant instrumental problem, however, which is that practical gradient coils generate gradients that are not constant over the active volume of the sample [8, 54]. Most gradient coil designs have a "sweet spot" in the very middle of the coil that provides the most uniform gradient, but the exact nature of how the gradient varies along the z-axis (and to a lesser extent as a function of x and y) depends on the gradient coil design. The effect of spatial non-uniformity of the field gradients means that the experimental signal decay, as described by Eq. (4), deviates from a pure exponential. Different parts of the sample will experience different gradients, and hence their signals will attenuate as a function of field gradient at different rates. The resulting net signal observed will show a diffusional attenuation which deviates increasingly from exponential as the attenuation increases. It is possible to map this gradient non-uniformity and subsequently use this information to express the gradients as a function of position within the probe. Applying a weak "read" gradient during the acquisition of DOSY data makes different positions within the sample correspond to different frequencies within the spectrum. Given the known timing of the experiment, the known strength of the read gradient, the appropriate Stejskal-Tanner equation for the pulse sequence used, and the diffusion coefficient of the standard used (collections of known diffusion coefficients can be found in [52] and [53]), it is possible to map the spatial dependence of gradient strength and use this

information to derive a corrected form for the Stejskal-Tanner equation, for example as the exponential of a power series in the normal Stejskal-Tanner exponent [8]. This is by some margin the most reliable calibration method, and allows accuracies of better than 1 % to be obtained.

2.2.3 Convection

Temperature can also affect the measurement of diffusion in a third way. Diffusion NMR experiments measure the random movement of the molecules in the sample. Any additional motion, such as the flow generated by convection, will lead to over-estimation of the diffusion coefficients. Typically, convection is seen as a critical phenomenon [55, 56]. When a sample of liquid is warmer at its base than at its top, the warmer, less dense, liquid will tend to rise, and the colder, denser liquid to sink. This is known as Rayleigh–Bénard convection [57] and, importantly, convection only starts when the vertical temperature gradient reaches a certain critical value determined not only by the sample geometry but also the dynamic viscosity, thermal diffusivity and thermal expansion coefficient of the liquid present in the sample.

Given the temperature control apparatus of most modern NMR spectrometers described in Section 2.1.1, it might be assumed that, so long as the sample temperature is set lower than room temperature, the bottom of the tube would always be colder than the upper reaches and that no convective flow would form. This is not the case. The highly asymmetric space within the probe breaks up the air flow around the tube, leading to the presence of both vertical and horizontal thermal gradients. Horizontal temperature gradients also drive convection, through Hadley flow [58-60]. Importantly, this convective flow is not a critical phenomenon. Additional sources of flow in the NMR sample can, therefore, never be completely removed, so care has to be taken in reducing their effect as much as possible.

Further complicating matters, it has been shown that, while the amount of convection present in a liquid NMR sample depends on sample-specific experimental parameters such as the fluid's viscosity, thermal conductivity and expansivity as well as the sample's size, shape and temperature, it also varies widely between different instruments and different probes. The parameter $\chi = \beta\eta\kappa$, where β is the volumetric thermal expansion coefficient in K^{-1}, η is the dynamic viscosity in Pa s, and κ is the thermal conductivity in W m^{-1} K^{-1}, is a measure of the ease with which a sample of a given liquid convects under a horizontal temperature gradient [59, 60].

The effects of convection on acquired diffusion coefficients range from the severe to the subtle. Convection can introduce an additional cosine modulation to the diffusional signal attenuation. In cases of severe convection, the distortion is obvious - signals acquired with higher gradients may well be negative. Mild convection can be indistinguishable from unaffected data, and a fit to the expected exponential function will appear to give a good result. However, this measured diffusion coefficient will be larger than expected due to the additional component of mass transfer.

Diagnosis of the presence of convection can take a number of forms. Perhaps the simplest is to exploit approximate relationship, Eq. (5) [61].

$$D_{acq} \approx D + \frac{\Delta\, v^2}{2} \tag{5}$$

The effect of convection on the acquired diffusion coefficient, D_{acq}, can be approximated by adding a term containing the convective flow velocity, v, and the diffusion delay time, Δ. Diffusion coefficients can be measured with increasing values of Δ under otherwise identical conditions. In the absence of convection, the diffusion coefficients obtained should not change. The presence of convection is revealed by a linear increase in the experimentally acquired diffusion coefficients with longer diffusion delay times.

Convection can also be identified, and quantified, by using a modified convection-compensated double stimulated echo pulse sequence. When used as originally intended, the total diffusion encoding period of the latter is split into two equal halves, so that the effects of convection in the first echo are exactly cancelled by their reversal in the second echo. If the experiment is run asymmetrically, with different periods, Δ_1 and Δ_2, there will only be a partial cancellation of the effects of convection. A series of 1D experiments, where Δ_1 and Δ_2 are varied systematically but their sum is held constant, will produce a spectra where the signal attenuation is related to the size of the imbalance between the two diffusion periods [62].

This method can be adapted to produce profiles of convection velocity, as a function of sample temperature. Fig. 3(a) shows data acquired from a modified convection-compensated sequence, based on a 2D *J*-resolved *i*DOSY experiment, used for such studies. This sequence is designed to cancel the effects of constant flow when the imbalance, $\Delta\Delta$, between two diffusion delays is zero, allowing diffusion-weighted data to be acquired without interference from convection. When $\Delta\Delta$ is non-zero, the signals from species with magnetogyric ratio, γ, moving with maximum *z* velocity v_{max} acquire a phase shift proportional to that velocity. Since a convecting NMR sample has equal net upward and downward flows of liquid, the net result of the phase shifts averaged over the sample is an amplitude modulation of the overall signal. A series of 1D NMR experiments is acquired for different values of the diffusion delay imbalance, $\Delta\Delta$. The experimentally obtained peak heights obtained at different values of $\Delta\Delta$ can be fitted to a *sinc* $(\sin(x)/x)$ function, Eq. (6), as in Fig. 3(a), where the convection measurement method is applied to a sample of 99.8 % $CDCl_3$ at 313 K to obtain measurements of the residual $CHCl_3$ signal, *S*, as a function of $\Delta\Delta$, and hence estimate v_{max}, at that sample temperature.

$$S(\Delta\Delta) = S_0 \frac{sin\,(\gamma\delta g \Delta\Delta v_{max})}{(\gamma\delta g \Delta\Delta v_{max})} \quad (6)$$

Measurements over a range of temperatures produce a profile of sample flow velocities as a function of sample temperature, as in Fig. 3(b) for samples of 99.8 % $CDCl_3$ in both a standard and a thick-walled NMR tube [63].

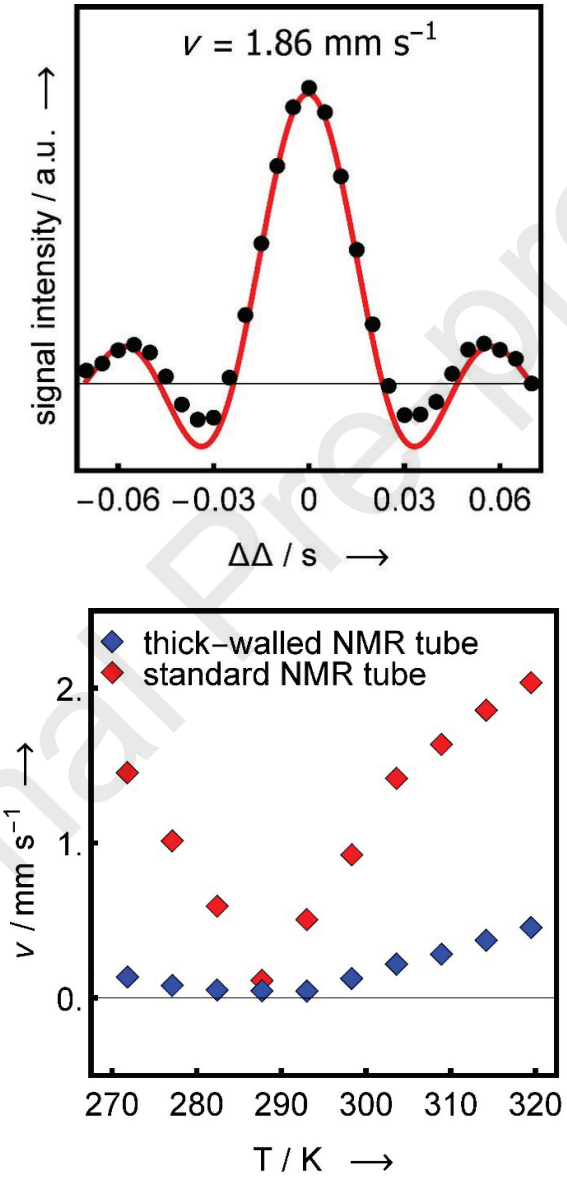

Figure 3: (a) Experimental measurements of $S(\Delta\Delta)$ (black circles) and fit to Eq. (6) (red line) for residual $CHCl_3$ in 99.8% $CDCl_3$ in a standard NMR tube at 313 K acquired using a modified convection-compensated sequence based on a 2D *J*-resolved *i*DOSY experiment

(upper). (b) Plot of maximum convection velocity, v_{max}, as a function of spectrometer temperature for 99.8% $CDCl_3$ samples in both a standard NMR tube (red diamonds) and a thick-walled NMR tube (blue diamonds) (lower). All data acquired using a Bruker Avance 300 MHz spectrometer equipped with a 5 mm PABBO BB-1H ZGRD probe. Both figures adapted from T.J. Rottreau, Application of liquid state nuclear magnetic resonance techniques for the study of porous materials, Aston University, 2018.

A number of recent studies [59, 60] have used this approach to reveal the nature of convective flow in a number of different probes. Essentially, all probes show some evidence of convective flow. The presence of Hadley convection, induced by horizontal temperature gradients, means that convection is observed at temperatures below ambient as well as temperatures above. The effects of convection on measured diffusion coefficients have, therefore, been historically underestimated. As a result of the near-ubiquity of convection in NMR experiments, a number of experimental methodologies have been developed by which its effects can be reduced or compensated for. The thermal conductivity of sapphire is approximately 25 times greater than that of borosilicate glass [64], so the use of sapphire NMR tubes will greatly reduce the temperature gradients that drive convection. Narrower-bore NMR tubes also reduce convective flow [65]. The advances in pulse sequence design detailed in Section 2.1 also include the development of convection-compensated diffusion NMR experiments. By using diffusion-encoding pulse sequence segments with equal but opposite velocity encoding, these experiments are designed to cancel the effects of laminar flow in the sample, albeit at the cost of loss of half of the signal [66, 67]. It is possible to predict how likely a solvent is to convect on the basis of its physical properties. Any quantitative study of diffusion coefficients should take care to reduce the effects of

convection by using narrower bore tubes, convection-compensated diffusion NMR pulse sequences, or both if signal-to-noise is sufficient.

2.3 Other Methods for the Measurement of Diffusion Coefficients

PFG NMR is not the only class of method by which diffusion coefficients of species in solution can be measured. An early name for self-diffusion was tracer diffusion, which gives a hint as to one method for its measurement [68]. In the tracer, or capillary, method, two solutions of the same liquid are prepared, one of which is labelled with a suitable radioactive "tracer" isotope. A capillary cell is filled with the tracer solution and then immersed in the unlabelled solution for a known length of time, over which normal, unrestricted diffusion can take place. The cell contents are then removed, dried thoroughly, and the radioactive content measured using standard counting equipment. This method found wide historical use in the study of water (light, heavy and super-heavy [69-72]) and the mobility of ions in water [73] and, even as recently as 2000, tracer diffusion methods were described as the status quo, although the advantages of diffusion NMR methods (faster measurement times, smaller sample volumes, easy application to wide chemical, pressure and temperature ranges) were noted [53].

Light scattering methods are more widely used, and are a common technique for particle size analysis in the nanometre range [74-76]. A laser is directed through a liquid sample. If there are particles in the sample, the incident laser light will get scattered in all directions as it passes through the sample. This scattered light can be detected over time as a fluctuating signal. Smaller particles, which move faster, will give rise to more rapid fluctuations in the scattered light than more slowly moving, larger particles. However, for most light scattering experiments, the intensity of the scattered light increases according to the 6^{th} power of particle radius. A particle 10 times wider will give rise to a signal one million

times more intense. This tends to limit light scattering techniques to nanometre to micrometre-sized species, such as nanoparticles, polymers, other colloids and proteins, rather than small molecules.

Diffusion coefficients are used in electrochemical techniques to describe mass transport phenomena close to the electrode surface [77]. If an electrochemical process is well-understood and the number of electrons being transferred is known, then electrochemical methods such as chronoamperometry [78], chronopotentiometry [79] and rotating disc electrode voltammetry [80] can be used to estimate the diffusion coefficients of the species involved. Taking chronoamperometry as an example, an electrochemical experiment where changes in electric current are measured as a function of time in response to a step change in the potential applied across the electrochemical cell, the measured current depends on the rate at which the molecule being studied diffuses to the electrode surface, giving rise to a $D^{½}$ dependence in the current [81].

The ability to use standard commercial instrumentation for such measurements on routine samples has obvious advantages over these alternative methods, such as radioactive tracer studies, for measuring diffusion. NMR techniques allow relatively fast measurements over a range of temperatures, in a range of solvents, and require neither specialised handling of radioactive isotopes nor specialised electrochemical equipment. The diffusion coefficients obtained by the alternative methods described here can still be interpreted by the methods introduced in Sections 3, 4 and 5 of this review. The underlying mass transport being studied remains the same – Brownian motion.

3. The Stokes-Einstein Equation

Any discussion of diffusion coefficients of small molecules in solution has to start with Eq. (7), the Stokes-Einstein equation [82]. This equation predicts diffusion coefficients, D, at a

given temperature, T, by considering a hard, spherical particle, with radius r_H, at infinite dilution in a continuum fluid with viscosity, η. The thermal energy of the system, $k_B T$, k_B is the Boltzmann constant, is balanced by the frictional resistance to movement of the particle, $6\pi\eta r_H$.

$$D = \frac{k_B T}{6\pi\eta r_H} \tag{7}$$

A number of related equations exist. A similar equation, Eq. (8), was proposed, at roughly the same time, working along similar lines and with similar arguments, by Sutherland [83]. One key difference is the introduction of a variable parameter, β, that determines the amount of friction between solute and solvent.

$$D = \frac{k_B T}{6\pi\eta r_H}\left(\frac{\beta r_H + 3\eta}{\beta r_H + 2\eta}\right) \tag{8}$$

If $\beta = 0$, corresponding to a "non-stick" or "slip" boundary between particles, the denominator of Eq. (8) reduces to $4\pi\eta r_H$. For larger molecules, the parameter increases until $\beta = \infty$, a "stick" boundary, and the Stokes-Einstein equation is reproduced. The Stokes-Einstein-Debye equation [84] has a similar form to both Eqs. (8) and (9), but is used to predict the rotational diffusivity, D_{rot}, of a molecule on the basis of its volume V. Wilke and Chang [85], in 1955, developed a generalised equation, Eq. (9), for predicting D from available properties of dilute solutions. While Eq. (9) is derived from the Stokes-Einstein equation, it is empirical in nature. Wilke and Chang's motivation was to estimate diffusion coefficients, D in $cm^2\ s^{-1}$, for engineering purposes.

$$D = 7.4 \times 10^{-8}\frac{(xMW)^{0.5} T}{\eta V^{0.6}} \tag{9}$$

In this equation, MW and V are the molecular weight and molar volumes of the diffusing species, respectively. There are two notable features in this equation. First is the introduction of the association parameter, x. This accounts for associated molecules behaving

like larger ones and therefore diffusing at a lower rate. Different solvents permit different degrees of association and values were presented for the most widely used solvents, ranging from $x = 2.6$ for water and $x = 1.9$ for methanol to $x = 1$ for benzene and heptane. Second is the use of explicit power laws for the mass and volume dependence of D. The Stokes-Einstein equation shows an inverse dependence of the diffusion coefficient on the hydrodynamic radius of the diffusing species and, therefore, D would be expected to show a cube root dependence on molecular weight if all species had the same density. This cube root dependence is not reproduced in the Wilke-Chang equation. While the Wilke-Chang equation has been widely used and cited (> 4600 citations as of August 2019, a small number of very recent citations are provided for the curious [86-88]), the association parameter causes difficulties when new systems are studied. For example, x was seen to fall from 2.6 to *ca*. 2.3 for the diffusion of small alcohols and glycerol through water.

The Wilke-Chang equation is one of a family of similar equations [89-93] that all address the same problem: the Stokes-Einstein equation tends to significantly underestimate diffusion coefficients for smaller molecules. Fig. 4 compares the viscosity-scaled diffusion coefficients of a range of 108 small organic molecules, estimated using the Stokes–Einstein equation, with those measured in 5 different deuteriated solvents using diffusion NMR techniques [94]. Species were chosen to be representative of those commonly encountered in synthetic and pharmaceutical NMR laboratories, but excluded those with heavy atoms (i.e. >Cl) or those known to aggregate in dilute solution. In order to calculate Stokes-Einstein diffusion coefficients, the molecules were assumed to be spherical in solution, the densities of the pure compounds were used to calculate the hydrodynamic radii used in the plot, and a packing factor, dependent on whether the pure compound is solid or liquid, was also included. As the molecules get larger, the differences between estimated and measured diffusion coefficients decrease and the Stokes-Einstein equation works for large molecules

and particles, but the under-estimation for fast moving, small molecules is clearly shown. Similar trends are observed for all five solvents.

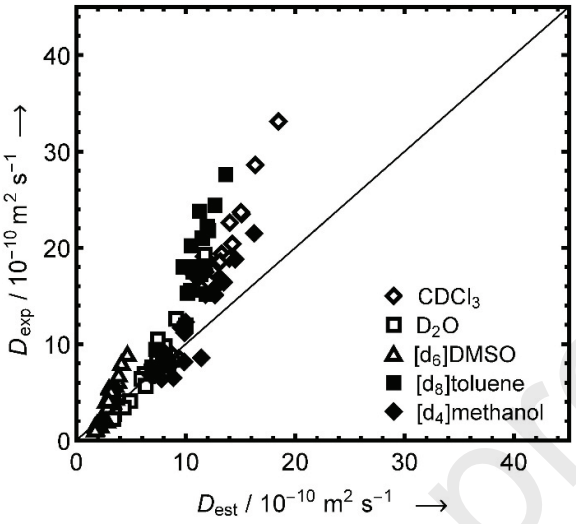

Figure 4: Measured diffusion coefficients plotted against diffusion coefficients calculated using the Stokes–Einstein equation for 108 samples of 44 small molecules in five deuteriated solvents, as detailed in the figure legend, with a solid line of unit slope. All data acquired on a Varian Unity 400 MHz spectrometer using the Oneshot sequence at 298 K. Adapted from Evans et al., *Angew. Chem. Int. E*d., **52** (2013) 3199-3202.

Another demonstration of how the Stokes-Einstein equation can sometimes struggle to predict small molecule diffusion coefficients can be found in electrochemical research by Gonzalez and Valencia [95, 96]. The diffusion coefficients of 29 molecules, a set spanning molecular weights from 100 to *ca*. 350 g mol^{-1} and containing quinones and polyaromatic compounds such as triphenylene and chrysene, as well as ferrocene and some derivatives, were obtained using chronoamperometry. A linear relationship between diffusion coefficient and inverse molecular weight was observed rather than the expected cube root relationship. To rationalise this, the Stokes-Einstein equation was modified by expanding the cube root molecular weight term into a power series. This was facilitated by introducing a molecular

density parameter, equal to MW/V, and assuming that the molecules studied were broadly spherical. If this molecular density can be assumed to be approximately constant for the set of molecules, then a first order series expansion of the Stokes-Einstein equation around a pivot mass M_0 produces a linear function that fits data over a small range of molecular weights. There are two important points to bear in mind here. First, the molecules chosen were almost all aromatic or polyaromatic and therefore would be rather inflexible, flat molecules. Second, when constructing the Stokes-Einstein equation, the constant on the denominator was not set to 6, but left as a variable, n (named the "Sutherland constant" in the text, reflecting the presence of the variable β in Eq. (8)). This "constant" was estimated using the diffusion coefficients and was found to < 4 for the three solvents studied, rather than the 6 typically used in the Stokes-Einstein equation.

Understanding how and why the Stokes-Einstein equation fails to predict small molecule diffusion coefficients is instructive. The original equation is based on two important assumptions. First, that the fluid through which molecules diffuse is a continuum, and second, that the molecules themselves are hard spheres. Related to this is the difficulty in relating the hydrodynamic radius of a molecule to its molecular weight. How these assumptions lead to the failure of the Stokes-Einstein equation in accurately predicting small molecule diffusion will be analysed and addressed now before moving on to more successful methods of predicting diffusion coefficients.

3.1 Fluid Friction

A continuum fluid is one where the individual, discrete fluid molecules are neglected and the fluid is modelled as a single, uniform substance. Real solvents are not continuum fluids, but consist of small molecules moving randomly, tumbling as they collide with other molecules in the liquid. In chemical systems, the sizes of the solute molecules are likely to be

in the same order of magnitude as the sizes of the solvent molecules. As implied by Eq. (8), differently-sized solute molecules will experience different frictional forces. A transition between these types of boundaries is sometimes invoked to explain apparent differences in frictional forces between larger and smaller molecules. It is clear that no one denominator will work across the entire range of possible molecular sizes.

3.2 Molecular Shape

The effects of molecular shape also modify the friction experienced by molecules. Molecules are not spheres; a better initial approximation is to describe them as as ellipsoids. Ellipsoids can be either prolate or oblate, as defined by their aspect ratio, the ratio of the minor to the major axis (b/a). For illustration, a rugby ball is a prolate ellipsoid with an aspect ratio *ca*. 1.6, while an athletics discus is oblate and has an aspect ratio of approximately 5. The effect of molecular shape were analysed by Perrin [97], who derived analytical equations (Eqs. (10)(a) and (10)(b)) for the effect on friction of increasing aspect ratio in ellipsoidal shapes, in the form of an extra shape friction factor f_s that multiplies the denominator of Eq. (7).

prolate ellipsoid

$$f_s = \frac{\sqrt[2]{1-\left(\frac{b}{a}\right)^2}}{\left(\frac{b}{a}\right)^{2/3} ln\left(\frac{a}{b}\sqrt[2]{1-\left(\frac{b}{a}\right)^2}\right)} \qquad (10)(a)$$

oblate ellipsoid (10)(b)

$$f_s = \frac{\sqrt[2]{\left(\frac{b}{a}\right)^2 - 1}}{\left(\frac{b}{a}\right)^{2/3} arctan\left(\sqrt[2]{\left(\frac{b}{a}\right)^2 - 1}\right)}$$

For aspect ratios lower than 5, i.e. molecules that are not long thin rods or wide thin disks, the effects are typically much less than 10 % and can often be safely ignored.

3.3 Estimation of Molecular Size and Density

The final aspect of the Stokes-Einstein equation to be discussed is the size of the molecules themselves. There are a number of methods for characterising the size of molecules. The hydrodynamic radius, r_{H}, only represents the radius of a hard sphere diffusing at the same speed as the particle being studied. Real molecular systems under investigation can be non-spherical, or can contain cavities and inlets, are flexible to a greater or lesser extent, and are solvated. Other measurements of radii exist, such as the van der Waals radius, r_{VdW}, the radius of gyration, r_{g}, the crystallographic radius, $r_{\mathrm{X-ray}}$, and radii derived from density or partial molar volume, r_{M}. The relationships between these different molecular dimensions are not always clear and depend on the molecules themselves. Some distinct trends can be observed. The space taken up by the atoms themselves, r_{VdW}, is often the lower limit for molecular radius. The hydrodynamic radius r_{H} can be viewed as a radius of a hypothetical hard sphere, which has the same diffusion coefficient as the studied particle. A lower limit for r_{H} is, therefore, the van der Waals radius, r_{VdW}. The two radii are only equal in the case of a compact molecule without any cavity inlet. The upper bound of the hydrodynamic radius can be estimated by the crystallographic radius $r_{\mathrm{X-ray}}$, which can be obtained by dividing the volume of the crystallographic unit cell by the number of molecules contained while assuming a spherical shape for the molecule [1]. Clearly, the actual

hydrodynamic radius of a molecule in solution depends on its chemical structure and any interactions with solvent.

The Stokes-Einstein equation can still be used in the analysis of large, approximately spherical species [98, 99]. However, this is clearly not the case for small molecules. Faced with the problems described in this section, empirical methods are required to estimate MW from experimentally measured diffusion coefficients. Two limiting cases exist. For very well-characterised problems, it should be possible to parameterise the relationship using measurements on a series of closely-related species. For more general problems, the assumptions inherent in the Stokes-Einstein equation can be revisited in order to find a universal, but necessarily more approximate, relationship that works across solvents, temperatures, and a wide span of chemistry. Note that both of these methods are based on equations that predict diffusion coefficients on the basis of the molecular weights of the species involved. The inverse problem of estimating mass from experimentally measured diffusion coefficients, whilst more useful to chemists and the interpretation of DOSY spectra, comes with increased (approximately tripled) uncertainties in the final molecular weight estimations.

4. Power Laws

One approach to inferring molecular weight from diffusion coefficient is to assume that the diffusion coefficient or, often, the relative diffusivity (the measured diffusion coefficient divided by that of an internal reference) can be expressed in terms of the molecular weight of the species, MW, raised to an empirical negative power, –α, as in Eq. (11).

$$D \propto MW^{-\alpha} \tag{11}$$

This use of a power law is reminiscent of Flory theory [100, 101] (Eq. (12)), where the radius of gyration of a polymer, R_g, is related to its molecular weight, MW, through a parameter, known as the Flory exponent, δ.

$$R_g \propto MW^{\delta} \tag{12}$$

The molecular weight of a polymer is an important quantity, because it determines many physical properties including the temperatures for transitions from liquids to waxes to rubbers to solids and mechanical properties such as stiffness, strength, viscoelasticity, toughness, and viscosity. It is tempting to relate the power law relationship to some physical quantity. In Flory theory (Eq. (12)), the reciprocal of the exponent, δ, is sometimes taken to represent the fractal dimension of the molecular chain. Fractal dimensions can be best understood as a measure of the way an object occupies three-dimensional space. While there may not be a direct link between a fractal dimension and the exponent obtained in diffusion NMR studies, the analogy can be useful in interpreting and understanding the diffusion data and, importantly, relating it to molecular structure. A purely one-dimensional object, such as an infinite rigid rod, will have a fractal dimension of 1, a completely packed sphere will have a fractal dimension of 3, and intermediate values correspond to molecules that partially fill empty space. These in turn give rise to limiting values of α of 1 and 0.33. These values can also be linked to the values predicted for polymers by Flory theory. Polymers fold differently in different types of solvent; the values of α for poor and good solvents are 0.333 and 0.588 respectively. For Θ-solvents (i.e. those where polymer-polymer interactions are equal to polymer-solvent interactions, and the polymer behaves like a Gaussian chain [102]), the value of α is 0.500.

Empirically-obtained power laws have found wide use in the study of macromolecules, in particular proteins, peptides and polymers, with the scaling parameters depending on the molecular structure of the species, as well as on experimental conditions

such as solvent choice and temperature. A plot of log$D$ against logMW, as in Eq. (13), for a series of structurally similar compounds can then be used to infer MW for an unknown compound of the same class from the measured D.

$$\log D = -\alpha \log MW + \log K \quad (13)$$

Each power law needs to be parametrized for the distinct class of compounds studied, producing a pair of parameters, log$K$ and, more importantly, α. This constant of proportionality between log$D$ and logMW indicates the relationship between the molecular weight of the species and its hydrodynamic relationship in solution. Using a double-logarithmic plot approach avoids direct discussion of some of the problems discussed in Section 2.1 of this review and has achieved good results for a range of macromolecules. While not small molecules, the power law relationships exhibited by proteins, polymers and oligosaccharides are instructive and give important context to their use in the interpretation of small molecule diffusion coefficients.

Globular proteins are an example of a class of chemical species where values of α tend towards 0.33. Over a range of protein sizes spanning several orders of magnitude, two studies, one by Augé et al. using diffusion NMR [103] and another by Enright and Leitner [104], computing the fractal index for a set of 200 proteins based on structures in the Protein Data Bank, both obtained a value of α for proteins of 0.39. Earlier work by Jones and Wilkins [105, 106] related the radius of gyration of the proteins, acquired using diffusion NMR, to the number of residues, with similar results. The exponents for globular proteins tended towards 0.33, while measurements in strongly denaturing solutions increased the value of α to approaching 0.6, similar to the exponent expected for a polymer in a good solvent. This difference in α can be used to distinguish between folded, disordered and denatured proteins. Dudás and Bodor [107] acquired diffusion coefficients of 12 globular proteins and 10 intrinsically disordered proteins with sizes of up 65 000 g mol^{-1}. This work obtained a value

of α for globular proteins of 0.381, consistent with previous work and near-spherical molecules. Intrinsically disordered proteins had an average exponent of 0.507, commensurate with their more extended, loosely packed structures. Small cyclic peptides have also been studied with diffusion NMR methods [108]. By closing the ring, these molecules have somewhat more constrained conformations compared to linear polypeptides. Two methods were used to estimate the hydrodynamic radii of a set of four polypeptides, one using a relative diffusion coefficient based on the simultaneous measurement of a small reference molecule, the other a direct calculation of radius from the Stokes-Einstein equation, estimating the viscosity of the mixed solvents used. The two estimates were found to be in close agreement for both peptides. While the analysis of the relationship between peptide length, related to MW, and the measured diffusion coefficient data was simplistic, the work shows that diffusion NMR can be readily applied to proteins of very different sizes. Diffusion NMR has also been used to estimate the molecular weights of human telomeric 22-mer DNA, and related mutants [109].

While proteins and oligopetides are constructed from chains of amino acids, with a number of different possibilities for each repeating unit, polymers are typically made from multiple repeats of the same unit. A number of qualitative applications of diffusion NMR to polymers have been proposed [110]. It is an effective and efficient method for the study of polymer mixtures [111], the determination of polymer molecular weight distributions [29], revealing and characterising colloid-like behaviour in di-block copolymers [112-114], and the structure elucidation of block copolymers [115, 116]. DOSY can also be used for the evaluation of the efficiency of purification processes, as traces of impurities such as unreacted monomers, degradation products and residual homopolymers can be identified not only through their chemical shifts but also through their faster diffusion. In addition, a

DOSY-based protocol was developed by Delsuc and co-workers to access the dispersity, *Đ*, of linear polymers [117].

Quantitative study of polymer molecular weights reveals that macromolecules show a wide range of behaviour in solution, with values of α/δ dependent on polymer identity, solvent and polymer mass. The relationship between mass and diffusion coefficient for linear polymers, including polyethylene oxide, polystyrene, and poly (methyl methacrylate), spanning a wide range of molecular weights has been studied in a number of different solvents. Comparisons can be made between different species. Table 1, taken from Reference 103, summarises the power law exponents obtained for polystyrene samples in a number of different solvents and for different polymer fractions. From the power law exponent, α, it is possible to estimate the fractal dimension of the folded polymer in solution, δ. These data show clearly that the structures of polymers in solution depend not only on solvent, as expected, but also on molecular weight.

solvent	α	δ
toluene-d_8	0.41	2.45
acetone-d_6	0.47	2.15
$CDCl_3$ (< 20 kD)	0.47	2.12
$CDCl_3$ (> 20 kD)	0.61	1.63
THF-d_8 (< 20 kD)	0.50	2.01
THF-d_8 (> 20 kD)	0.62	1.61

Table 1: Experimentally obtained values of α and $\delta = 1/\alpha$ for a series of polystyrene samples measured in common deuteriated NMR solvents. Data adapted from Augé et al., *J. Phys. Chem. B* 113 (2009) 1914 – 1918.

By showing that the relationship between logMW and log$D$ is maintained over 4 orders of magnitude for a series of polyethylene oxide standards, Augé et al. used double logarithmic plots as calibration curves to estimate the molecular weights of a number of different polymer samples. This method has since been successfully demonstrated for, e.g., polystyrene [118], poly(L-lactide) [119], and poly(N-acryloylmorpholine) [120], as well as being used to distinguish between different polymerisation mechanisms in the synthesis of poly(methylmethacrylate) [121].

Two recent diffusion NMR studies of polymers stand out due to their implications for similar studies of small molecules. Solubility is an important consideration in the study of polymers. Some combinations of molecular weight, temperature and solvent can render a polymer insoluble. However, a wider range of solvents and conditions are available to NMR than to chromatographic techniques. Poly(ethylene terephthalate) (PET) is one of the most common oil-based plastics, used widely in bottles and other food packaging. Poly(ethylene furanoate) (PEF) has been proposed as a bio-based replacement. Molecular weight determination for PET and PEF is severely hindered by their insolubility in most common solvents. Hot tetrachloroethane, trifluoroacetic acid (TFA), and hexafluoroisopropanol (HFIP) have proven to be the only solvents capable of dissolving these two polymers. While chromatographic methods are possible, the equipment needs to be resistant to the solvents and strict care and attention to health and safety needs to be maintained throughout. Using a series of PET standards to generate calibration curves for both M_n and M_w, DOSY NMR was used to measure average molecular weights of both PET and PEF samples in TFA-d, including those from commercial packaging samples. The diffusion NMR values obtained for M_n and M_w match those from light scattering techniques closely, with a near one-to-one correlation. The calibration curves revealed a power law relationship with $\alpha = 0.54$ ($\delta = 1.85$),

consistent with other polymers studied using diffusion NMR. While measured diffusion coefficients were smaller, changing the solvent from TFA-d to HFIP-d_2 had very little effect on α [122]. With extended π-bonding networks, it might be expected that conjugated polymers and copolymers, such as poly(3-hexylthiophene) (P3HT), would have very stiff backbones and therefore exhibit diffusion behaviour in solution consistent with an extended configuration. Four P3HT samples with distinct molecular weights (M_n of 5, 10, 20, and 40 kg mol^{-1}) and narrow weight distributions were used to construct a double-logarithmic calibration curve, where $\alpha = 0.56$ ($\delta = 1.78$). This was then used to estimate the molecular weights of a series of samples of an alternating copolymer comprising cyclopenta-[2,1-b:3,4-b′]-dithiophene and pyridal-[2,1,3]-thiadiazole. Note that chromatography is ill-suited to the study of these conjugated polymers. First, the stiff backbones and low solubility in most common solvents means that they interact with and adsorb onto chromatographic columns. Second, the extended conjugated π-bonding network means that they can strongly absorb the wavelengths of light typically used in detection. Quantitative validation of the polymer molecular weights could therefore not be easily attempted. The molecular weights calculated from the acquired diffusion data agreed qualitatively with increasing red shift in the optical spectra of the polymers [123]. These two examples show that calibration curves for one group of compounds may find use for structurally similar compounds, and that choice of solvent can be important, whether by allowing access to otherwise inaccessible materials or by changing the structures it forms in its solvated state.

Poly- and oligo-saccharides can possess more complex structures, with highly branched macromolecules common. Polysaccharides such as pullulan [124] and dextran [125] have been used as standard examples of linear, water-soluble, polysaccharides to demonstrate how diffusion NMR methods can be applied more generally. For pullulan, a water-soluble linear polysaccharide consisting of α-1,6-linked maltotrioses, an exponent α =

0.49 (δ = 2.07) was obtained from the diffusion NMR data for 6 fractions spanning two orders of magnitude in molecular weight. The value of the exponent fits well with the fact that water is nearly a Θ-solvent for polysaccharides. This power-law information was used to characterise both single component samples and mixtures of pullulans and dextrins. It was further noted that sucrose, α-, β-, and γ-cyclodextrins, dextrans and a mannose-rich oligosaccharide also fitted the pullulan calibration curve. This suggests that the pullulan calibration curve could be used to provide rough estimation of molecular weights for both linear and slightly branched water soluble uncharged polysaccharides [50]. Hydroxyethyl starches are more disperse, branched polysaccharide structures, with both α-1,6- and α-1,4-linkages between sugar motifs. Diffusion coefficients for 15 samples were acquired and a range of fitting methods applied. These produced values for the power-law exponent between 0.38 and 0.41, consistent with a more spherical solution state structure [126].

The use of power laws is not limited to the analysis of polymers and other macromolecules. In theory, the cyclisation of a linear molecule into a ring should have a significant effect on the molecular shape. There is a restriction in the conformational freedom of the molecules and imposed organisation of the structure. Diffusion coefficients, and the interpretation of power laws based on the acquired diffusion coefficients, allow for the effect of cyclisation on diffusion to be studied. Diffusion coefficients of a matched set of macrocycles, from 12- to 29-membered rings, and their linear analogues were acquired in both $CDCl_3$ and DMSO-d_6. The compounds were designed to span the molecular weight range typically associated with drug molecules (for example, the immunosuppressant cyclosporin is a 33-membered ring [127]) and to possess functional groups found in biologically-active molecules. The linear analogues all differed from the cyclic compounds in the breaking of a single carbon-carbon bond. Plots of log$D$ against logMW indicated power law relationships for all species, linear and cyclic, in both solvents. As perhaps expected, the

cyclic compounds all diffused faster than the linear analogues, corresponding to a *ca.* 10 % difference in molecular weight. However, the slopes of the double-logarithmic plots for each matched set in a given solvent were very consistent, suggesting that the linear and cyclic molecules form similarly packed structures in solution [128].

For generic small molecules, such similarities between the packing and folding of structures in solution cannot be relied upon. In the previous example, the same functional groups are present in both of the paired molecules. Polymers consist of many repetitions of the same units, with the same groups repeating. As has been shown in this section, the polymer functional groups and solvents interact so as to give polymers different structures in solutions, depending not only on functional groups but also on sizes, with the atoms packed together differently as a result. Small molecules are much less flexible, and the incorporation of different functional groups can impart different degrees of rigidity and polarity into their chemical structures. As the next section will show, in the same solvent, small molecules can, however, behave similarly enough to one another to allow for the use of power laws in the quantitative interpretation of their diffusion coefficients.

4. 1 Power Laws for Estimating Molecular Weights of Small Molecules

Power laws have also found use in attempts to deduce the molecular weights of small molecules from their diffusion coefficients. This is typically achieved by the use of calibration curves, double logarithmic plots of diffusion coefficient against molecular weight for a particular set of calibrant compounds. Hence, all of the following power law methods follow the same general approach. The diffusion coefficients of an appropriate series of reference compounds are measured, and appropriate double-logarithmic plots are used to generate the two parameters needed for each power law. This calibration is then used to predict the diffusion coefficient of a compound on the basis of its molecular weight, or to

estimate the molecular weight of an unknown species from its diffusion coefficient. Such methods can be divided into two distinct categories, depending on whether the multiple different reference materials are added to the sample (internal calibration) or measured separately (external calibration). Their use in the quantitative study of small molecules was first demonstrated by Crutchfield and Harris [129]. There is also an important distinction to be drawn between internal and external referencing when calculating the diffusivity of an analyte: in the former, the diffusion coefficients of analyte and reference material are measured in the same sample, in the latter, in different samples.

Seeking a quantitative relationship between diffusion and molecular weight for common, small, organic and water-soluble compounds, Crutchfield and Harris measured diffusion coefficients for two sets of molecules, dissolved in either D_2O or $CDCl_3$ with residual water or tetramethylsilane (TMS) as internal reference molecules respectively. Double-logarithmic plots of the data yielded two different power law relationships between relative diffusivity and molecular weight, with the same exponent, $1/\alpha = 1.72$ ($\alpha = 0.58$). The test set of molecules spanned a range of molecular weights from 2 to 1300 g mol^{-1}. These data, and the resulting calibration curves, are shown in Fig. 5. Note that a wide range of compounds with different sizes and functional groups was included in each calibrant set. While the polymer work of the previous section suggests that, for best results, each chemically distinct set of compounds would need to be parametrised appropriately, general trends can be shown by using a very large number of different compounds. Clear correlations are seen between diffusion coefficient and molecular weight for a given solvent, with most species having a diffusion coefficient within ±30 % of the average for that MW.

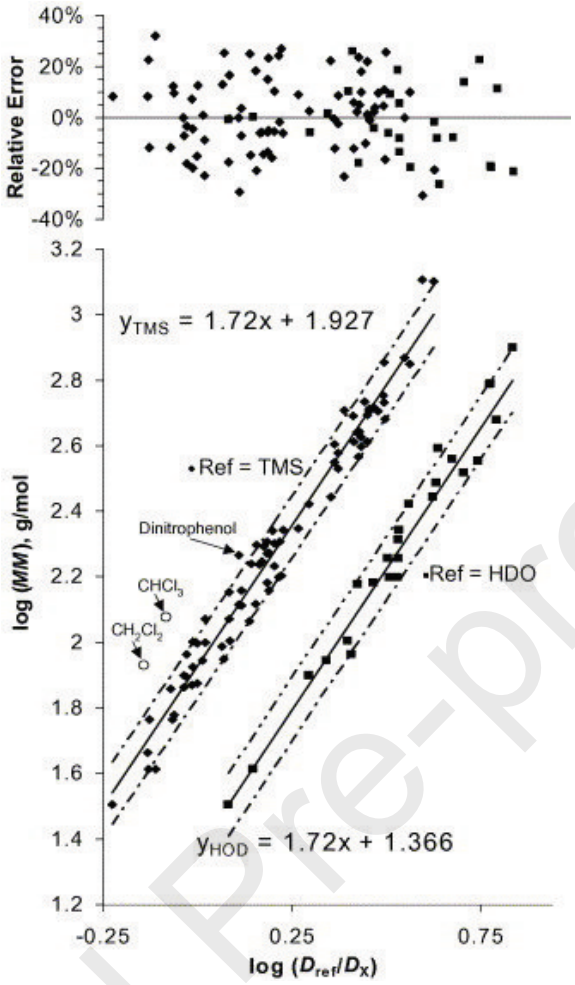

Figure 5: Pair of calibration curves relating molecular weight and relative diffusivity for small molecules; diamonds signify the use of TMS as an internal reference (for solutions in $CDCl_3$), squares signify HDO (for solutions in D_2O). Molecules of abnormally high density, CH_2Cl_2 and $CHCl_3$, or low density, H_2 (data not shown in this figure), are not included in the fit. The upper figure is a residual analysis plot that retains the same symbols. All data acquired on a Bruker Avance 400 MHz spectrometer. Reproduced with permission from C. A. Crutchfield and D. J. Harris, *J. Magn. Reson.*, **185** (2007) 179-182. Copyright (2007) Elsevier.

Certain aspects of the Crutchfield and Harris methodology warrant further discussion. First, the diffusion coefficients are measured relative to the diffusion coefficient of an internal

reference. This use of relative diffusivity (Eq. (14)) ensures that the measurements are independent of sample viscosity and relatively robust to experimental flaws.

$$D_{\mathrm{rel,ref}} = \frac{D_{\mathrm{ref}}}{D_{\mathrm{X}}} \tag{14}$$

This relative diffusivity now corresponds to the relative size of the analyte, *X*, compared to the size of the reference molecule. The exponents produced in their studies are then analogues of the fractal dimension, and are reciprocals of those used elsewhere.

A stated aim of the Crutchfield and Harris approach was to minimise experiment time. This was achieved by assuming that their data fitted the Stejskal-Tanner equation, so it should be possible to obtain an accurate measurement of relative diffusivity from measurements with just two gradient values, as in Eq. (15).

$$D_{\mathrm{rel,ref}} = \frac{D_{\mathrm{ref}}}{D_{\mathrm{X}}} = \frac{\ln\left(S_{\mathrm{ref}}, g_{\max}/S_{\mathrm{ref}}, g_{\min}\right)}{\ln\left(S_{\mathrm{X}}, g_{\max}/S_{\mathrm{X}}, g_{\min}\right)} \tag{15}$$

This approach reduces experiment times to just a few minutes, although at some risk of loss of precision in the measurement. A significant amount of attenuation is required in order to obtain accurate values, but this comes at the risk of low signal-to-noise in the most attenuated spectrum. In the original work, diffusion coefficients obtained in this way were within 2 % of those found from non-linear regression of the complete diffusion NMR data set, with 32 increments of the gradient strength. For samples with low signal-to-noise ratio, caution may be well advised.

Two examples of the methodology applied to practical examples have been demonstrated. In the original paper, the methodology was used to study a sample of virgin olive oil. The molecular weight of the main component of the oil, oleic triglyceride, was estimated to within 7 %. The olive oil sample also contains a number of aldehydic components, found at *ca.* 9.5 ppm in the NMR spectrum, which typically elude identification. A number of signals were identified in the spectrum, with a sharp peak at 9.74 ppm and a

number of smaller peaks found between 9.4 and 9.6 ppm. The average molecular weights were estimated to be 350 ± 100 g mol^{-1} for the sharp peak, suggesting that it is a larger compound than those tentatively assigned to this peak, hexanal and heptanal [130]. The smaller peaks were found to be heavier still, ruling out oxidized fragments of oleic acid. The molecular weight estimation gives an additional source of information, ruling out certain assignments and giving additional insight into possible compounds present.

A further example of the application of the methodology is the analysis of derivatised compounds [131]. Derivatisation of functional groups aids in the analysis of mixtures and impurities by removing the original signals and introducing new, functional-group specific resonances, in unobscured regions of the NMR spectrum. This can overcome one of the key problems in diffusion NMR experiments, when overlap hinders the successful resolution of NMR signals and analysis of a sample. Molecular information beyond the immediate vicinity of the functionalised groups may be difficult to obtain, but the accurate estimation of molecular weight provides additional information for the classification of molecules, particular in chemically cognate groups of molecules and homologous series.

In this work, two different derivatisation agents were used. For a sample set containing alcohols, thiols, amines and carboxylic acids, trichloroacetyl isocynate (TAI) was used. Two calibration curves were generated, with TMS used as a reference for all experiments, obtaining the same value of α as in the original study. Difunctionalised compounds such as methylsalicylic acid were found to be derivatised with TAI twice, with accordingly lower diffusion coefficients. In order to handle the two sets of compounds, and two calibration curves, an empirical correction factor, dependent on the number of reactive functional groups in the molecule, was added. The second derivatisation agent, chlorophosphane, reacts with alcohols and carboxylic acids to introduce a phosphorous-containing group into the molecule. This allows the use of ^{31}P NMR. The sparser phosphorus

spectrum reduces the amount of overlap between signals and should allow for better spectral resolution of peaks in the spectrum and identification of compounds present. Diffusion coefficients were measured for a sample set of alcohols and carboxylic acids in 1:1 pyridine:$CDCl_3$, with (derivatised) bisphenol-A as the reference compound. Two calibration curves were generated, both with the same exponent as in the original study [129] and also the TAI-derivatised set of compounds. Difunctionalised compounds such as 1,3-propanediol were found to be derivatised with chlorophosphane twice, with accordingly slower diffusion. As with the TAI-derivatised set of compounds, an additional calibration factor was added to account for the additional molecular weight present. The combination of derivatisation and molecular mass estimation was demonstrated with a lubricant oil. First, the oil was derivatised with chlorophosphane, then ^{31}P NMR was performed on the derivatised sample. Integrals relative to derivatised bisphenol A gave an indication of the relative concentrations of the species present. Difunctional compounds could be partially identified from pairs of resonances with equal integral areas. A combination of interpretation of chemical shifts and additional diffusion coefficient information allowed for the identification of terminal and secondary alcohols, phenolic groups, and carboxylic acids, with molecular weights between 180 and 460 g mol^{-1}. No further identification of compounds was performed, in spite of several peaks in the spectrum corresponding to primary alcohols, with different estimated molecular weights.

The work by Crutchfield and Harris appears to be the first application of the power law method to small molecules for deductive purposes. While the use of relative, rather than absolute, diffusion coefficient has become quite widespread, as will be seen later, only a study of terpene hydroperoxide chemistry in citrus oils has directly acknowledged the original methodology [132]. In this study, a new calibration curve was generated from 19 perfumery compounds in cyclohexane-d_{12} with TMS as both chemical shift and diffusion

coefficient reference. This method would now be categorised as an *external* calibration method: the diffusion coefficients of a sample set of representative compounds were experimentally measured individually and a double-logarithmic plot of the data generated for use as a calibration curve. A single reference compound was used in the sample of the species of interest, and its molecular weight estimated from its relative diffusion coefficient. An alternative approach would have been to generate the calibration curve using diffusion coefficients measured from multiple calibrant compounds added to the sample: an *internal* calibration method.

4.2 Internal Calibration

Key to the successful use of any power-law based method is an appropriate calibration curve. As the name suggests, an *internal* calibration method uses reference species contained within the sample, with the diffusion coefficients measured synchronously with those of the species of interest. In much internal calibration work, just three co-solutes are added to samples to provide parameters for the power law. Using only two co-solutes, or the solvent itself, makes the calibration less reliable and removes any check on internal consistency. A fitted curve, based on the experimentally-derived diffusion coefficients for the three references, is generated and the molecular weight of the unknown is then calculated from this curve. Not all potential reference materials are suitable: they must be inert, soluble, non-aggregating, and cover a suitable range of molecular weights around that of the analyte being studied. Reactive and coordinating groups (alcohol/amide/ether/carbonyl) should be avoided. A suitable range of molecular weights needs to be spanned by the reference compounds, for example benzene (MW = 78 g mol^{-1}), cyclooctene (MW = 110 g mol^{-1}), and 1-tetradecene (MW = 196 g mol^{-1}). This mixture covers diffusion coefficients ranging from 8.42×10^{-10} m^2 s^{-1} (1-tetradecene in cyclohexane-d_{12}) to almost 40×10^{-10} m^2 s^{-1} (benzene in

CD_2Cl_2). A further requirement is that the signals of the internal references must not overlap with those of the other components in the sample. A significant general issue with diffusion NMR is that the addition of more signals to the NMR spectrum increases the likelihood of spectral overlap, displacing the peaks in the diffusion dimension. This can, for example, rule out the use of TMS as an internal diffusion reference as its single peak sometimes overlaps with organolithium complexes as well as common impurities such as vacuum grease. Temperature dependence is also important. Organolithium compounds, amongst others, are typically studied at low temperatures. Changes in temperature mean changes in the rates of exchange between structures. In particular, the multiplet structures exhibited by exchanging signals can be sensitive to differences in their rates of exchange.

Proof of principle of internal calibration was achieved using diisopropylamine (DIPA), studied in four deuteriated solvents (toluene-d_8, cyclohexane-d_{12}, CD_2Cl_2 and $CDCl_3$), with 1-tetradecene, cyclooctene and benzene as internal references, as in Fig. 6(a) [133, 134]. All four compounds could be resolved and identified in the DOSY spectrum of a sample in toluene-d_8 (Fig. 6a), and diffusion coefficients could then be estimated. Fig. 6(b) has been adapted from [134] using the experimental data contained within the DOSY spectrum and detailed further in the original work. First, a log$D$-logMW calibration curve was plotted, here giving the relationship log$D$ = –0.7374 logMW – 7.2783, with R^2 = 0.98. The diffusion coefficient of DIPA, the "unknown" in this sample, was also measured (D = 17.9 $m^2\ s^{-1}$) and from this logMW and MW could then be calculated. For this sample, where [DIPA] = 1.12 M, the internal calibration method gave MW = 98.5 g mol^{-1} for the amine, a 2.7 % difference from its actual MW of 101.2 g mol^{-1}

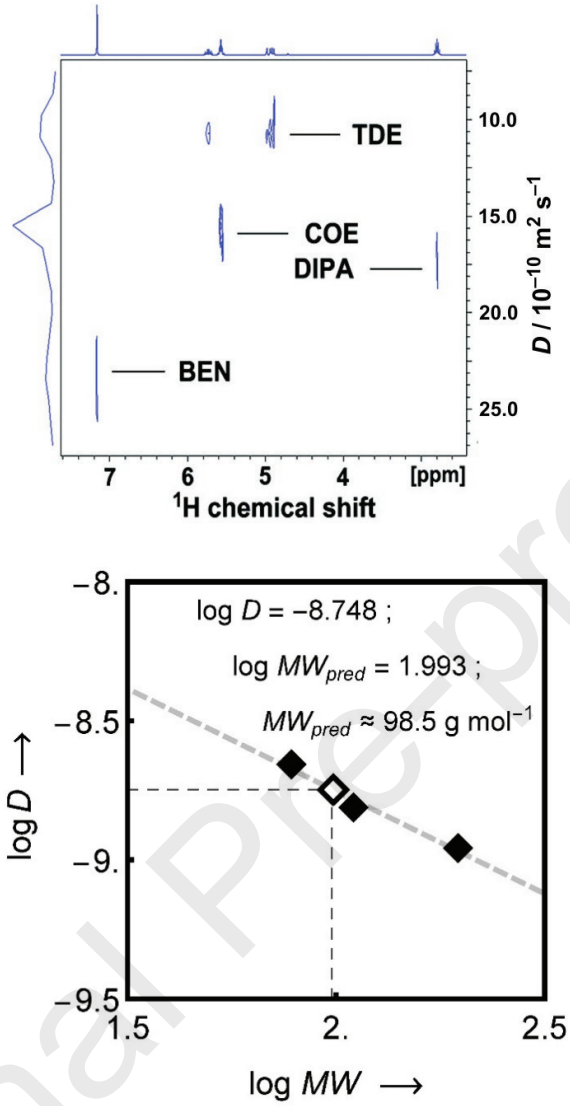

Figure 6: (a) ^{1}H DOSY spectrum of 1.12 M diisopropylamine (DIPA), and three internal references (benzene (BEN), cyclooctene (COE) and 1-tetradecene (TDE)), in toluene-d_8 (upper). All data acquired on a Bruker DRX 400 MHz spectrometer. Adapted from Li et al., *J. Am. Chem. Soc.*, **131** (2009) 5627-5634. Copyright (2009) American Chemical Society. (b) Internal calibration curve constructed from DOSY spectrum in (a), consisting of a log−log plot of diffusion coefficients acquired for BEN, COE and TDE (black diamonds) as a function of *MW* and the acquired diffusion coefficient of DIPA (white diamond)

superimposed with subsequent deduction of molecular weight (lower). Adapted from Li et al., *J. Am. Chem. Soc.*, 131 (2009) 5627-5634.

The first demonstration of the wider utility of the method used a mixed trimeric organolithium complex, containing 1 equivalent of *n*-butyllithium (*n*-BuLi) and 2 equivalents of a lithium amide [135], with MW = 678.1 g mol^{-1}. Diffusion coefficients for the three internal references and the complex were acquired for a number of different concentrations. Taking the data at 0.248 M as an exemplar set, values for α and log$K$ of 0.552 and –7.689 were obtained. The measured coefficient of the mixed complex was 5.6 × 10^{-10} m^2 s^{-1}, extrapolated to estimate a MW of 673.6 g mol^{-1}, an error of only 0.7 %. Across all five concentrations of complex studied, the molecular weight of the species was estimated to within < 2 % in all samples.

These proof of principle results were part of a larger study of the methodology and, importantly, its robustness and reliability [134]. log$D$-logMW curves were parametrised for four deuteriated solvents for a range of sample concentrations, for a total of 28 different samples. While toluene-d_8 and cyclohexane-d_{12} showed consistent trends in α and log$K$ as the concentration fell, the denser $CDCl_3$ and CD_2Cl_2 did not. It is noteworthy that the trends in α and log$K$ as a function of concentration tend to mirror each other, a potential artefact of the two-parameter fit employed. However, as the internal calibration methodology plots a separate, independent calibration curve for each sample, the actual values of α and log$K$ should not matter, albeit at the expense of any physical insight these parameters might have provided. Notably, these changes in do not appear to affect the reliability of the molecular weight estimation, with R^2 values > 0.9 obtained for every sample tested. Sample densities and viscosities were also measured for these samples. These behaved as expected, with broadly linear changes with composition. Diffusion coefficients were observed to increase

with decreasing viscosity, again as expected, and there was no clear relationship between the measured diffusion coefficients and the sample densities. Solvent identity played more of a role in the reliability of the techniques. R^2 was observed to fall markedly for the halogenated compounds and there was a concomitant increase in the observed values of ΔD, so much so that the authors advised against the use of halogenated compounds in these studies.

4.3 Internal Calibration with Nuclei Other Than ^1H

While the high abundance and gyromagnetic ratio of the proton ensure adequate signal-to-noise ratio for most diffusion applications, it has already been shown that ^{1}H DOSY can suffer greatly from overlapping resonances in the chemical shift dimension. With a relatively narrow frequency range and splitting of peaks due to near-ubiquitous homonuclear coupling, the addition of a number of internal references will crowd the spectrum further and increase the possibility of resonances overlapping. When two peaks overlap, normal diffusion processing methods struggle, and fail to provide a reliable diffusion coefficient for either signal. In order to avoid this, a range of internal calibration methods using nuclei other than ^{1}H has been developed. In every case, the aim is to produce a sparser NMR spectrum, with fewer overlapping signals, and better resolution of the peaks of interest. Before moving on to wider applications of the internal calibration method, these methods will be briefly summarised. Analysis of organometallic compounds, such as alkyllithiums, often uses a range of different nuclei to probe the chemical structure. This section identifies the nuclei used and any special experimental considerations needed. Specific applications and examples will follow in Section 4.4.

4.3.1 ^{13}C

The major advantages of using ^{13}C diffusion NMR are better resolution, a wider chemical shift range (extending to over 200 ppm), and the absence of any homonuclear coupling in natural abundance samples. A proton-decoupled experiment will produce only a single peak in the NMR spectrum for each distinct carbon atom in the sample. These advantages come at a cost. A low natural abundance, 1.1 %, a low gyromagnetic ratio, *ca*. 25 % that of ^{1}H, and long relaxation times conspire to make most ^{13}C diffusion experiments prohibitively long in duration if sufficient signal-to-noise is to be obtained. A further problem is that the Stejskal-Tanner equation (Eq. (4)) contains a γ^2 term in the exponent. To achieve an equivalent amount of diffusion encoding, the gradient pulses would need to be proportionally stronger or their durations longer. Concatenation with a polarisation transfer experiment is one solution, albeit at the expense of losing quaternary signals. Both refocused INEPT- and DEPT-based DOSY experiments have been devised. In these experiments, it is the proton magnetisation that is spatially encoded by pulsed field gradients, and subsequent transfer to the ^{13}C nuclei produces diffusion-encoded carbon spectra [136]. The use of the INEPT sequence increases the signal-to-noise according to the ratio of the gyromagnetic ratios of the nuclei involved, 4 in the case of ^{13}C and ^{1}H. In the absence of significant *J* modulation, a spin echo can be used to introduce the required diffusion-encoding gradient pulses. The two-fold increase in signal-to-noise compared to a stimulated echo results in improved resolution in the diffusion dimension in the final 2D DOSY spectrum [137].

The combination of the internal calibration method for estimating molecular weight and ^{13}C INEPT-DOSY was first demonstrated in a confirmation of the aggregation state of lithium diisopropylamide (LDA) in THF [138]. This non-nucleophilic Brønsted base [139] has found wide use in organic synthesis, but its polymeric solid state structure was only determined in 1991 [140] and, while its solid-state structure and aggregation are well established having been determined by X-ray crystallography [141], its solution state

structure is highly dependent on both solvent and temperature. However, LDA is known to exist in a single form in THF: a di-solvated dimer $LDA_2.THF_2$. The internal references chosen for this proof of principle were 1-octadecene (MW = 252.3 g mol^{-1}), *cis*-cyclododecene (MW = 166.3 g mol^{-1}), *trans*-cyclododecene (MW = 166.3 g mol^{-1}), and benzene (MW = 78.1 g mol^{-1}). Ethylbenzene (MW = 106.2 g mol^{-1}) was also present as an impurity in the LDA-THF solution. The 2-dimensional DOSY presentation of the data (Fig. 7(a)) allows for the extraction of one-dimensional spectral slices for each resolved component in the DOSY spectrum, showing the spectrum of a component at a given diffusion coefficient. This slice contains the complete spectral shift information of that component, aids assignment of all the signals of all components, and allows for the comparison of the identified components with spectra obtained from pure samples, as in Fig. 7(b). While this presentation of the data is certainly possible in the ^{1}H DOSY experiments, the sparser ^{13}C spectrum allows for the retrieval of clean sub-spectra with all chemical shift information intact. Fig. 7(b) shows that the INEPT spectral slices extracted from the 2D INEPT DOSY experiment resolve all the chemical shift information of all the components in the sample. In particular, the ^{13}C signals of the oxygen-attached carbons in THF and the LDA methane carbons were present in the same slice, confirming that they are present in a single associated species. Also of note was the observation that the isomers of cyclododecene were resolved in the DOSY spectrum. Individual INEPT spectra of the two isomers could be retrieved. ^{13}C INEPT-DOSY has also been used to characterise chiral mixed trimeric lithium complexes [133].

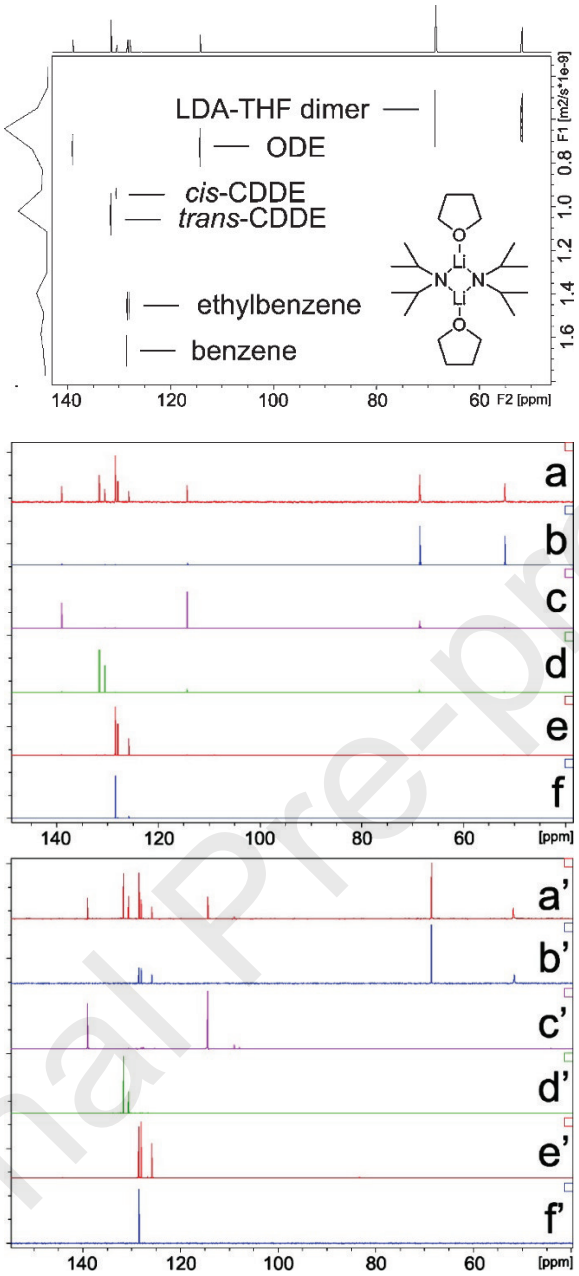

Figure 7: (a) ^{13}C INEPT DOSY spectrum of THF-solvated LDA dimeric aggregate in toluene-d8 with internal references at 298 K (top). (b) Comparison between slices of ^{13}C INEPT DOSY spectra (a-f) with ^{13}C INEPT NMR spectra of authentic samples (a'-f'). (a) and (a'): (b) LDA dimer with internal references, (b) and (b'): LDA dimer without internal references, (c) and (c'): ODE, (d) and (d'): *cis*- and *trans*-CDDE mixture, (e) and (e'): ethylbenzene, (f) and (f'): benzene (lower). All data acquired on a Bruker DRX 400 MHz

spectrometer. Reproduced with permission from Li et al., *Acc. Chem. Res.*, **42** (2009) 270-280. Copyright (2009) American Chemical Society.

The use of polarisation transfer sequences also allows for spectral editing of ^{13}C spectra. The refocused INEPT sequence contains two pairs of delays, the latter of which can be altered to edit the acquired spectrum according to the multiplicities of the carbons present. By defining an angle, $\theta = 180J\Delta_2$, the expected intensities of signals with different numbers of protons attached can be calculated as functions of this angle. A delay, Δ_2, corresponding to $\theta = 45°$ produces all responses, while one corresponding to $\theta = 135°$ will invert methylene groups relative to methyl and methine. The closely-related DEPT experiment allows for similar editing, through the modification of the flip angle of the third proton RF pulse. Indeed, the same results as INEPT are obtained, with an angle of 45° producing a spectrum with all non-quaternary carbons positive, and an angle of 135° inverting the methylene signals. As the editing is achieved by manipulation of a pulse flip angle in DEPT, it is more robust with respect to differences in one-bond coupling constant. In turn, this means that the editing efficiency of DEPT tends to be superior to that of INEPT when a range of *J* values is encountered, as it is in most cases. While INEPT- and DEPT-based sequences have been used in diffusion NMR experiments, the use of edited spectra has not yet been reported but may prove to be a useful complement to the existing pulse sequences and methodologies.

It is also possible to reduce experiment times by increasing the abundance of ^{13}C in the samples [142]. While it is possible to use commercially available ^{13}C-labelled internal references, a set of internal references can be synthesised using relatively inexpensive ^{13}C-labelled iodomethane. While the criteria for internal molecular weight references remain the same, the set of compounds previously used as internal references in ^{13}C diffusion NMR experiments, barring benzene, becomes less useful as they are neither readily available with

^{13}C enrichment nor are easy to synthesise or modify with ^{13}C labelled groups. Therefore, in addition to benzene-$^{13}C_6$, a set of internally labelled references was synthesised by Su et al. 2-methoxy-2-methyloctane-$^{13}C_1$ was synthesised from octan-2-one, reacted first with the ^{13}C labelled Grignard reagent $^{13}CH_3MgI$, and then methylated to form the methoxy ether (MW = 159.3 g mol^{-1}). A second labelled ether was synthesised, albeit with a C_{23} backbone. In this compound, the methoxy-ether was ^{13}C labelled by methylation of a tertiary alcohol (MW = 369.7 g mol^{-1}). The set of labelled references was completed by heptadec-2-ene, synthesised by terminally labelling hexadec-1-yne with $^{13}CH_3$, followed by partial hydrogenation (MW = 239.4 g mol^{-1}). As two of the species used were ethers, the possibility of them coordinating with the lithium aggregates typically studied had to be ruled out. Any association of the compounds would lead to a reduction in the measured diffusion coefficient, rendering any log$D$-logMW correlation using these compounds meaningless. The concentration of these ethereal, ^{13}C-labeled internal references is many orders of magnitude less than the ethereal solvent used in the NMR samples. Additionally, these ethers are sterically hindered, especially compared to the solvent. It was therefore assumed that the reference ethers did not coordinate with the complexes significantly in either diethyl ether or THF.

To illustrate the use of isotopically labelled compounds, *N*-Boc-piperidine was synthesised, with a ^{13}C label present in the *t*-butyl group. All species gave resolved signals in the DOSY spectrum produced, and a log$D$-logMW plot was generated from the four internal references. From the internal calibration curve, the formula weight of labeled *N*-Boc-piperidine was deduced to be 179 g mol^{-1}, within 5 % of the actual formula weight of 186 g mol^{-1}. In spite of this promising early validation work, the set of internal references was revisited. The C_{23}-ether tended to precipitate out of diethyl ether solution at temperatures approaching 273 K, making it unsuitable for the variable temperature work typically required for organolithium studies. A squalene derivative containing a ^{13}C-labelled methoxy group (

MW = 443.8 g mol^{-1}) was typically used instead, with little change to the quality of the internal calibration curve. With the ^{13}C-labelled internal calibration method validated, it was used to investigate a number of organolithium systems. First, the aggregation state of methyllithium (MeLi) dissolved in diethyl ether, with and without the presence of several tertiary diamine ligands, was determined. MeLi is observed to exist as a tetramer in diethyl ether. As the content of LiI is increased, a range of other structures form, with iodine atoms incorporated into the structures. Two separate peaks were observed in the ^{13}C spectrum. For the peak assigned as $(MeLi)_4$, the internal calibration method gave a molecular weight of 407 g mol^{-1}, suggesting a tetrameric species with diethyl ether coordinating to each Li on the vertices of the cube. The method failed for the proposed $(MeLi)_3(LiI)$ mixed species, perhaps a result of the increased density of the incorporated iodine atom. The successful characterisation of complexes incorporating N,N,N′,N′-tetramethylethylenediamine, racemic N,N,N′,N′-tetramethyl-1,2-diaminocyclohexane, N,N′-dimethylbispidine, N,N,N′,N′,N″-pentamethyldiethylenetriamine and (−)-sparteine were also reported [139]. Of note was spectral evidence for the presence of minor amounts of mixed dimeric complexes consisting of one equivalent of MeLi and one equivalent of LiI in the presence of both N,N,N′,N′-tetramethyl-1,2-diaminocyclohexane and N,N′-dimethylbispidine.

4.3.2 ^{2}H

The cost and effort of introducing ^{13}C labels into most organic compounds makes the approach detailed in Section 4.3.1 expensive and impractical. It is both cheaper and easier to label organic compounds with ^{2}H rather than ^{13}C. ^{2}H is fundamentally different to ^{1}H and ^{13}C in that it has a nuclear spin quantum number of 1. Nuclei with I > ½ possess a nuclear quadrupole moment in addition to their nuclear magnetic moment. While this can cause complications with 1D spectra, with broader peaks and hence lower sensitivity, the major

problem in diffusion experiments is the effects of the quadropolar moment on the relaxation of the spins. Quadropolar relaxation depends on a number of parameters, such as any local electric field gradients and the rotational correlation time of the species. The latter depends on tumbling rate, which depends on the experimental conditions. NMR spectra acquired at lower temperatures show longer correlation times, shorter relaxation times, and broader peaks. All diffusion experiments contain a delay during which the molecules in the sample diffuse through solution. If this delay is too long, longitudinal relaxation will return all of the magnetisation back to equilibrium before the end of the delay, and render the experiment useless. A further practical limitation of the use of ^{2}H NMR in these studies is therefore that the diffusion experiment delay time (Δ) must be shorter than or comparable to T_1 for all peaks of interest. This does lead to some constraints on the diffusion NMR methodology. It was suggested that the T_1 times for all ^{2}H signals utilized for molecular weight estimated should be longer than 50 ms and that the experimental temperature should not be lower than 253 K. For most small molecules, and solvents such as H_2O and D_2O, diffusion coefficients are measured at ambient temperatures. This is often not the case for organometallics, which can be studied at temperatures far below 273 K. For larger molecules, the longer rotational correlation times may necessitate experiments at temperatures at ambient temperature or higher [143].

Correlation of diffusion coefficients with molecular weights requires that the compounds compared all have similar densities. For atoms in the first period of the periodic table, this is usually the case. A deuteron is the same size as a proton but has twice the mass. The more deuterium nuclei are introduced into a molecule, the greater its density will be. For a given organic compound containing C, H, N and O only, the proton nuclei may well be the most numerous in the molecule but will contribute only a small percentage of the compound MW. In order to test the effect of perdeuteriation on any possible log$D$-logMW correlation,

the diffusion coefficients of four commercially available perdeuteriated compounds (acetone-d_6, ethylbenzene-d_{10}, chrysene-d_{12}, acenaphthene-d_{10}) and a synthetically produced methyl-d_3 oleate ester were measured. The plot of log$D$ against logMW gave a straight line for four of the compounds, with $\alpha = 0.61$, with only chrysene-d_{12} being an outlier. Given the flat shape of chrysene and the role shape plays in diffusion coefficients, this was perhaps not an unexpected finding. Using a mixture of both partially and perdeuteriated compounds, ^{2}H DOSY successfully estimated the molecular weight of lithium diisopropyl amide, known to exist as a di-solvated dimer in THF. In 10:1 excess of THF, the MW of the species in solution was estimated to within 5 % [143].

Synthetic deuterium labelling can be an arduous and expensive process. The most efficient and convenient method of deuterium labelling is exchange of labile protons with solvent deuterons. This is used in amides so as to obtain information about the local structure and dynamics of proteins. To test whether this labelling strategy could be used as part of a MW estimation experiment, the MW of acetanilide was first estimated, in the presence of small amount of D_2O, using ^{1}H DOSY and the ^{1}H NMR references benzene, cyclooctene, 1-tetradecene and squalene. While the MW found in aqueous solution was higher than the expected molecular weight of the species, a discrepancy attributed to solvation and aggregation, a ^{2}H DOSY experiment in similar conditions reproduced the measurement to within 10 %, suggesting that in-situ labelling of exchangeable groups could be a strategy for determining MW [140]. As the MW estimation previously proved robust to the amount of deuteriation in the reference compounds, it would not necessarily be required to know the number of exchangeable protons in the analyte molecule in advance. However great caution should be exercised when using diffusion measurements on exchangeable hydrogens, because of the risk of chemical exchange with water leading to faster average diffusion [21].

4.3.3 ^{6}Li

As noted previously, one of the most common applications of the internal calibration method has been in organometallic chemistry, particularly organolithium chemistry. While the initial diffusion NMR studies used the protons present in the complexes, lithium has two magnetically active isotopes, ^{6}Li and ^{7}Li. 92.4 % of lithium is ^{7}Li, but it is spin-3/2, with very short relaxation times. The remaining 7.6 % is ^{6}Li, a spin-1 nucleus but with only a small nuclear quadropole moment, allowing for the acquisition of sharp lines, particularly when the Li is in a symmetrical environment. It is therefore possible to use ^{6}Li in diffusion NMR studies of organometallics, with rapid and unambiguous assignment of peaks in the NMR spectrum, and the diffusion information giving access to aggregation and solvation state. It is also possible to synthesise ^{6}Li-enriched compounds, removing one of the drawbacks of the technique. While both ^{6}Li NMR and ^{6}Li-^{15}N heteronuclear multiple-quantum coherence (HMQC) studies of chiral amide bases give evidence of chemical structures [144], they do not easily address the degree of aggregation. Several possible complexes with different degrees of aggregation can exist that are consistent with these experimental NMR results. Studies of compounds using ^{6}Li NMR have therefore made use of multinuclear, multidimensional techniques, such as ^{6}Li heteronuclear Overhauser effect spectroscopy (HOESY) [145] and ^{1}H-^{6}Li heteronuclear multiple bond correlation spectroscopy (HMBC) [144], to bridge the highly resolved ^{6}Li NMR data to the ^{1}H DOSY experiments from which the log$D$-logMW correlation is obtained.

Well-resolved peaks in the ^{6}Li spectra are indirectly assigned to diffusion coefficients obtained from ^{1}H DOSY, while well-established references present in the sample provide the internal calibration curve. Fig. 8 shows this approach applied to a mixed chiral lithium complex that contains three Li atoms. The structure of the complex is shown in an insert in Fig. 8(a), along with the ^{6}Li DOSY spectrum. Two distinct peaks, in an approximate 2:1

ratio, are observed. The correlations of the two lithium atoms to the two different ligands in the complex are revealed by the $^{6}Li\{^{1}H\}$ HOESY spectrum (Fig. 8(b)). Finally, the ^{1}H DOSY spectrum of the internal references, which have well-resolved peaks away from the signals produced by the two ligands, can be used to produce a log*D*-log *MW* calibration curve, from which the molecular weight of the complex can be estimated [146]. Such combined $^{1}H/^{6}Li$ NMR strategies will be discussed further in Section 4.4.

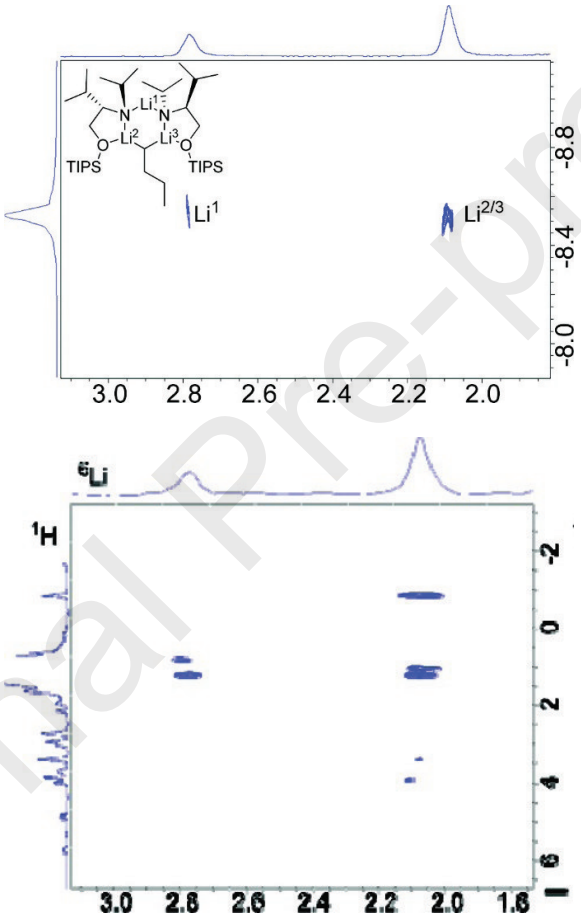

Figure 8: (a) ^{6}Li DOSY spectra of a mixed lithium complex, shown as inset, in toluene-d_8 (upper). (b) $^{6}Li\{^{1}H\}$ HOESY spectra of the same mixed lithium complex in toluene-d_8 (lower). All data acquired on a Bruker DRX 400 MHz spectrometer. Reproduced with permission from Kagan et al., *Org. Lett.*, **12** (2010) 520-523. Copyright (2010) American Chemical Society.

It is also possible to perform ^{7}Li DOSY experiments, despite its unfavourable relaxation times and quadrupole moment. While no formal report of the methodology required appears to have been published, ^{7}Li DOSY was used in the first study of *n*-BuLi, and the measured diffusion coefficients were consistent with those acquired by ^{1}H NMR. ^{7}Li DOSY experiments have also been reported in studies of mixed-lithium-zinc complexes [147]. Combined with, for example, the use of ^{7}Li residual quadrupolar couplings [148] and analysis of the ^{2}J(Li-Li) coupling, and its variable temperature behaviour, between ^{7}Li atoms [149], there is plenty of scope for the development and wider use of ^{7}Li techniques in the study of small molecules and organolithium compounds.

Where ^{7}Li NMR has found notable recent use is in the characterisation of lithium-ion battery electrolytes. A recent combined ^{1}H and ^{7}Li DOSY study of electrolyte solutions has determined the solvation state of the component ethyl methyl carbonate in the absence and in the presence of $LiPF_6$ [150], as well as characterised common electrolyte solvents according to their solvating ability [151, 152]. While described as internally referenced studies, only a single reference, toluene, is used to control for viscosity effects on the acquired diffusion coefficients) There is clear potential for wider use of combined multinuclear diffusion NMR studies in this field in this area in order to better understand the relationships between lithium-ion battery performance and the diffusion behaviour of the species involved [153].

4.3.4 ^{19}F

Like ^{1}H NMR, ^{19}F NMR uses a spin-1/2 nucleus that is 100 % abundant. A typical ^{19}F spectrum consists of sharp peaks spanning a very wide range of chemical shifts. The nucleus exhibits a high sensitivity of its chemical shift to local environment, meaning that the likely lack of overlap of signals makes ^{19}F DOSY a potentially useful experimental tool for systems with fluorine atoms already present. While its gyromagnetic ratio is marginally lower than

that of ^{1}H nuclei, it is still almost 4 times greater than that of ^{13}C, allowing for efficient diffusion encoding of signals.

Chiral Brønsted acids, particularly phosphoric acids, have been shown to act as powerful asymmetric catalysts in a number of organic transformations. Key to effective enantiosynthesis is close proximity between a chiral element of the catalyst and the reaction site. Many Brønsted acid catalysts, such as chiral *N*-triflylphosphoramides, contain fluorine atoms, as do several Lewis acid counterions such as BF_4^-, $(CF_3SO_2)_2N^-$, and PF_6^-. Many of the substrates that are used in catalytic reactions also contain fluorine atoms. Dual labelling, with fluorine atoms present in both acid and substrate, should also be possible as many of the substrates used in the catalytic reactions also contain fluorine atoms. DOSY spectra of dual labelled systems will help in the understanding of the ion pairs, complexes and aggregates formed between Brønsted acids and their basic substrates. If extensive complexation occurs, with slow exchange, then fluorine signals associated with both substrate and acid will show similar, if not the same, diffusion rates. The internal standards chosen were trifluoromethylbenzene (MW = 146 g mol^{-1}), 1,4-bis(trifluoromethyl)benzene (MW = 214 g mol^{-1}) and 1,3,5-tris(trifluoromethyl)benzene (MW = 282 g mol^{-1}). The method was used to infer the molecular weights of three test compounds, all Brønsted acids, to within 5 % accuracy [154].

With a proof of concept obtained, the method was then applied to a Brønsted acid-basic substrate system using TFA and a trifluoromethyl-labelled acylimidazole. A ^{19}F DOSY spectrum of the system showed that the diffusion coefficient of the TFA fell below that of the three standards, to the same as the acylimidazole. This is strong evidence for complexation and aggregation. Using the internal calibration method, the MW of the acid was estimated at 343 g mol^{-1}, close to the expected mass of a 1:1 complex. The analysis was repeated using two stronger Brønsted acids, bis(trifluoromethane)sulfonimide and trifluoromethanesulfonic,

or triflic, acid. When diffusion data could be acquired, the internal calibration method indicated a range of 1:1 and 2:2 complexes between Brønsted acids and the basic substrates. It is also possible to use singly labelled systems, with diffusion coefficients of ^{19}F-labelled acylimidazole acquired in the presence of phosphoric acid. While additional spectral information concerning the acid's diffusion coefficient is lost, the MW deduction proved robust and suggested a 1:1 complex between the Brønsted acid and substrate base. This methodology has subsequently been successfully used in a number of fields, particularly by Day and Weaver to help confirm their successful synthesis of 2,3,5,6-tetrafluoro-4-(nitromethyl)pyridine [155] and by Yousefi et al. to confirm the stoichiometry of complexes formed during carbon dioxide capture/cyclization reactions performed using chiral Brønsted acid catalysts [156].

There have been a number of recent advances in the field of ^{19}F NMR that should aid in its wider usage. The wide chemical shift range, while useful in terms of assuring a sparse NMR spectrum, cannot all be uniformly excited at any one time. Off-resonance effects lead to anomalies even when only a narrow range of the spectrum is being studied. Very- and ultra-broadband techniques using swept-frequency "chirp" pulses have recently been developed to overcome these issues [157, 158]. Even if only a small region of the chemical shift range is being studied, the large ^{19}F-^{19}F couplings, of up to 200 Hz, can lead to *J*-modulation of multiplets even when short delay periods are used, resulting in negative signals in the spectra acquired and artefacts in DOSY spectra. The Oneshot-45 sequence, a Oneshot diffusion NMR sequence extended by a 45° RF pulse, has proved robust enough to remove the influence of *J*-modulation from such spectra [159].

4.3.5 ^{31}P

Phosphorus-containing ligands, such as phosphines and phosphine oxides, are widely used in organometallic chemistry. The 100 % abundant isotope, ^{31}P, is spin-1/2, making it a good choice for NMR analysis. While the gyromagnetic ratio is not as high as that for ^{1}H, it is still higher than that of ^{13}C, so acquisition of spectra, and diffusion NMR data, is relatively rapid. With relatively sharp, well-resolved peaks and a very wide chemical shift range, ^{31}P DOSY also avoids the severe overlap often observed in ^{1}H DOSY. Proof of principle experiments were performed using dimethylphenylphosphine (MW = 138.15 g mol^{-1}), triphenylphosphine (MW = 262.29 g mol^{-1}), and tri-*n*-octylphosphine (MW = 370.64 g mol^{-1}) as internal references, and hexamethylphosphoramide (HMPA) as a test analyte. All four components had well-resolved peaks in the chemical shift dimension, and correspondingly well-resolved peaks in the diffusion dimension of the resulting DOSY spectrum. A linear log$D$-logMW plot was produced from the acquired diffusion coefficients, with values for α and log$K$ of 0.7246 and –8.0263 respectively. This method successfully gave the MW of the test analyte, 179.2 g mol^{-1}, to within a percentage point [160]. When trying to characterise the complex formed by lithium hexamethyldisilazide (LiHMDS) and HMPA, only a single HMPA peak was observed in the ^{31}P spectrum, coincident with the chemical shift of free HMPA in solution. However, the diffusion coefficient of HMPA in this sample was notably lower than that observed for the free compound, indicating that HMPA remains complexed with LiHMDS in solution. Integration of the ^{1}H signals of the two species indicated a 1:1 stoichiometry and the MW estimated from the diffusion coefficient, 598 g mol^{-1}, was consistent with a [(LiHMDS)•(HMPA)]$_2$ complex. The coincident chemical shifts suggest binding between the oxygen of the phosphorus compound and the lithium complex [160].

Further complications were soon noticed in the study of manganese complexes, as phosphorus-containing ligands, such as phosphines, have a strong tendency to bind to metals. The ^{31}P spectra of phosphine oxides were observed to broaden and overlap when the latter

were added to a sample containing a manganese complex containing phosphine ligands. In order to ensure absolutely no interactions between the internal references and the compounds being studied, it proved necessary to physically separate the references from the rest of the sample. This can be achieved, for example, by the inclusion of glass capillaries within a standard 5 mm NMR tube. While diffusion coefficients do depend strongly on sample temperature and viscosity, it can reasonably be expected that the sample temperatures in both tubes will be the same and that, if low concentrations of material are used, then the viscosities in a capillary and in the main sample will also be the same. A ^{31}P DOSY spectrum resolved the three phosphine oxide internal references, trimethyl phosphate (MW = 137 g mol^{-1}), triphenylphosphine oxide (MW = 297 g mol^{-1}) and tri(*n*-octyl)phosphine oxide (MW = 370 g mol^{-1}), and a suitable log$D$-logMW calibration curve was generated. Three manganese complexes, all containing phosphorus ligands, were successfully characterised to within 8 % of their molecular weights. The physical separation of references is therefore a powerful supplementary methodology for systems where interactions between references may be difficult to avoid [161].

4.4 Internal Calibration – Examples and Applications

An important area in which DOSY, and the internal calibration method in particular, has been used to characterise composition, solvation and aggregation state is organolithium chemistry. The aggregation states of organolithium compounds in solution remain one of the fundamental unknowns of the area [162]. Access to both aggregation state and solvation degree helps in understanding and controlling their reactivity as bases or nucleophiles. Solid state measurements do not necessarily reflect the solution state structure, and any structures formed are likely to be highly temperature- and solvent- dependent. While X-ray crystallography remains the most widely used method for solid-state structure determination,

there will always be questions concerning how a material behaves in solution. Does the structure change? Is there any exchange between different structures? Does the compound form several species in solution, of which the solid-state characterisation only represents one, if that? Reactive intermediates stretch this issue further. As the name suggests, they tend only to form for a relatively short period of time. Analysis of the X-ray crystal structures of many organolithium compounds showed that they typically have similar densities (~ 1.0 g cm^{-3}) and approximately spherical structures. This markedly simplifies the use of the Stokes-Einstein equation, and allows for a general logarithmic relationship between D and MW.

The first demonstration of diffusion NMR in organolithium chemistry was the identification of both dimeric and tetrameric structures in THF-solvated *n*-BuLi [163]. While, strictly, this is not a demonstration of a power law related method, it is a good demonstration of the general utility of diffusion NMR methods. Theoretical values for the diffusion coefficients were calculated on the basis of both gas-phase and crystal structures. These predicted a difference of *ca.* 10 % between the tetramer and dimer, a small difference but a measurable one. ^{1}H NMR spectra of 0.2 M *n*-BuLi in THF-d_8 were acquired at 189 K. Resonances assigned to α-CH_2 groups could be identified at –1.00 and –1.22 ppm. The DOSY spectrum of the sample resolved these peaks, with the dimeric species moving with a greater diffusion coefficient (10.1×10^{-10} m^2 s^{-1}) than the tetrameric (8.83×10^{-10} m^2 s^{-1}). It was also possible partially to resolve the β- and γ- CH_2 signals at 1.5 ppm although, as expected, peaks not resolved in the NMR spectrum (i.e. -CH_3 groups at *ca.* 1.0 ppm) were not resolved in the diffusion dimension. While the ^{7}Li spectrum showed two distinct peaks, ^{7}Li DOSY failed, in this report, to reproduce the signals of the dimeric species.

The combined use of ^{6}Li and ^{1}H NMR allows unambiguous assignment of resonances to specific species and aggregates in *n*-BuLi systems. *n*-Bu^{6}Li was synthesised from ^{6}Li metal, artificially increasing the abundance of the required isotope. Using squalene,

cyclooctene and benzene as internal references, two aggregates, with different chemical shifts and diffusion coefficients, were identified in both ^{1}H DOSY and ^{6}Li DOSY experiments. A ^{6}Li{^{1}H} HOESY experiment showed cross-peaks from the upfield *n*-Bu^{6}Li peak in the 1D ^{1}H NMR to the upfield *n*-Bu^{6}Li peak in the 1D ^{6}Li NMR, and also from the downfield *n*-Bu^{6}Li peak in the 1D ^{1}H NMR to the downfield *n*-Bu^{6}Li peak in the 1D ^{6}Li NMR, confirming that the peaks had been assigned correctly. Molecular weight estimations were attempted, which confirmed the presence of a tetrasolvated dimer, a tetramer, and also the presence of free THF [164]. The combined ^{1}H/^{6}Li approach was also applied to LiHMDS, where the observed diffusion coefficient indicated the presence of an unsolvated dimer in toluene-d_8 [146], and provided evidence from NMR that isopropyllithium (*i*PrLi) forms a 1:2 monomer-dimer mixture in THF-d_8 [165].

The typically broad multiplets found in ^{1}H NMR lead to extensive overlapping of component spectra in a mixture, even at the highest fields. Pure shift ^{1}H NMR seeks to replicate the resolution of ^{13}C NMR, by suppressing the effects of homonuclear coupling, and collapsing multiplets into singlets [166-169]. A pure shift spectrum consists of a single peak for each chemically distinct site, effectively increasing the resolution of the signals by almost an order of magnitude. The deleterious effects of signal overlap on DOSY spectra have already been discussed. Pure shift DOSY techniques have been developed as a response to this problem [170, 171]. The increase in resolution achieved by pure shift acquisition means that individual peaks in the ^{1}H spectrum now do not overlap even with very near neighbours, and well-resolved peaks are produced in the DOSY spectrum. These more advanced NMR methods revealed additional information about the complex aggregates formed by a mixed *n*-BuLi/*n*-BuOH system. Even in the first reports of NMR studies of the *n*-BuLi equilibrium, an unidentified signal was observed at *ca*. 0.8 ppm. This signal was found to depend on trace concentrations of oxygen, leading to a tentative assignment to a butoxide or butylperoxide

species. Addition of *n*-BuOH increased the intensity of this peak, confirming the initial assignment, but introduced additional peaks into the spectrum. The region of the spectrum corresponding to α-CH_2 peaks rapidly became too crowded to interpret. These changes in the NMR spectra correspond to the successive replacement of alkyl groups by alkoxy groups in the tetrameric *n*-BuLi structure. The degree of solvation and the aggregation states of the compounds eluded analysis by standard ^{1}H methods. First, the ^{1}H pure shift (PS-)DOSY spectrum of LDA and *n*-BuLi in THF-d_8 using three internal references (squalene, triphenylbenzene and cyclododecene) was acquired. This experiment confirmed that LDA is present in solution as a series of di-solvated LDA dimers. The ^{1}H PS-DOSY spectrum of *n*-BuLi/*n*-BuOLi in THF-d_8 using four internal references (squalene, triphenylbenzene, cyclododecene and LDA) showed efficient separation of eight components that could be clearly identified in the proton dimension. The corresponding peaks in the DOSY spectrum were also well resolved. The DOSY spectrum suggested the presence of a number of lithium species, both homogeneous and mixed. The internal references were used to generate a calibration curve, allowing estimates of molecular weight for all four species. This data suggested the presence of a tetrasolvated mixed tetramer (*n*-BuLi)$_2$/(*n*-BuOLi)$_2$•THF_4 (MW = 589 g mol^{-1}), a tetrasolvated homogeneous tetramer (*n*-BuLi)$_4$•THF_4 (MW = 534 g mol^{-1}), a disolvated homogeneous dimer (LDA)$_2$•THF_2 (MW = 312 g mol^{-1}) and a disolvated mixed dimer (LDA/*n*-BuLi) •THF_2 (MW = 300 g mol^{-1}). Overlap still hindered the analysis of the full ^{1}H spectrum. A third experiment, this time without added LDA, was used to identify two further species in this region. Molecular weight estimates suggested that these were a tetra-solvated mixed tetramer (*n*-BuLi)$_3$/(*n*-BuOLi)$_1$•THF_4 (MW = 579 g mol^{-1}) and tetra-solvated homogeneous dimer (*n*-BuLi)$_2$•THF_4 (MW = 490 g mol^{-1}). This analysis is consistent with known organolithium chemistry: LDA forms dimers, while cubic aggregates of the *n*-Bu and *n*-BuO species are also observed, in which case, lithium atoms are all monosolvated [172].

Other organolithium complexes characterised using an internal calibration method include chiral enolate aggregates [173], THF-solvated 1,4-dienolates [174], 2,2,6,6-tetramethylpiperidides [175, 176], pinacolone enolate [177], aryl and alkyl gem-dilithium phosphido-boranes [178], chiral lithium amides derived from valinol derivatives [179, 180], N-isopropyl alaninol [181] and *S*-valine [182], as well as the identification of hexameric and octameric *sec*-butyllithium/*sec*-butoxide mixed aggregates [183]. Such studies are not limited to single metal complexes. Because they easily form mixed aggregates with other organometallic species, lithium halides are known to exert a significant influence on the behavior of organometallic reagents, affecting both the reactivity and the selectivity. In the case of MeLi, known to form a tetrameric species in solution, the effects of the addition of LiCl were studied using a combination of combined ^{1}H and ^{7}Li variable temperature NMR spectroscopy on monolabeled and doubly labelled $^{13}CH_3{}^{6}Li$, quantum mechanical calculations and diffusion NMR. Results indicated the formation of a single heterodimeric species, trisolvated in THF [184]. A related area in which internal calibration methods have been widely used is the field of Grignard (RMgX) [185] and turbo-Grignard (RMgCl·LiCl) [186] reagents. Mixed metal species such as Grignard reagents and mixed lithium-cadmium compounds have also been characterised through their diffusion coefficients in solution, with molecular weights deduced by the internal calibration method [187, 188]. Further discussion of diffusion NMR-based molecular weight characterisation of these, and related, organometallic compounds will be found in Section 4.6.

Thus far, the use of diffusion NMR has only confirmed the aggregation state and estimated the likely numbers of solvent molecules coordinated. Diffusion NMR also allows access to the binding constants, K_a, of the aggregation process. Such experiments are common in supramolecular chemistry [4], where there is a significant difference in diffusion coefficients between the large, supramolecular, host molecule and the smaller guest

molecules. This can also be the case for higher-order aggregates of organolithium complexes. While a titration experiment monitored by chemical shift will access very similar information, diffusion coefficients are used because they are less sensitive to the presence of impurities than are chemical shifts. LiHMDS was chosen for a preliminary study [189]. It forms an unsolvated dimer in toluene-d_8 in the absence of any additional ligands, while the addition of even a small amount of an ethereal ligand leads to the formation of a range of solvated $(LiHMDS)_n$ aggregates. Binding constants can be estimated by titrating LiHMDS to a fixed concentration of ethereal ligand L and observing the change in diffusion coefficient of the ligand. A general equilibrium binding constant, K_a, between a LiHMDS molecule and ligand, L, to form a LiHMDS-ligand complex can be expressed by Eq. (16)

$$a[\mathrm{LiHMDS}] + b[\mathrm{L}] \rightleftharpoons c[\mathrm{LiHMDS}_a{\bullet}\mathrm{L}_b]$$

$$K_a = \frac{[\mathrm{LiHMDS}_a{\bullet}\mathrm{L}_b]^c}{[\mathrm{LiHMDS}]^a[\mathrm{L}]^b} \tag{16}$$

where $[\mathrm{LiHMDS}_a{\bullet}\mathrm{L}_b]$ represents the LiHMDS−ligand complex, [LiHMDS] is the concentration of free LiHMDS, and [L] is the concentration of free ligand. The likely aggregates were characterised by the use of a series of internal references and logD-log MW calibration curves generated from the acquired diffusion coefficients. Different aggregates were observed for different ligands. LiHMDS solvated by THP, methyl tertiary-butyl ether, or tert-butyl acetate forms a 1:1 complex ($a = b = c = 1$, in Eq. (16)) while LiHMDS solvated by THF or diethyl ether forms a 2:1 complex ($a = c = 1$ & $b = 2$ in Eq. (16)). The appearance of ^{1}H NMR spectra is dependent on both K_a and the rate of ligand exchange. Here, only a single peak is seen for the ligand, suggesting that this system is in the fast exchange regime. Therefore, concentrations of free and bound [L] and [LiHMDS] can be estimated by titrating LiHMDS to a fixed concentration of ethereal ligand L and measuring the diffusion coefficient of the ligand. The observed diffusion coefficient of the ligand peak (D_{obs}) is the weighted

average of bound (D_{complex}) and free (D_{free}) ligands (Eq. (17), sometimes called Lindman's Law [190]), and x_{B}, the fraction of bound ligand, can be calculated from these diffusion data (Eq. (18)).

$$D_{\text{obs}} = x_{\text{B}} D_{\text{complex}} + (1 - x_{\text{B}}) D_{\text{free}} \tag{17}$$

$$x_{\text{B}} = \frac{D_{\text{obs}} - D_{\text{free}}}{D_{\text{complex}} - D_{\text{free}}} \tag{18}$$

For both 1:1 and 2:1 models, K_{a} for the association equilibria can be estimated by determining x_{B} from a series of measured diffusion coefficients and then performing a non-linear fit to Eq. (19)(a) for the 1:1 model and to Eq. (19)(b) for the 2:1 model.

$$x_{\text{B}} = \frac{K_a[\text{LiHMDS}]}{1 + K_a[\text{LiHMDS}]} \tag{19}(a)$$

$$x_{\text{B}} = \frac{2K_{\text{a}}[\text{LiHMDS}]}{1 + 2K_{\text{a}}[\text{LiHMDS}]} \tag{19}(b)$$

Fig. 9 shows the diffusion coefficients of methyl *tert*-butyl ether acquired in a series of titration experiments, where LiHMDS was added to the sample in increasing amounts (Fig. 9(b)), and the calculated fraction of bound ether molecules for each experiment, from which a value of K_{a} was estimated using a non-linear fit of the data to Eq. (19)(a). Using this method, binding constants between LiHMDS and five ligands, THP, methyl *tert*-butyl ether, *tert*-butyl acetate, THF and diethyl ether were estimated. LiHMDS showed a greater affinity for cyclic ligands (THP, $K_{\text{a}} = 8.40 \times 10^2\ \text{M}^{-2}$ and THF, $K_{\text{a}} = 6.39 \times 10^2\ \text{M}^{-2}$) than for non-cyclic (diethyl ether, $K_{\text{a}} = 2.85 \times 10^2\ \text{M}^{-2}$ and methyl *tert*-butyl ether, $K_{\text{a}} = 1.40 \times 10^2\ \text{M}^{-2}$). Both methyl *tert*-butyl ether and *tert*-butyl acetate contain bulky groups. The higher binding constant for *tert*-butyl acetate ($K_{\text{a}} = 12.50 \times 10^2\ \text{M}^{-2}$) can be attributed to the strong coordination between lithium atoms and carbonyl group.

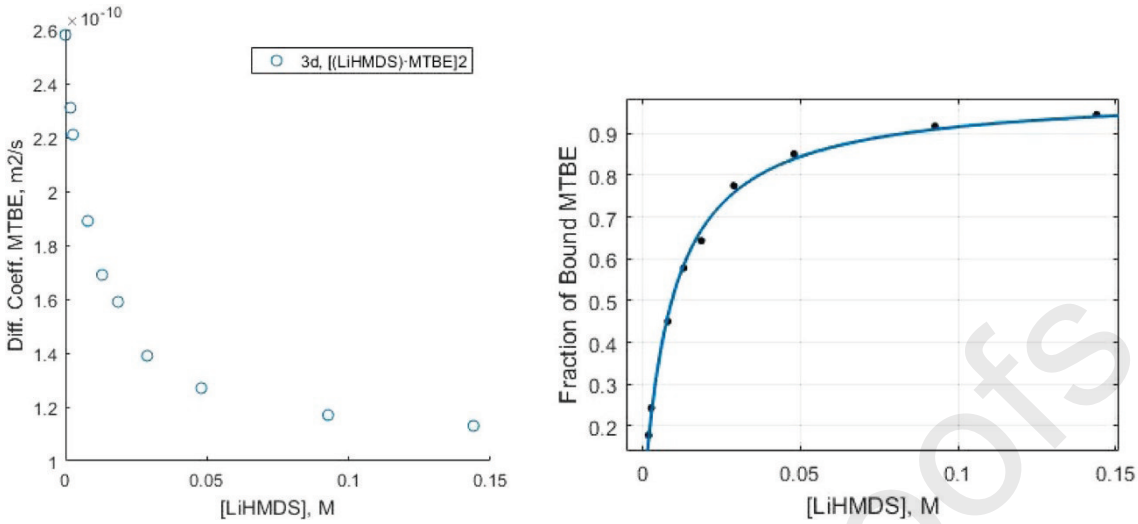

Figure 9: (a) Diffusion coefficients of methyl *tert*-butyl ether acquired in a series of titration experiments with increasing concentration of LiHMDS (left). (b) Fraction of methyl *tert*-butyl ether bound to complex calculated using Eq. (19)(a) for each titration experiment given that $D_{complex}$ is $(1.03 \pm 0.04) \times 10^{-10}$ m^2 s^{-1} and D_{free} is 2.87×10^{-10} m^2 s^{-1}. (right). Reproduced with permission from Tai et al., *Org. Lett.*, **82** (2017) 6223-6231. Copyright (2017) American Chemical Society.

While most of the applications of the internal calibration method demonstrated here are found in organometallic chemistry, the method should find use in any field which can use diffusion NMR methods. Biodiesel is a renewable and biodegradable alternative to petrol, and is derived from the oils and fats of plants and animals [191-193]. Its production relies on the transesterification of a triglyceride to form methyl esters and glycerol, often in the presence of a suitable catalyst [194]. Mono- and di-substituted species are formed as intermediates in the process. Standard 1D ^{1}H analysis of these reaction mixtures is complicated by the severe overlap of signals from similar chain length species. The extent of transesterification will correlate strongly with molecular weight, with a diacylglycerol moving faster than a tri- substituted one and a monoacylglycerol moving faster still. In order

to prove that the methodology could work, the individual ^{1}H spectra of the acylglycerols were examined to identify peaks that could be resolved in a mixture. While relatively close in terms of their chemical shifts, methylene peaks in the triolein (δ = 4.26 ppm), 1,3-dioleoylglycerol (δ = 4.02), 1,2-dioleoylglycerol (δ = 3.78 and 3.49), a methine signal of 1-oleoyl-*rac*-glycerol (δ = 3.64) and a strong methyl signal (δ = 3.35) in the methyloleate product were selected as readily identified signals that would not overlap. Diffusion NMR data of a test mixture containing triolein, 1,3- and 1,2- dioleoylglycerol, 1-oleoyl-*rac*-glycerol, squalene, methyl oleate and benzene, in toluene-d_8, were acquired [195]. As expected from the analysis of the 1D spectra, enough peaks were resolved in the proton dimension to produce a well-resolved DOSY spectrum, with all five species resolved, and diffusion coefficients measured. Squalene and benzene were added to the sample to act as internal references, alongside the triolein starting material. While the method worked well for the ester product and the singly transesterified product, it worked less well for 1-oleoyl-rac-glycerol. This was only analysed via the distinctive multiplet signal of the methine group. The method was further tested on two mixtures produced from transesterification reactions on virgin olive oil and waste cooking oil. Prior to heating with methanol, the samples showed the presence only of triacylglycerols. In both cases, the presence of both methyl ester products and 1,3- substituted products was identified. The identity of the products was confirmed by log$D$-logMW analysis yielding the MW of the products to within 6 % in both samples.

Much of the molecular weight estimation work discussed so far was carried out in non-aqueous solvents, such as tetrahydrofuran. Different sets of internal diffusion references are needed for different solvents. The same requirements for suitable internal references in aqueous solution apply as for organic solutions: the references must span a reasonable range of molecular weights, must have a reasonable spread of chemical shifts, avoiding overlap if

possible, must be soluble, and must not interact with the analyte. The relatively limited range of available functional groups and soluble species compatible with these requirements severely limits the range of possible references. An initial set of references, based on tetraalkylammonium salts, failed as higher molecular weight salts, such as tetrahexylammonium chloride, were found to be barely soluble. The high likelihood of longer-chain salts forming aggregates in solution also limits their potential utility. A second set of compounds, tris-(hydroxymethyl) aminomethane (TRIS, MW = 121 g mol^{-1}), 2-(*N*-morpholino) ethanesulfonic acid (MES, MW = 195.2 g mol^{-1}), 4-(2-hydroxyethyl)-1-piperazineethanesulfonic acid (HEPES, MW = 283.3 g mol^{-1}) and piperazine-N,N′-bis(2-ethanesulfonic acid) (PIPES, MW = 302.4 g mol^{-1}), all based on biological buffers, was then tested. The strong similarities in chemical structure between MES, HEPES and PIPES lead to severe overlap between signals between 2 and 4 ppm. In the light of this, MES and HEPES were replaced with t-butanol (MW = 74.12 g mol^{-1}) and the resulting DOSY spectrum resolved all three components, allowing for the generation of a linear log$D$-logMW calibration graph with the R^2 value for the data again approaching 1. The physical separation of samples finds further use in aqueous systems. In a study of two complexes, one rhodium and one manganese, both containing hydroquinone (HQ), the analytes were placed in capillaries, which were in turn placed within an NMR tube. The ^{1}H DOSY spectrum of the internal references matched that obtained in the absence of the analyte capillary. The rhodium complex, Rh(HQ)(cyclooctadiene), dissolved in D_2O, exhibited signals for both the cyclooctadiene and the hydroquinone signals. The major component was estimated to have a MW = 300 g mol^{-1}, within 10 %. of the true value. Of the two remaining ligand signals, the hydroquinone was found to be consistent with free hydroquinone, while the cyclooctadiene was found to be consistent with a single molecule bound to rhodium. This evidence suggests some dissociation of the complex in D_2O. The manganese complex ($Mn(CO)_3HQ$) exhibited

similar behaviour, as shown in Fig. 10, with the molecular weight of the complex correctly estimated to within 1 %, and evidence of dissociation with free HQ found in the sample [196].

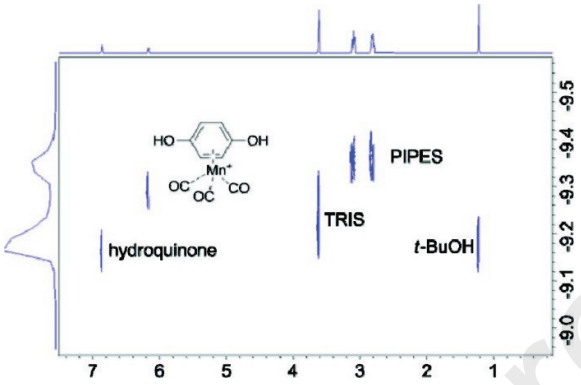

Figure 10: ^{1}H DOSY spectrum of ($Mn(CO)_3HQ$) in D_2O with physically-separated references PIPES, TRIS and *t*-BuOH. Additional signals due to free hydroquinone can be found at *ca*. 7 ppm. All data acquired on a Bruker DRX 400 MHz spectrometer. Reproduced with permission from Li et al., *Org. Lett.*, **12** (2010) 2698-2701. Copyright (2010) American Chemical Society.

4.5 External Calibration

With the constraints on choice of internal calibration references highlighted in the previous sections, calibration curves produced external to the sample are the logical next step [197, 198]. Instead of three or four additional reference compounds placed within the sample, and a calibration curve based on the acquired diffusion measurements, the diffusion coefficients of a suitably large number of compounds can be acquired to generate an external calibration curve. An internal reference compound is still needed for calculating diffusivity, but now only a single species need be added to the NMR sample. The calculation is a two-step process. First, the relative diffusivity, as defined by Crutchfield and Harris [129], is used to reduce the influence of solvent and of some types of experimental uncertainty (including

gradient calibration, but not gradient non-uniformity) that can affect diffusion NMR. A linear, normalised, equation (Eq. (20)) is then defined.

$$\log D_{\mathrm{x,\,norm}} = \log D_{\mathrm{ref,fix}} - \log D_{\mathrm{ref}} + \log D_{\mathrm{x}} \tag{20}$$

In this equation, the measured diffusion coefficient of the analyte is D_{x} and the measured diffusion coefficient of the reference is D_{ref}. In order to produce a normalised diffusion coefficient, a fixed value for the diffusion coefficient of the reference, $D_{\mathrm{ref,fix}}$ is needed. Eq. (20) produces a normalised relative diffusion coefficient for the analyte, $D_{\mathrm{x,\,norm}}$ which can then be used in Eq. (21), a reiteration of the power law, where log$K$ and α are the parameters determined from the relevant external calibration curve (ECC).

$$MW = 10^{\left(\frac{\log D - \log K}{\alpha}\right)} \tag{21}$$

As with the power laws discussed in Section 4.1, the values of log$K$ and α produced depend strongly on the nature of the solvent and also on the shape of the molecule being studied.

4.5.1 Classification of Shapes

Different classes of molecules can exhibit subtly different behaviour in solution, reflecting differences in conformational freedom and solvation as well as shape, resulting in different relationships between molecular weight and molecular size for a given solvent. While the shapes of molecules studied are an important consideration for both methods, the ECC method addresses it directly. For each solvent studied, three different ECC curves were produced, with different power law parameters for each shape class, as in Fig. 11(a). These three different ECC curves therefore distinguish between “compact spheres” (CS, blue), “expanded discs” (ED, green), and “dissipated spheres and ellipsoids” (DSE, red), intermediate in shape between the previous two. The three curves are coincident for a range of intermediate molecular weights, but deviate at the extremes. A single merged ECC curve

can be generated from all data acquired, but it works less well away from the intermediate *MW* region. An additional sub-classification was made for DMSO-d_6 and cyclohexane-d_{12}, where linear fitting of log*D* for molecules classified as compact spheres resulted in a poor fit. To resolve this, molecules were further sub-divided into hydrocarbons, and those containing other elements such as nitrogen or silicon [197, 198]. Fig. 11(b) shows the two further CS calibration curves generated and the resulting improvement in fit. Table 2 contains values for log*K* and α obtained for the three shapes classes of molecules in Fig. 11(a), the sub-classification in Fig. 11(b), and a single merged curve, in cyclohexane-d_{12}. Similar tables exist for a wide range of deuteriated solvents (toluene-d_8 and THF-d_8 in [197], benzene-d_6, $CDCl_3$, CD_2Cl_2, DMSO-d_6, cyclohexane-d_{12} in [198]).

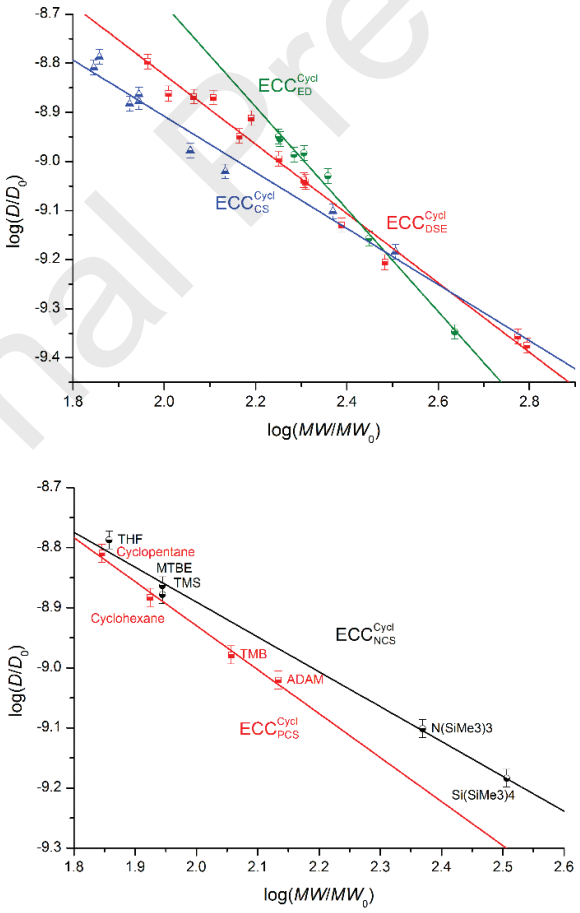

Figure 11: (a) Three external calibration curves (ECCs), plots of $\log(D/D_0)$ vs $\log(MW/MW_0)$, for 30 model compounds in cyclohexane-d_{12}, sorted by their molecular shape ("expanded discs" (ED, green); "dissipated spheres and ellipsoids" (DSE, red) and "compact spheres" (CS, blue)) (upper). (b) Two further ECCs for purely hydrocarbon (PCS, red) and non-hydrocarbon (NCS, black) compact spherical model compounds for C_6D_{12} (lower). Values of log*K* and α for all five curves presented here, and the merged calibration curve, are reproduced in Table 2. Data acquired on two spectrometers: (1) Bruker Avance 400 MHz spectrometer and (2) Bruker Avance III HD 400 MHz spectrometer. Reproduced with permission from Bachmann et al., *Chem. Eur. J.*, **22** (2016) 8462 – 8465. Copyright 2016 Wiley-VCH.

cyclohexane-d_{12}		
Shape	log*K*	α
expanded discs (ED)	–6.59	1.04
dissipated spheres and ellipsoids (DSE)	–7.41	0.707
compact spheres (CS)	–7.76	0.572
purely hydrocarbon CS	–7.47	0.732
non-hydrocarbon CS	–7.73	0.580
merged	–7.62	0.620

Table 2: Compilation of values of log*K* and α in cyclohexane-d_{12} for calibration curves for the three shape classes of molecules in Fig. 11(a) and for hydrocarbon and non-hydrocarbon CS species; and values of log*K* and α in cyclohexane-d_{12} for a merged curve for all the species studied. Data adapted from Bachmann et al., *Chem. Eur. J.* **22** (2016) 8462 – 8465

and S. Bachmann, Estimating Molecular Weights of Organometallics in Solution with Diffusion NMR Techniques, George-August-Universität Göttingen, 2017.

The values of α obtained are consistent with both those obtained by Crutchfield and Harris, and with the polymer data listed in Table 1. For the more spherical molecules, α tends towards its lower limit of 0.333. As molecules become flatter and more disk-like, the value of α increases. Clearly the accuracy of molecular weight estimation depends on correct classification of the shape of molecule. This classification of molecules can be done on an *ad hoc* basis. Compact small molecules, highly symmetrical species, and those that are densely packed are best described as compact spheres. Most molecules can be described as ellipsoidal, even if they possess cavities or projecting functional groups. Small disc-shaped molecules can be classified as ellipsoid, but larger disc-shaped molecules need to be classified separately. Incorrect classification may well lead to incorrect estimation. Use of either the dissipated sphere or the merged curve is likely to avoid the biggest errors. It is possible to quantify the shapes of the molecules on the basis of the moments of inertia of the molecule. Two methods exist. Given a set of three principal moments of inertia (I_{xx}, I_{yy}, and I_{zz}), it is possible through Eq. (22) to calculate the relative anisotropy of the molecular shape, κ^2.

$$\kappa^2 = 1 - \frac{3(I_{xx}I_{yy} + I_{yy}I_{zz} + I_{zz}I_{xx})}{(I_{xx} + I_{yy} + I_{zz})^2} \tag{22}$$

The value of κ^2 will always lie between 0 (a perfectly spherical molecule) and 1 (a perfectly linear one). Relative anisotropies for the set of molecules used to generate Fig. 11 were calculated and found to lie between 0 % (TMS, $Si(Si(Me)_3)_4$) and *ca.* 14 % (2-phenylpyrene and anthracene). It is also possible to quantify the anisotropy of the molecule based on the relative sizes of the three perpendicular moments of inertia. If they are broadly

the same ($I_{xx} = I_{yy} = I_{zz}$), then κ^2 tends towards 0. Two other classes of molecule can be distinguished by this method, both of which have two similar moments of inertia and one that is significantly different ($I_{xx} < I_{yy} \approx I_{zz}$ and $I_{xx} \approx I_{yy} < I_{zz}$). Whilst not perfect, the approach allows for some quantification of shape, as spherical and linear compounds can be differentiated from one another. While most compounds fit the compromise curve, those closest to the extremes of spherical and linear shapes do not. These are easily identified by the use of either of the methods described [199].

4.5.2 Reference Molecules

The original external calibration paper [197] specified two possible reference molecules, adamantane (ADAM) for use in toluene-d_8 and 2,2,3,3-tetramethylbutane (TMB) for use in THF-d_8. There is a wide range of possible reference molecules for each solvent. First, the residual solvent signals (i.e. the signals from residual protons in deuteriated solvents) can be used. These have been demonstrated to also give excellent estimation of MW [197]. Any of the molecules used to generate a calibration curve could also be used as a reference. However, both ADAM and TMB can be used in a wider range of solvents than just toluene-d_8 and THF-d_8, and it is likely that a standard NMR reference, such as TMS, will be used in most NMR experiments. Values of log $D_{ref,fix}$ for a number of molecules have been summarised in Table 4 of [197] and Table 4 of [198]. The values of log $D_{ref,fix}$ for these three possible references in all seven solvents are shown in Table 3, as well as data for solvent residual proton signals. The entry n/a indicate a lack of such measurement reported in the original paper, where insolubility meant that the material could not be used as a reference.

	log $D_{ref,fix}$			
compound	solvent	TMS	ADAM	TMB

toluene-d_8	–8.73	–8.74	–8.85	–8.80
THF-d_8	–8.63	–8.70	n/a	–8.77
CD_2Cl_2	–8.52	–8.63	–8.70	–8.68
$CDCl_3$	–9.18	–8.72	–8.82	–8.79
benzene-d_6	–8.69	–8.71	–8.88	–8.78
cyclohexane-d_{12}	–8.88	–8.88	–9.02	–8.98
DMSO-d_6	–9.18	–9.21	–9.33	–9.30

Table 3: Compilation of values for reference diffusion coefficients of three possible reference molecules and residual solvents in seven common deuteriated solvents. Data adapted from Bachmann et al., *Chem. Eur. J.* **22** (2016) 8462 – 8465.

4.5.3 Concentration and Temperature Dependence

Both internal and external calibration methods work best for dilute solutions. The Stokes-Einstein equation is strictly only valid for infinitely dilute solutions. Higher concentrations mean increased interactions between solute molecules as well as the possibility of obstruction effects. While obstruction effects are more easily observed in solutions of large molecules such as surfactants [190] and proteins [200], they can still have an effect on the diffusion coefficients of small molecules at high concentrations. Increasing the concentration of the analysed species from 15 mM to 120 mM had only a small effect on the average deviation of estimated MW [197]. The biggest errors were observed with species likely to exhibit intermolecular interactions such as aromatic compounds.

The effects of temperature gradients and changes on experimentally acquired diffusion coefficients has been covered in Section 2.1.3. If convection can be avoided or, at the very least, mitigated through the use of narrow-bore NMR tubes and/or convection

compensated pulse sequences, then the external calibration method should be applicable over a range of temperatures. Viscosity changes can be compensated for by the use of an internal reference species. Care must be taken in the choice of the reference: at lower temperatures, intermolecular interactions have a much greater effect. The use of residual THF signals produced significant errors in MW estimation, whereas the use of ADAM or toluene-d_8 gave no such errors. This is likely due to interactions between polar THF molecules [197].

4.5.4 Incorporating Heavier Atoms

The external calibration curves devised and discussed above were all derived for simple organic molecules. By restricting the chemical structures studied to molecules containing only C, H, O and N, the molecules can be assumed to have very similar average molecular densities. As Fig. 12(a) indicates, the densities of atoms, estimated from van der Waals volumes, increase down the periodic table. The presence of Cl, P and S atoms within a molecule makes the reliable estimation of MW more difficult. Fig. 12(a) even suggests that a high number of N and O atoms, common in organic chemistry, will have a detrimental effect on estimation of MW. It is however possible to generate ECCs for specific groups of such compounds, for example mono- or di-brominated compounds. As expected, increasing the average density of the molecule by incorporating increasingly denser atoms leads to steeper slopes in the log$D$-logMW curves. Fig. 12(b) shows plots of log$D$ against logMW for four different groups of compounds dissolved in benzene-d_6. The blue curve shows the original, merged, calibration curve for simple organic molecules. The other curves correspond to monobromo- (black), dibromo- (red) and monoiodo (green) molecules. The parameters of fit using these curves are comparable to those in the original study. For systems where, for example, the nature and degree of halogenation are known, this method should be reliable for MW estimation [201].

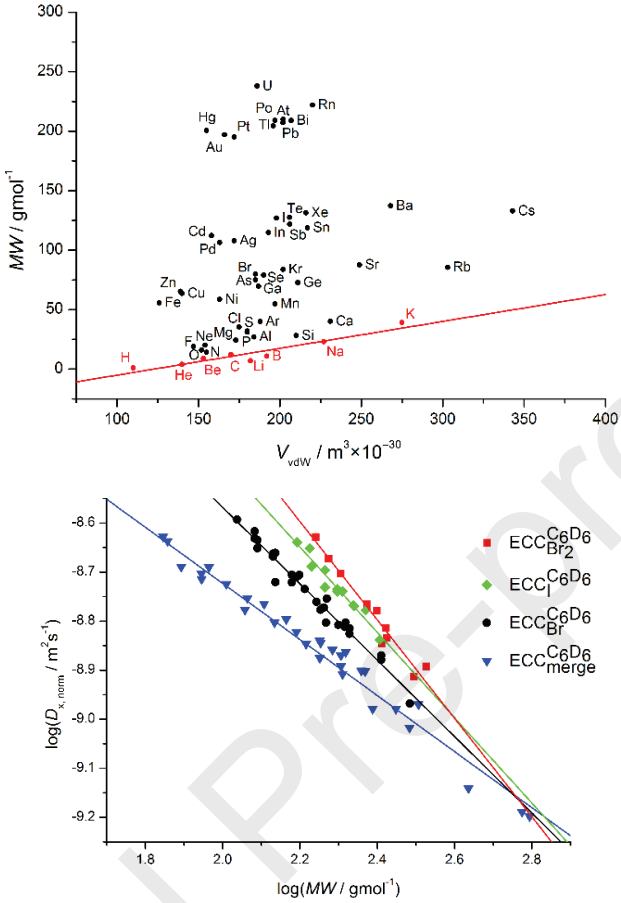

Figure 12: (a) Plot of *MW* against van der Waals volume, V_{vdW}, for a selection of elements. The red line corresponds to elements in the first and second periods of the periodic table (upper). (b) Plots of log$D_{x,norm}$ against log*MW* for different categories of compounds in benzene-d_6. The blue fit shows the original merged ECC established with simple organic molecules. The other fits correspond to mono- (black) and dibrominated (red) as well as monoiodated (green) compounds respectively (lower). Data acquired on two spectrometers: (1) Bruker Avance 400 MHz spectrometer and (2) Bruker Avance III HD 400 Mz spectrometer. Reproduced with permission from Kreyenschmidt et al., *ChemistrySelect.*, **2** (2017) 6957-6960. Copyright (2017) Wiley-VCH.

A more general approach has been suggested that might find wider use, particularly in the study of transition metal and organometallic systems [201]. First, MW_{det}, the molecular weight is estimated using the merged calibration curve for the solvent being used. This estimated molecular weight is then scaled by a correction factor, X_{corr} (Eq. (23)(a)) to obtain an improved estimate MW_{calc}. This factor X_{corr} for a given molecule is estimated from the molar van der Waals density, *MD*, of the molecule, in units of g cm^{-3}, through a saturation growth equation, Eq. (23)(b), stated here for C_6D_6. A different set of three parameters will be required to generate similar equations for use with different solvents such as THF-d_8.

$$MW_{\text{calc}} = X_{corr}\, MW_{\text{det}} \qquad (23)(a)$$

$$X_{corr} = \frac{2.555}{1 + \exp(-1.638(MD - 0.956))} \qquad (23)(b)$$

It should be noted that Eq. (23)(b) is purely empirical, as an analytical correlation between *MD* and X_{corr} could not be determined. However, for this particular set of experimental data, containing mostly brominated and iodated compounds in C_6D_6, it has proven effective, particularly for other highly halogenated compounds. It performed less well for transition metal complexes. Where different oxidation states of transition metals might be present, the model failed to give reliable estimates, presumably because of uncertainties in the van der Waals radii of the metal ions involved.

4.6 External Calibration – Examples and Applications

As with the internal calibration method, the external calibration method for estimating molecular weights from diffusion coefficients should be applicable to many different fields of chemistry. It has found wide use in the characterisation of organometallics, including organolithium compounds similar to those described in Section 4.4. This section will first focus on the application of the external calibration method to organolithium compounds,

before moving on to cover other s-block metals, mixed metal complexes and selected transition metals, before finishing with some examples from organic and environmental chemistry.

Prior to the development of the external calibration method, diffusion NMR had been used in the qualitative analysis of organolithium compounds, for example illustrating how hexameric trimethylsilylmethyllithium interacts with different solvents to give chiral tetrameric species in diethyl ether and *tert*-butylmethyl ether but only a dimer in the chelating solvent dimethoxyethane [202]. The introduction of the external calibration method allowed quantitative interpretation of diffusion coefficients and more definite assignment of degree of aggregation. Accurate *MW*s for small molecules with different geometries, independent of differences in temperature or viscosity, can be obtained. A first example of the application of external calibration curves to organolithium chemistry is in the further characterisation of LDA [203]. Variable temperature ^{1}H NMR spectra of LDA in toluene-d_8 show a range of different multiplets. At temperatures below 248 K, at least three multiplets can be observed in the spectrum. As the temperature increases, the peaks broaden and merge until only a single peak is observed at 373 K. Molecular weights of the species were estimated from diffusion coefficients acquired at three different temperatures, consistent with the presence of tri-, tetra-, penta- and, potentially, hexameric species at 198 K. Only signals from the tri- and tetrameric aggregates were observed at room temperature, with integration of the two multiplets indicating a 2:1 ratio of trimers to tetramers. The diffusion coefficient of the single peak observed at higher temperatures suggested a molecular weight consistent with a trimeric species. The additional information concerning the molecular weights and, therefore, aggregation states obtained gives a clear indication both of the aggregation of LDA in toluene and of the temperature dependence of aggregation. LDA is present as a mixture of different aggregates, ranging from trimers and tetramers through to higher oligomers. As the

temperature decreases, successively larger aggregates form. The lower the temperature, the closer the solution structure approaches the polymeric solid-state structure.

While ferrocene may lay claim to being the most well-known cyclopentadienide, its discovery in 1951 [204] post-dates that of both sodium and potassium cyclopentadienides by over 50 years [205]. Alkali metal cyclopentadienidyl complexes (CpM) are important starting materials in organometallic synthesis, used to synthesise both sandwich and half-sandwich transition metal complexes, which go on to have a wide range of further applications. Crystal structure analysis shows that the compounds, in the absence of any chelating agents, form polymeric chains that are linear for lithium and sodium, but bent for potassium, rubidium and caesium. Complementing a 1D NMR study using ^{1}H, ^{13}C, ^{6}Li, ^{7}Li, ^{23}Na and ^{133}Cs, that confirmed the presence of a number of species, low temperature diffusion NMR experiments were performed to estimate the molecular weights of all five known group 1 CpMs in THF. Molecular weights were estimated from the diffusion coefficients measured in THF and compared to the possible molecular weights of likely monomeric [CpM.THF$_n$] and dimeric aggregates [(CpM)$_2$•THF$_n$] with n = 0–4 for M = Li, Na, K, Rb, and Cs. The "dissipated spheres and ellipsoids" calibration curve [197] for THF was considered the most appropriate. As an additional check, the densities of the proposed structures were checked to ensure that they were consistent with the test set of molecules and would not induce any deviations in the MW estimation. Given that Cp and THF have similar molecular weights, it is worth noting that it proved impossible to distinguish between metallocene complexes (i.e. containing two Cp groups) and those containing only a single Cp group and an additional THF molecule solvating the metal ion. The diffusion NMR data acquired, and subsequent molecular weight estimations, best fitted monomeric species with either two, for Li and Rb, or three, for Na and K, THF molecules bound. The Cs analogue, on the other hand, exhibited diffusion coefficients consistent with penta- or hexameric aggregates [206]. A range of s-block metal

complexes, containing ligands such as hexamethyldisilazide [207], the bulky bis(4,6-tbutylbenzoxazol-2-yl)methane [208], and 1-(trimethylsilyl) cyclopropyllithium [209] have all successfully been characterised by a combination of diffusion NMR and external calibration calculations.

The success of diffusion NMR methods in organolithium chemistry is a result of lithium's place in the periodic table, tucked in between H and C. Molecular weight estimation from diffusion coefficients has also been applied to both heavier s-block metals, and alkaline earth metals such as magnesium. Already introduced in Section 4.4, organomagnesium compounds, such as Grignard reagents and Hauser bases, find wide use in organic synthesis. Grignard reagents are formed by the reaction of magnesium metal with alkyl or alkenyl halides, producing a compound with typical formula RMgX. They are good nucleophiles, reacting with electrophiles such as carbonyl compounds (aldehydes, ketones, esters, carbon dioxide, etc) to form new carbon-carbon bonds. In addition, they are also very strong bases.

Hauser bases are similar to Grignard reagents but contain an amido group instead of an alkyl one, producing a compound with the typical formula R_2NMgX. It was soon discovered that the addition of LiCl to both sets of reagents improved their solubility and also enhanced their reactivity. Understanding the solution phase structures formed, and the role the additional lithium plays in them, is vital to better understanding and use of both turbo-Grignard and turbo-Hauser reagents. Grignard reagents RMgX in ethereal solutions undergo disproportionation (the Schlenk equilibrium) to afford both R_2Mg and MgX_2. As part of a wider study also using mass spectrometry, conductivity measurements and quantum mechanical predictions of the structures formed, diffusion NMR of a series of Grignard reagents, where R = Et, Bu, Hex, Oct, Dec, and *i*Pr, was used to characterise the structures formed by the reagents in THF-d_8 in the absence and in the presence of LiCl. The molecular weights estimated from the diffusion coefficients measured in the absence of LiCl matched

those calculated for the di-solvated Grignard, [RMgCl•$(THF)_2$], very well. Only BuMgCl was studied in the presence of LiCl. ^{1}H and ^{13}C NMR revealed no differences in spectra after the addition of LiCl, while the single peak in ^{7}Li was shifted slightly compared with that observed for pure LiCl. The molecular weight estimated from the ^{1}H DOSY spectrum was consistent with a 1:1 complex between LiCl and [RMgCl•$(THF)_2$]. The other experimental methods suggested that a more complicated series of equilibria were actually occurring in solution [210]. Similar studies were conducted on other mixed metal complexes, such as the Hauser bases, *i*Pr_2NMgCl [211] and TMPMgCl [212] and their turbo-derivatives, revealing that the Schlenk equilibrium can be replaced by a more complicated series of equilibria between different aggregations states and identifying the effect of more hindered amides [213] on the solution phase structures. Other alkaline earth metal species characterised by diffusion NMR methods and external calibration calculations include s-block bimetallic catalysts containing two magnesium atoms, stabilised by differing amounts of $Na(THF)_3$ depending on the solvent used [214], and multinuclear complexes of calcium- and containing π ligands [215].

The accuracy of the ECC approach is highly dependent on the choice of model parameters. As demonstrated by Fig. 12, the density of an element is related to its position in the periodic table, and the presence of a heavier atom in a molecule or complex can render the use of a purely organic calibration curve inappropriate. Thus in the study of species containing heavier metals, an appropriate calibration curve containing a range of model compounds with similar densities to the expected complexes needs to be generated. This approach is well demonstrated in the case of gold (I) complexes [216]. The interactions between cationic gold(I) complexes, their counter-ions, and the chosen substrate play an important role in the use of such complexes in homogeneous catalysis. With a van der Waals radius of 166 pm and an atomic weight of 196 g mol^{-1}, a gold atom has a molecular density

of 1.03×10^{31} g mol^{-1} m^{-3} (17.1 g cm^{-3}), far outside the range covered by carbon, hydrogen and other elements found in simpler organic molecules. As expected, calibration curves based on a selection of compounds containing only C, H and O lead to failures in MW estimation. Instead, external calibration curves were constructed using 13 mono- and di-gold complexes. Separate curves, with different values of log$K$ and α, were required for the two separate classes of gold complex. The reason for this difference may not be due to the single additional denser atom. Indeed, a comparison of the molecular densities of the mono- and di-gold species shows that the average molecular densities for the two groups of complexes differ by less than 3%. Their shapes, on the other hand, do differ markedly: qualitatively, monometallic complexes are mostly spherical-like molecules, while di-gold complexes have a more elongated shape. Fig. 13 shows the ^{1}H DOSY spectrum of $(Ph_3P)AuCl$ in CD_2Cl_2 with adamantane as a reference molecule. The MW of the gold complex diffusion coefficient can be estimated using values of logK and α taken from the appropriate calibration curve (–7.30 and 0.65 respectively) and a normalised logarithm of the diffusion coefficient, $\log D_{x,\,norm} =$ –9.04, to give an estimate of molecular weight within 1 % of the actual weight of the complex. The curves were also used to estimate the molecular weights of species formed by the interaction of the gold complexes, (JohnPhos)AuCl, (IPr)AuCl and $(Ph_3P)AuCl$, with AgOTf. For all complexes, the diffusion coefficients measured indicated the presence of an ion pair. This observation was validated by ^{1}H and ^{19}F diffusion NMR experiments, both of which produced the same measured diffusion coefficient. Adding an excess of an alkyne to these samples makes them representative of gold-catalyzed alkyne transformations. Both (JohnPhos)AuCl and $(Ph_3P)AuCl$ formed monogold species with the alkynes and AgOTf. On the other hand, the diffusion coefficient and corresponding molecular weight for the species in the sample containing (IPr)AuCl, AgOTf and phenylacetylene did not correspond to a simple monogold complex. Instead, better agreement was found with the digold complex

$[\{(IPr)Au\}_2(\eta^1,\eta^2\text{-}C{\equiv}C{-}C_6H_5)]^+[OTf]^-$. Similar approaches have also proved successful for tantalum [217] and could prove useful for studies of other coinage metals (copper [218] and silver [219]).

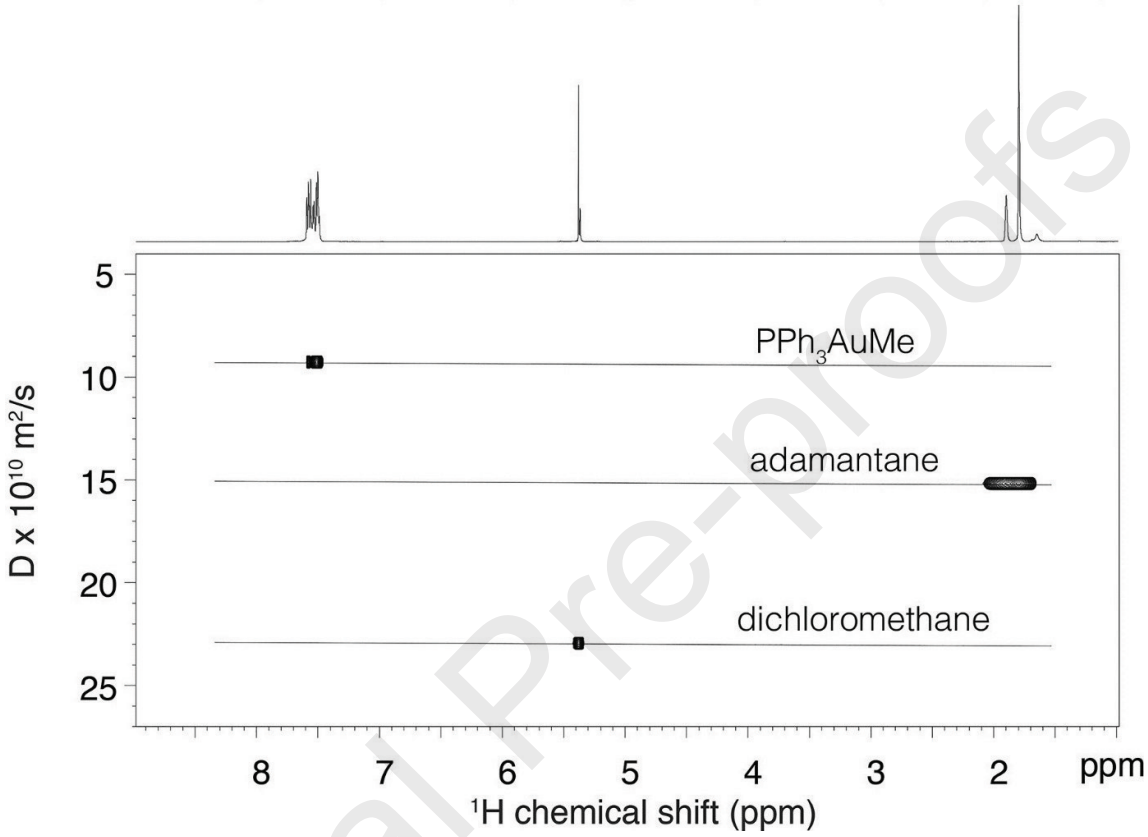

Figure 13: ^{1}H DOSY NMR spectrum of $(Ph_3P)AuMe$ complex in CD_2Cl_2, with adamantane as an reference compound. Estimation of molecular weight of $(Ph_3P)AuCl$ is described in the main text. All data acquired on a Bruker Avance 600 MHz spectrometer. Reproduced with permission from Hamdoun et al., *Organometallics*, **37** (2018) 4692-4698. Copyright (2018) American Chemical Society.

The external calibration method is not limited to organometallic chemistry, and has been used to investigate glycosylation reactions at low temperature [220], the hydrolysis and dehydration of inulin in water [221], and the observed reduction of carbazole fluorescence in the presence of isolable carbenes [222]. Samples in more complicated aqueous solutions have

also been studied. Phosphorous-containing compounds are common in environmental chemistry, and can be crucial for plant nutrition. Soil samples can contain up to 3 g of phosphorous per kilogram of soil, with species such as phosphate diesters, monoesters and phosphonates reported. Chemical shifts of phosphorus species can depend on sample matrix properties such as pH and ionic strength. Multidimensional NMR approaches, such as ^{31}P-^{1}H correlation spectroscopy, can offer a route to firm identification of species. Diffusion NMR has recently been shown to be an effective additional spectroscopic tool for such analysis [223], using a mixture of 14 different model phosphorus compounds, including phosphonic acids, phosphate and pyrophosphate salts. Three "unknown" compounds were also included in the sample: lipoteichoic acid (LTP) from *Staphylococcus aureus*, RNA, from torula yeast Type VI, and DNA, from salmon testes. Some of the compounds, notably the RNA, degraded in solution introducing additional signals to the spectrum. However, the sparse phosphorus spectrum allowed the resolution of almost every peak in the 1D ^{31}P spectrum. A log$D$-log MW plot was produced using this set of compounds, with an exponent, α, of 0.455, consistent with many of the log$D$-logMW correlations shown so far in this review. The masses of the two remaining "unknowns", DNA and LTP, could then be estimated, as 75.7 kDa and 2.4 kDa respectively. Further interpretation of these diffusion coefficients requires caution. These species are not single, well-defined molecules but distributions of macromolecules with different sizes. The signals observed will stem from phosphorus nuclei in species with a broad range of molecular weights and, therefore, diffusion coefficients. Analysis of these peaks as if the species were monodisperse will give poor fits to the Stejskal-Tanner equation, large errors in estimated diffusion coefficients and large uncertainties in the estimated molecular weights while not correctly describing their dispersity. Here, the difference in size of over a power of ten between DNA and LTP does allow for the two species to be distinguished. If information about the range of molecular weights present is required, some

of the methods used in the study of polymers may prove useful [27, 29, 117]. For the smaller molecules in the sample, the accuracy of the MW estimation was within 10 % of the true weights for all species. While this proof of principle work measured all reference species in a single DOSY spectrum, arguably providing a comprehensive internal calibration curve, the number of model compounds used means that it could also be used to provide an external calibration curve.

The external calibration method and all related ECCs have been implemented as both an Excel spreadsheet and a standalone Java package, available for free download from http://www.stalke.chemie.uni-goettingen.de/mwestimation/.

5. A Return to the Stokes-Einstein Equation

The much more general problem of estimating the *MWs* of unknown species in a range of solvents can be approached from a different angle by returning to the discussion of the Stokes-Einstein equation. Each key assumption in the equation can be isolated and appropriate modifications made. This approach is both more general than the use of a power law to describe the diffusion of a particular class of species in a particular solvent, and, necessarily, more approximate.

The first problem to address is that of the finite size of solvent molecules: the breakdown of the continuum model has a large effect on predicted diffusion coefficients. The effect of changing particle size on the friction experienced by a solute species can be included in the Stokes-Einstein equation by the introduction of a variable friction factor, *f* to the denominator of Eq. (7), just as Perrin did for the effect of solute shape. For solute species much smaller than the solvent, the denominator of Eq. (7), corresponding to friction acting on the solute, will change to $4\pi\eta r_{\mathrm{H}}$, corresponding to a "slip" boundary between solute and solvent rather than a "stick" boundary. Two expressions have been proposed to describe the

transition between these limits, both expressed as functions of the ratio of the radius of solvent to the radius of molecule, r_S/r_H. The first, developed by Gierer and Wirtz [224] (Eq. (24)(a)), uses microfrictional theory, the second, described by Chen and Chen [225] (Eq. (24)(b)), was obtained by converting the Gierer-Wirtz expression into one containing only a single term in r_S/r_H, with two adjustable parameters determined by fitting diffusion data for a small set of model compounds.

$$f_{GW} = \left(\frac{3r_S}{2r_H} + \frac{r_H}{r_H + r_S}\right)^{-1} \quad (24)(a)$$

$$f_{CC} = \left(1 + 0.695\left(\frac{r_S}{r_H}\right)^{2.234}\right)^{-1} \quad (24)(b)$$

Using the same test set of compounds used in Fig. 4, these variable friction approaches can be tested, as shown in Figs. 14(a) and 14(b). Diffusion coefficients of the small test set of molecules used to generate Fig. 4 were estimated using the Stokes–Einstein equation modified by the Gierer-Wirtz (Fig. 14(a)) and Chen-Chen (Fig. 14(b)) methods, and then compared with those measured using diffusion NMR.

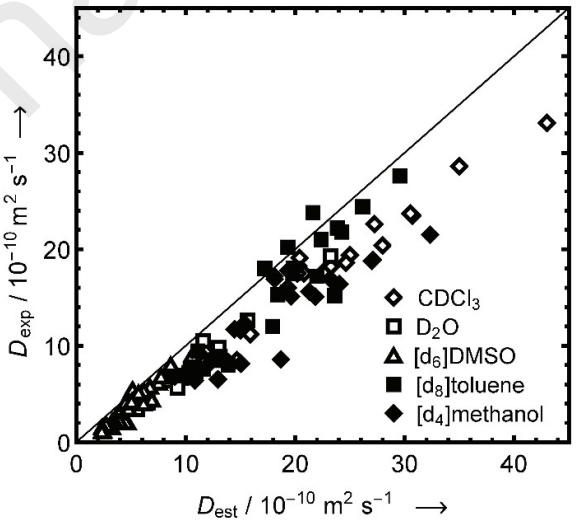

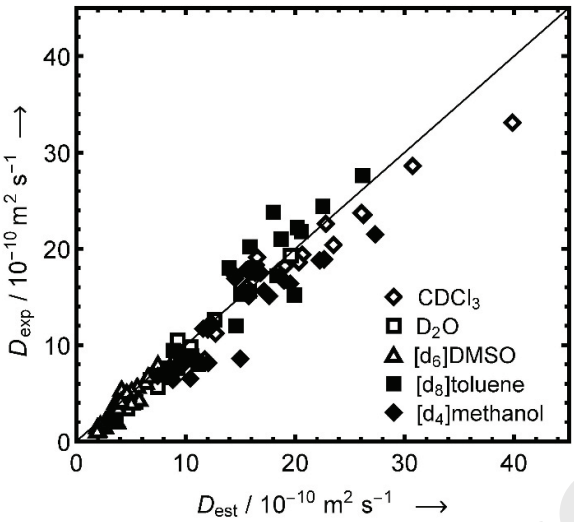

Figure 14: Measured diffusion coefficients plotted against diffusion coefficients calculated using (a, upper) the Gierer-Wirtz (Eq. (24)(a)) and (b, lower) the Chen-Chen (Eq. (24)(b)) modifications to the Stokes–Einstein equation (Eq. (7)) for 108 samples of 44 small molecules in five deuteriated solvents, as detailed in the figure legend, together with a solid line of unit slope. All data acquired on a Varian Unity 400 MHz spectrometer using the Oneshot sequence at 298 K. Adapted from Evans et al., *Angew. Chem. Int. Ed.*, **52** (2013) 3199-3202.

Why the Gierer-Wirtz model fails to accurately predict the experimental diffusion coefficients is important. Both methods succeed in flattening the data onto something approaching a unit slope. The Gierer-Wirtz approach, which has no adjustable parameters, overshoots, predicting faster diffusion than is actually measured, i.e. the solute molecules have larger hydrodynamic radii in solution than expected. By using two adjustable parameters, the Chen-Chen method corrects the overshoot. It should be noted that attempts to extend the Chen-Chen model to crown ethers and alkanes in ethanol and butan-1-ol were less successful [225]. One obvious problem with the Chen-Chen equation is the choice of crown

ethers as the calibration set of compounds. Such molecules are highly flexible and, particularly for the larger species, will show increased hydrodynamic radii.

In principle it should be possible to calculate f directly from the known molecular structures of solute and solvent, but this would be a formidable challenge. A more tractable alternative is to use a simplified "bead" model of solute structure and, with the aid of empirical parameters optimised for a suitable training set of species, use hydrodynamic calculations to find a diffusion tensor and hence the value of f [226]. As expected, the values of f obtained tends towards 1 as solute molecules increase in size; they are close to those obtained by Gierer and Wirtz and, in all cases, lower than the Chen and Chen modification.

The second problem is that the effective hydrodynamic radius of a solute species is determined not only by its *MW*, but also by its effective density, shape, solvation and flexibility. The effect of shape on the shape frictional coefficient f_s can typically be safely ignored for aspect ratios lower than 3, which covers the great majority of small molecules, but in the absence of prior information factors such as composition, solvation and flexibility cannot be treated explicitly. In seeking a general relationship between D and *MW*, therefore, one important simplification is to restrict the search to species that do not contain heavy atoms, and hence may be assumed to have an effective density typical of organic molecules. A second simplification is afforded by restricting the range of species considered to small to medium-sized (up to *ca*. 1 kDa) molecules. Solutes are therefore all assumed to be hard spheres with a density ρ_{eff} that is treated as a sole parameter to be optimised. This empirical effective density will be lower than would be predicted from a consideration of molecular mass and geometry, because the effects of solvation and flexibility will increase the solute hydrodynamic radius.

This thus provides a mechanism for estimating a hydrodynamic radius for a given *MW*, which can be used together with the Stokes-Einstein equation Eq. (7) and the Gierer-

Wirtz equation Eq. (24)(a) to calculate a diffusion coefficient *D*. The Gierer-Wirtz equation requires knowledge of the solvent to solute radius ratio r_S/r_H, but since the solute radius is being estimated using the hard sphere approximation with an effective density ρ_{eff}, it is reasonable to apply exactly the same logic to estimating the solvent radius. The radius ratio then simplifies to the cube root of the ratio of the solute and solvent solute molecular weights.

These modifications to the Stokes-Einstein equation thus lead to Stokes-Einstein-Gierer-Wirtz estimation (SEGWE), Eqs. (25)(a) and (25)(b), which links the diffusion coefficient expected in a solvent with a given viscosity η at a given temperature *T* to the solute and solvent molecular weights MW and MW_S, through a single adjustable parameter, the effective density ρ_{eff}:

$$D = \frac{k_B T\left(\frac{3\alpha}{2} + \frac{1}{1+\alpha}\right)}{6\pi\eta\sqrt[3]{\frac{3MW}{4\pi\rho_{eff}N_A}}} \quad (25)(a)$$

$$\alpha = \frac{r_S}{r} = \sqrt[3]{\frac{MW_S}{MW}} \quad (25)(b)$$

where N_A is the Avogadro number.

The problem of deriving a general relationship between molecular weight and diffusion coefficient then reduces to that of finding an optimum value for the effective density ρ_{eff}. The original study [94] used a training set of experimental diffusion coefficients, *D*, all measured at 298 K, for 109 combinations of 44 test compounds and 5 common solvents. Fig. 15 compares the viscosity-scaled diffusion coefficients of the same set of 109 small organic molecules as in Fig. 4, estimated now using SEGWE, with those measured in 5 different deuteriated solvents using diffusion NMR. Numerical optimization was used to estimate the required effective density, ρ_{eff} = 0.619 g cm^{-3}. As expected, this is much smaller than the typical densities of solid or liquid organic materials, because of the effects, in

roughly decreasing order of importance, of solvation, flexibility and shape. These would all make the molecule effectively larger in solution than when solid. The systematic errors observed in Fig. 4 have been successfully removed, and the root-mean-square difference between estimated and experimental diffusion coefficients for the training set of measurements was 14.6 %. This can be contrasted with a value of 45 % for the corresponding Stokes-Einstein prediction (Fig. 4).

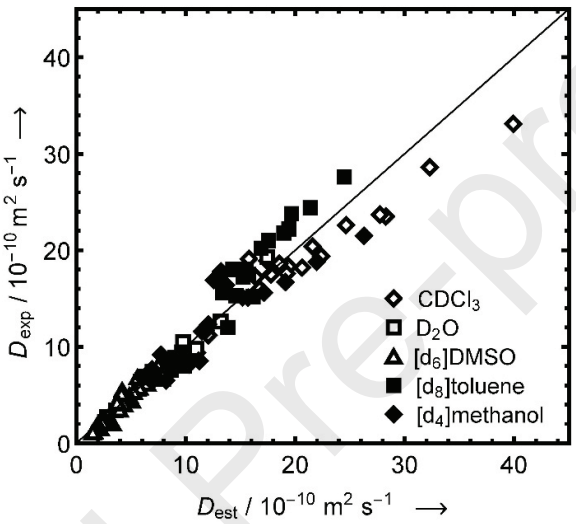

Figure 15: Measured diffusion coefficients plotted against diffusion coefficients calculated using the SEGWE modification (Eqs. (25)(a) and (b)) of the Stokes–Einstein equation (Eq. (7)) for 108 samples of 44 small molecules in five deuteriated solvents, as detailed in the figure legend, with a solid line of unit slope. All data acquired on a Varian Unity 400 MHz spectrometer using the Oneshot sequence at 298 K. Adapted from Evans et al., *Angew. Chem. Int. Ed.*, **52** (2013) 3199-3202.

More recently, the model has been tested further by incorporating measurements of small molecules in dilute systems drawn from literature studies of small molecule diffusion [4, 35, 52, 53, 95, 129, 134, 143, 197, 198, 227-239] in the training set. With 548 additional measurements, this set of data spans a wider range of chemical space than the initial training

set, increases the range compound masses up to *ca*. 1.5 kDa, increases the number of solvents covered from 5 to 23, and removes the previous temperature restriction of 298 K. Not all of the available sources of data were used. Five criteria were used to determine the likelihood that literature data were reliably acquired and, therefore, suitable for inclusion in the literature data set.

Systematic Miscalibration. Sections 2.2.1 and 2.2.2 discussed a number of possible sources of systematic errors in diffusion NMR experiments [230, 240]. If a paper contained evidence of lack of, or mis-, calibration, its data were excluded from the literature data set. In particular, sets of experimentally acquired diffusion coefficients with systematically large deviations from prediction in every measurement reported were excluded.

Evidence of Convection. The most likely source of unreliability in acquired experimental diffusion NMR data is convection. Section 2.2.3 has detailed how it is not a critical phenomenon in diffusion NMR experiments, but is likely to be present to some degree in almost every NMR experiment. The presence of convection in a sample is likely to lead to higher diffusion coefficients than expected [59, 60]. Variable temperature studies, or those in solvents particularly prone to convection, that showed systematically higher diffusion coefficients than predicted were excluded from the literature data set.

Inconsistent Diffusion Coefficients. Related to the first criterion, if a repeated measurement of the same species had inconsistent diffusion coefficients reported within a single experimental report, it is highly likely that there were significant problems with the experiments, and the data were excluded from the literature data set.

Scope. Solutes with molecular weights greater than 1.5 kDa were not included. (The use of diffusion NMR in characterizing proteins and polymers was discussed in Section 4.1).

Evidence of Aggregation. Species that form aggregates diffuse more slowly than single molecules. Systems that might be expected to aggregate and that had lower diffusion

coefficients than predicted were therefore excluded from the literature data set. The use of diffusion NMR in the study of aggregation is an interesting topic in its own right; a number of reviews and papers are recommended [2-4, 237, 241]. This criterion meant that one datum included in the original data set, trimesic acid (benzene-1,3,5-tricarboxylic acid) in DMSO-d_6, was excluded from later analysis and from Figs. 4, 14, 15 and 16 presented here. This compound exhibited a diffusion coefficient *ca*. 60 % smaller than predicted, indicating significant aggregation. This should have been expected; trimesic acid is known to form extended self-assembled structures in both the solid state [242] and at liquid–solid interfaces [243], producing extended hexagonal networks with either "chicken wire" or "flower" structures.

Fig. 16 compares the measured diffusion coefficients of both the original set of 108 small organic molecules, and an additional 558 diffusion coefficients taken from the literature [244], with those estimated with SEGWE using the same optimized effective density, ρ_{eff} = 0.619 g cm^{-3} as derived from the original data set.

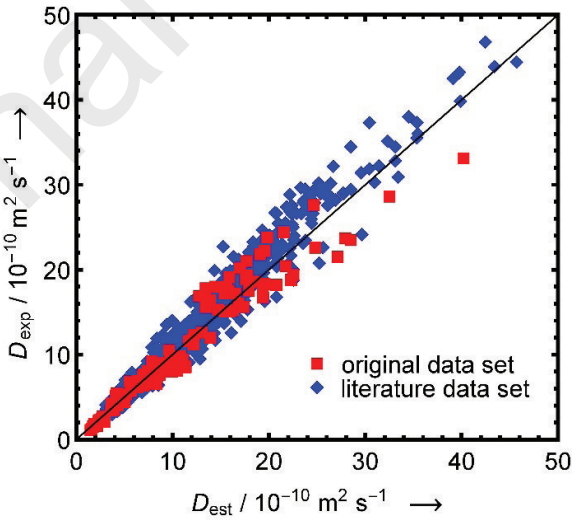

Figure 16: Measured diffusion coefficients plotted against diffusion coefficients calculated using the SEGWE modification (Eqs. (25)(a) and (b)) of the Stokes–Einstein equation (Eq. (7)) for 108 samples of 44 small molecules in five deuteriated solvents (original data set,

filled red squares) and 558 samples in 23 solvents, in both deuteriated and protiated solvents (literature data set, filled blue diamonds), together with a solid line of unit slope. Adapted from Evans et al., *Anal. Chem*., **90** (2018) 3987-3994.

Certain subsections of the literature data warrant closer inspection. In Section 3, electrochemically-acquired data were discussed, as they appeared to show an inverse correlation between D and MW [95, 96]. These data was included in the further testing of the SEGWE model. For the larger dataset [95], containing a total of 59 diffusion coefficients of 29 molecules measured in three different solvents, acetonitrile, dimethyl sulfoxide and dimethyl formamide, SEGWE performed admirably, with an RMS error of well under 5 %.

The temperature dependence of the SEGWE predictions can also be tested. In order to estimate diffusion coefficients at different temperatures, an Arrhenius model for solvent viscosity was used with Eq. (25)(a). For all liquids used in the literature data set, as well as protiated analogues of all deuteriated solvents, two parameters were used to fit the solvent viscosities as exponential functions of temperature. The effectiveness of this extension can be judged by considering the data contained in [129], a compilation of 200 diffusion coefficients measured in D_2O and in $CDCl_3$ at both 298 and 303 K. While some systematic trends were observed, all diffusion coefficients were estimated by SEGWE to within 25%. As the temperature dependence of viscosity is likely to be independent of the other modifications to the Stokes-Einstein equation incorporated in the SEGWE model, it is perhaps not surprising that the temperature dependence of diffusion is well represented. Some small deviations are observed, mostly increased experimental diffusion coefficients for samples in $CDCl_3$; these are likely to be the result of sample convection. As a consequence of its viscosity, density and thermal expansion coefficient [60, 244], $CDCl_3$ is over ten times more likely to convect than D_2O under the same thermal conditions.

SEGWE has been implemented as an Excel spreadsheet and as a standalone Matlab package, as well as being incorporated into the GNAT processing software, all available for free download from http://nmr.chemistry.manchester.ac.uk/.

5.1 Stokes-Einstein-Gierer-Wirtz Estimation – Examples and Applications

As with both the external and internal calibration methods, the SEGWE estimation model has found use in organometallic chemistry as well as in more traditional organic chemistry and in the identification of natural products [245, 246]. Its application has tended to be more fragmentary than both internal and external methods where distinct classes of reagents were subjected to concerted, methodical characterisation.

One particular aspect of its utility is as a check on whether species are aggregating or not. Aggregation processes have been found to affect the absorption and distribution of bioactive molecules *in vivo*. DOSY spectra of a fluorescence-based Cu^+ sensor developed by Giuffrida et al. were therefore acquired to test for the presence of aggregates. The diffusion coefficient acquired, $D = 3.51\times10^{-10}$ m^2 s^{-1}, for a 1 mM sample of the sensor in D_2O was consistent with both the predicted hydrodynamic radius and the molecular weight of the compound [235]. On the other hand, the method has been used to identify the presence of dimers and larger aggregates, as in the cases of π-stacked [247], halogen- [239] and hydrogen-bonded [248-251] species in solution. Indeed, rather large and complex aggregates can be monitored and characterised. 5-ureidosalicylic acid is known to form cyclamers in the solid state. DOSY spectra confirmed the persistence of at least a trimeric species in acetone-d_6 [252]. Larger still are the oligomeric aggregates of shuttlecock-like penta-modified C_{60} fullerenes. At increasing concentrations, diffusion coefficients consistent with aggregates of up to seven modified fullerenes were measured [253].

While the SEGWE method was explicitly designed for small molecules, containing only lighter atoms such as C, H, and O, this has not stopped its use in the analysis of compounds and complexes containing aluminium [254-256], cobalt [257], copper [258, 259], gold [260], heavy alkaline earth elements [261], all heavier Group 14 elements [262], iridium [263], nickel [264], palladium [236, 265, 266], samarium [267], selenium [268], silver [269, 270], titanium [271], uranium [272], yttrium [273, 274], and zinc [275, 276]. While caution might be well advised in the extrapolated use of an effective density optimised using a training set consisting solely of small, organic molecules, it was noted in [259] that for the species studied therein, the ligand units used made up the bulk of the molecular weight, 540 g mol^{-1}, compared with the heavier Cu (64 g mol^{-1}) atom and halides (35 g mol^{-1} for Cl, 127 g mol^{-1} for I).

The utility of the SEGWE model depends on the research question being asked. For example, diffusion NMR analyses of the complexes of tris(pyridylcarboxylate)-1,4,7-triazacyclononane ligands with yttrium showed that the estimated MW depended on the solvent used. In polar solvents, DMSO-d_6 and methanol-d_4, the estimated molecular weights were very similar, but the estimated mass in CD_2Cl_2 was twice as large and the estimated mass in $CDCl_3$, the least polar solvent used, was a further three times larger. This is perhaps unsurprising: solvation of the complex is weak in $CDCl_3$, and hydrophobic π–π stacking can freely occur between the aromatic rings. Other aspects of the study were hindered by severe line-broadening, presumably due to the slow rate of molecular tumbling of the very large complexes formed in this solution. The DOSY experimental data and SEGWE calculation provided valuable additional information, but only as part of the wider, multiple technique, study [273].

6. Discussion

6.1 Interpreting Size or Interpreting Weight?

The relationship between diffusion coefficient and molecular size is relatively simple: there is an inverse relationship, made clear in the Stokes Einstein equation (Eq. (7)). The complication, addressed by all the approaches described in this review, remains clarifying the link between molecular size and molecular weight. A neat example of this can be found in the recent paper by Zaccaria et al. [277]. Diffusion NMR data were acquired for a series of transition metal bis-cyclopentadienyl complexes Cp_2MCl_2 (M = Ti, Zr, Hf). In spite of a nearly 50 % increase in MW, the diffusion coefficients of the complexes were found to be the same, within experimental error. Here, the changing metal core does not materially affect the size of the overall species.

So what effect does introducing heavier atoms into molecules have? In the previous section, SEGWE was shown to have been used, quantitatively, in the analysis of species containing a range of increasingly heavy metals. The diffusion NMR study of gold complexes in [216] showed that, while a different calibration curve was needed for di-gold complexes, their average molecular densities only changed by *ca*. 3 %. Furthermore, Zaccaria et al. [277] generated a calibration curve, using a wide range of chemistry from small molecules to aluminium complexes, a silsesquioxane diol and a zirconium complex containing a *t*-butyl-substituted-bis(indenyl)dimethylsilane. While an excellent degree of fit was achieved for this particular set of 11 compounds, the calibration curve failed to work for three seemingly similar compounds. The silsesquioxane was reacted with $Ti(OiPr)_4$ to form a species that consisted of two cages, bridged by a single Ti atom. The indenyl ligands in the zirconium complexes were substituted with smaller groups, such as methyls, or replaced with smaller cyclopentadienyl groups. These changes in structure and shape lead to very poor estimations of MW from the original calibration curve. Just because a good linear log$D$-logMW

correlation is obtained for a certain group of molecules, it does not imply that it can be used as a reliable calibration for all similar molecules.

In supramolecular chemistry, there is also the issue of cavities in molecules. While diffusion NMR and DOSY spectra can be of great use in the characterisation of molecular cages and self-assembled systems, the existence of a hollow space in the centre of the molecule may complicate matters. A neat example is the case of ring-in-ring, or Russian doll, complexes consisting of a nested assembly of two different macrocycles [278]. The diffusion coefficient of the larger zinc-containing dodecameric ring was not observed to change when a smaller ring was assembled within it. Clearly, the hydrodynamic radius of the new complex remained - as expected - broadly the same as its precursor.

6.2 Quality Control

Together with the increasing numbers of studies acquiring small molecule diffusion coefficients as part of their characterisation, the development of the external calibration method and SEGWE have also generated and collated large sets of molecular diffusion coefficients. A key theme of this review, covered in detail in Section 2, has been that diffusion coefficients have to be measured carefully. Convection and aggregation, in particular, will lead to diffusion coefficients higher and lower than expected, respectively, while miscalibrations of the pulsed field gradient will lead to systematic errors in the diffusion coefficients acquired. Reference 244 developed a series of criteria that sets of data should pass before inclusion in any test literature data set. A quick “sanity check” of any set of acquired diffusion coefficient data according to these criteria should reduce any doubts as to the quality and self-consistency of acquired data, and aid in the later quantitative interpretation of the data. The same paper also collated the Arrhenius parameters of solvent viscosity for all deuteriated and protiated solvents used in the literature data set. This library

of variable-temperature viscosity data will also help with better understanding and interpretation of acquired diffusion coefficients.

6.3 Competing Methods

The various literature reports of quantitative estimation of molecular weight from small molecule diffusion coefficients, and vice versa, have been broadly grouped into three competing methods. These have been introduced, discussed and specific applications highlighted to show how each technique works, and to give some idea as to what it can be applied to in the future. Each method has found a particular niche in the quantitative interpretation of small molecule diffusion coefficients.

SEGWE is necessarily an approximate approach and tends to have the largest uncertainties in its predictions. However, as the majority of its published applications show, it is still precise enough to be capable of resolving simple chemical arguments: Are these species associating? Is the compound a monomer or a dimer? What is the approximate molecular weight of my unknown? While SEGWE needs robustly acquired and accurate diffusion coefficients, this review has addressed the key difficulties of temperature control, gradient calibration and convection. It is strongly recommended that any diffusion NMR study addresses these three issues before the acquisition of any data.

While a clear antecedent, the internal calibration method has not been completely superseded by the external calibration method. As the reference compounds are present in the same tube as the analyte, so long as the NMR signals do not overlap, the effects of many experimental imperfections will be compensated for. Where NMR spectra are suitably sparse, there is still room for this methodology to be used.

While the ECC method will likely find wide use for generic small organic molecules as well as for organometallic chemistry, it is essential to generate a specific calibration curve

for the range of species to be studied. For series of compounds with similar structures and containing atoms with similar atomic densities, the ECC approach to molecular weight estimation should be robust and accurate.

7. Summary

NMR measurements of diffusion coefficients, such as in diffusion-ordered spectroscopy (DOSY) experiments, have historically been used only in a qualitative manner, separating out signals in a manner akin to chromatography. The Stokes-Einstein equation implies that the relationship between diffusion coefficient and molecular size is simple. It is the relationship between hydrodynamic radius and molecular weight that is most uncertain for small molecules. This is not the case for macromolecules. While this review nominally concerns only the estimation of small molecule molecular weights, there is plenty of overlap with the application of diffusion NMR methods to macromolecules, such as proteins, polymers and polysaccharides, and a small section on these areas has been included. The power laws that govern the relationships between the molecular weights of these species and their diffusion coefficients in solution give insight both into the interactions between solvent and macromolecule, and into the three-dimensional structures these large, polymeric species fold into. They also give important context for the later small molecule work

Three different general methods for estimating molecular weight from acquired diffusion coefficient have been detailed in this review along with guides as to their use and the calculations required. Two are based on power law methods, differing only in how the diffusion of the unknown compound is compared to that of known reference molecules. The third method, a direct modification of the Stokes-Einstein equation, is more general and, as a result, more approximate, but highlights the importance of making pragmatic decisions about the systems being studied. All three methods discussed have their merits. As this review has

described and discussed, there is an ever-growing body of work, spanning almost the entire periodic table, of on the use of experimentally-acquired diffusion coefficients for estimating and validating small molecule and organometallic molecular weights. This, in turn, allows for the solution of many chemical problems, including identification and quantification of aggregation, determination of association constants, solvation, ion pairing, determination of effective sizes and structures of reactive intermediates, and the characterisation of organometallic systems and complexes.

While writing this review, three points became clear. First, this is not a new problem. The failure of the Stokes-Einstein equation to quantitatively predict small molecule diffusion coefficients was spotted very early on, and attempts to correct it started almost immediately. The Wilke-Chung equation, in particular, is still widely used and cited, even though it handles and simplifies the assumptions within the Stokes-Einstein equation in a completely empirical manner. Second, care and attention in the acquisition of diffusion NMR data reaps dividends. This review has summarised some of the important experimental considerations that need to be both before any experimental work begins, and during acquisition of data. In particular, convection can be the bane of experimental diffusion NMR studies, but it can be identified, it can be measured, and it can be compensated for. As increasingly reliable measurements of diffusion coefficient can be made, so can increasingly quantitative uses of the measured diffusion coefficients. NMR spectrometers are now ubiquitous in modern chemical research labs, and most are equipped with the hardware necessary for diffusion NMR experiments. The experiments themselves are increasingly robust, and can be used to acquire good quality, accurate diffusion coefficients. Finally, the range of distinct areas of chemistry where diffusion coefficients, acquired by NMR or otherwise, have been used to estimate molecular weights and, hence, solve chemical problems, is vast. The range of organometallic chemistry probed by diffusion NMR techniques and molecular weight

estimation would be worthy of comprehensive review on its own. This review has tried to highlight historically interesting studies and key aspects from an NMR point of view, but could not hope to cover, or do justice to, the full range of complexes and reagents reported in the literature. What is clear is that there is significant scope, and great opportunity, for the increased use of diffusion NMR and all of the various molecular weight estimation methodologies described in this review.

Acknowledgements

The author thanks Iain Day for help throughout, reading earlier iterations, and offering feedback. I would also like to thank some previous members of the Evans group at Aston: Taylor Rottreau, Mizan Matin, Arun Sandhu, Benjamin Lowe, Yiannis Bero, Burhan Uddin, Bridget Tang, Jamie Guest, Robbie Clark, Mitchell Antony and Joseph Jones for hard work, helpful discussions and helping me get this show on the road.

This research did not receive any specific grant from funding agencies in the public, commercial, or not-for-profit sectors.

References

[1] A. Macchioni, G. Ciancaleoni, C. Zuccaccia, D. Zuccaccia, Determining accurate molecular sizes in solution through NMR diffusion spectroscopy, Chem. Soc. Rev. 37 (2008) 479. doi:10.1039/B615067P.

[2] L. Avram, Y. Cohen, Diffusion NMR of molecular cages and capsules, Chem. Soc. Rev. 44 (2015) 586. doi:10.1039/C4CS00197D.

[3] Y. Cohen, S. Slovak, Diffusion NMR for the characterization, in solution, of supramolecular systems based on calixarenes, resorcinarenes, and other macrocyclic arenes, Org. Chem. Front. 6 (2019) 1705. doi:10.1039/C9QO00329K.

[4] Y. Cohen, L. Avram, L. Frish, Diffusion NMR spectroscopy in supramolecular and combinatorial chemistry: An old parameter - New insights, Angew. Chem. Int. Ed. 44 (2005) 520. doi:10.1002/anie.200300637.

[5] K.F. Morris, C.S. Johnson Jr, Diffusion-ordered two-dimensional nuclear magnetic resonance spectroscopy, J. Am. Chem. Soc. 114 (1992) 3139. doi: 10.1021/ja00034a071.

[6] H. Barjat, G.A. Morris, S. Smart, A.G. Swanson, S.C.R. Williams, High-resolution diffusion-ordered 2D spectroscopy (HR-DOSY)-a new tool for the analysis of complex mixtures, J. Magn. Reson. 108 (1995) 170. doi:10.1006/jmrb.1995.1118.

[7] G.A. Morris, Diffusion-Ordered Spectroscopy, in: eMagRes, John Wiley & Sons, Ltd, 2007. doi:10.1002/9780470034590.emrstm0119.pub2.

[8] M.A. Connell, P.J. Bowyer, P.A. Bone, A.L. Davis, A.G. Swanson, M. Nilsson, G.A. Morris, Improving the accuracy of pulsed field gradient NMR diffusion experiments: Correction for gradient non-uniformity, J. Magn. Reson. 198 (2009) 121-31. doi:10.1016/j.jmr.2009.01.025.

[9] E.L. Hahn, Spin Echoes, Phys. Rev. 80 (1950) 580. doi:10.1103/PhysRev.80.580

[10] H.Y. Carr, E.M. Purcell, Effects of Diffusion on Free Precession in Nuclear Magnetic Resonance Experiments, Phys. Rev. 94 (1954) 630. doi:10.1103/PhysRev.94.630.

[11] E.O. Stejskal, J.E. Tanner, Spin diffusion measurements: spin echoes in the presence of a time-dependent field gradient, J. Chem. Phys. 42 (1965) 288. doi:10.1063/1.1695690.

[12] A. Botana, J.A. Aguilar, M. Nilsson, G.A. Morris, J-modulation effects in DOSY experiments and their suppression: the Oneshot45 experiment, J. Magn. Reson. 208 (2011) 270. doi:10.1016/j.jmr.2010.11.012.

[13] J.E. Tanner, Use of the stimulated echo in NMR diffusion studies, J. Chem. Phys. 52 (1970) 2523. doi:10.1063/1.1673336.

[14] S.J. Gibbs, C.S. Johnson Jr, A PFG NMR experiment for accurate diffusion and flow studies in the presence of eddy currents, J. Magn. Reson. 93 (1991) 395. doi: 10.1016/0022-2364(91)90014-K

[15] G. Wider, V. Dötsch, K. Wüthrich, Self-compensating pulsed magnetic-field gradients for short recovery times, J. Magn. Reson. A. 108 (1994) 255. doi:10.1006/jmra.1994.1120

[16] I.J. Day, Phase cycling, in: eMagRes, John Wiley & Sons, Ltd, 2013. doi:10.1002/9780470034590.emrstm1344.

[17] M.D. Pelta, G.A. Morris, M.J. Stchedroff, S.J. Hammond, A one-shot sequence for high-resolution diffusion-ordered spectroscopy, Magn. Reson. Chem. 40 (2002) S147. doi: 10.1002/mrc.1107.

[18] I.V. Nesmelova, D. Idiyatullin, K.H. Mayo, Measuring protein self-diffusion in protein–protein mixtures using a pulsed gradient spin-echo technique with WATERGATE and isotope filtering, J. Magn. Reson. 166 (2004) 129. doi:10.1016/j.jmr.2003.09.004.

[19] G. Zheng, T. Stait-Gardner, P.G. Anil Kumar, A.M. Torres, W.S. Price, PGSTE-WATERGATE: An STE-based PGSE NMR sequence with excellent solvent suppression, J. Magn. Reson. 191 (2008) 159. doi:10.1016/j.jmr.2007.12.001.

[20] J.A. Aguilar, M. Nilsson, G. Bodenhausen, G.A. Morris, Spin echo NMR spectra without J modulation, Chem. Commun. 48 (2012) 811. doi:10.1039/C1CC16699A.

[21] J.A. Aguilar, R.W. Adams, M. Nilsson, G.A. Morris, Suppressing exchange effects in diffusion-ordered NMR spectroscopy, J. Magn. Reson. 238 (2014) 16. doi:10.1016/j.jmr.2013.10.018.

[22] H.C. Torrey, Bloch equations with diffusion terms, Phys. Rev. 104 (1956) 563. doi:10.1103/PhysRev.104.563.

[23] D. Sinnaeve, The Stejskal-Tanner equation generalized for any gradient shape – an overview of most pulse sequences measuring free diffusion, Concept. Magn. Reson. A. 40 (2012) 39. doi:10.1002/cmr.a.21223.

[24] A.A. Istratov, O.F. Vyvenko, Exponential analysis in physical phenomena, Rev. Sci. Instrum. 70 (1999) 1233. doi:10.1063/1.1149581.

[25] M. Nilsson, M.A. Connell, A.L. Davis, G.A. Morris, Biexponential fitting of diffusion-ordered NMR data: practicalities and limitations, Anal. Chem. 78 (2006) 3040. doi:10.1021/ac060034a.

[26] G. D. Poggetto, L. Castañar, M. Foroozandeh, P. Kiraly, R.W. Adams, G.A. Morris, M. Nilsson, Unexploited Dimension: New Software for Mixture Analysis by 3D Diffusion-Ordered NMR Spectroscopy, Anal. Chem. 90 (2018) 3695. doi:10.1021/acs.analchem.8b04093.

[27] S.W. Provencher, CONTIN a general purpose constrained regularization program for inverting noisy linear algebraic and integral equations, Comput. Phys. Commun. 27 (1982) 229. doi:10.1016/0010-4655(82)90174-6.

[28] I.J. Day, On the inversion of diffusion NMR data: Tikhonov regularization and optimal choice of the regularization parameter, J Magn Reson. 211 (2011) 178. doi:10.1016/j.jmr.2011.05.014.

[29] K.F. Morris, C.S. Johnson Jr, Resolution of discrete and continuous molecular size distributions by means of diffusion-ordered 2D NMR spectroscopy, J. Am. Chem. Soc. 115 (1993) 4291. doi:10.1021/ja00063a053.

[30] A. Chen, D.H. Zu, C.S. Johnson Jr, Determination of molecular weight distributions for polymers by diffusion-ordered NMR, J. Am. Chem. Soc. 117 (1995) 7965. doi:10.1021/ja00135a015.

[31] P. Stilbs, K. Paulsen, P.C. Griffiths, Global least-squares analysis of large, correlated spectral data sets: application to component-resolved FT-PGSE NMR spectroscopy, J. Phys. Chem. 100 (1996) 8180. doi:10.1021/jp9535607.

[32] J.A. Ostlund, M. Nyden, P. Stilbs, Component-resolved diffusion in multicomponent mixtures. A case study of high-field PGSE-NMR self-diffusion measurements in asphaltene/naphthenic acid/solvent systems, Energy Fuels 18 (2004) 531. doi:10.1021/ef030126s.

[33] P. Stilbs, Automated CORE, RECORD, and GRECORD processing of multi-component PGSE NMR diffusometry data, Eur. Biophys. J. 42 (2013) 25. doi:10.1007/s00249-012-0794-8

[34] M. Nilsson, G.A. Morris, Speedy component resolution: an improved tool for processing diffusion-ordered spectroscopy data, Anal. Chem. 80 (2008) 3777. doi:10.1021/ac7025833.

[35] A.A. Colbourne, S. Meier, G.A. Morris, M. Nilsson, Unmixing the NMR spectra of similar species - vive la difference, Chem. Commun. 49 (2013) 10510. doi:10.1021/ac7025833.

[36] M.A. Delsuc, T.E. Malliavin, Maximum entropy processing of DOSY NMR spectra, Anal. Chem. 70 (1998) 2146. doi:10.1021/ac9800715.

[37] W. Windig, J.P. Hornak, B. Antalek, Multivariate Image Analysis of Magnetic Resonance Images with the Direct Exponential Curve Resolution Algorithm (DECRA): Part 1: Algorithm and Model Study, J. Magn. Reson. 132 (1998) 298. doi:10.1006/jmre.1998.1390.

[38] B. Antalek, J.P. Hornak, W. Windig, Multivariate Image Analysis of Magnetic Resonance Images with the Direct Exponential Curve Resolution Algorithm (DECRA): Part 2: Application to Human Brain Images, J. Magn. Reson. 132 (1998) 307. doi:10.1006/jmre.1998.1391.

[39] B. Antalek, J.M. Hewitt, W. Windig, P.D. Yacobucci, T. Mourey, K. Le, The use of PGSE NMR and DECRA for determining polymer composition, Magn. Reson. Chem. 40 (2002) S60. doi:10.1002/mrc.1116.

[40] I. Toumi, B. Torresani, S. Caldarelli, Effective processing of pulse field gradient NMR of mixtures by blind source separation, Anal Chem. 85 (2013) 11344. doi:10.1021/ac402085x.

[41] A.A. Colbourne, G.A. Morris, M. Nilsson, Local covariance order diffusion-ordered spectroscopy: a powerful tool for mixture analysis, J. Am. Chem. Soc. 133 (2011) 7640. doi:10.1021/ja2004895.

[42] B.R. Martini, V.A. Mandelshtam, G.A. Morris, A.A. Colbourne, M. Nilsson, Filter diagonalization method for processing PFG NMR data, J. Magn. Reson. 234 (2013) 125. doi:10.1016/j.jmr.2013.06.014.

[43] M. Nilsson, The DOSY Toolbox: A new tool for processing PFG NMR diffusion data, J. Magn. Reson. 200 (2009) 296. doi:10.1016/j.jmr.2009.07.022.

[44] L. Castañar L, G. Dal Poggetto, A.A. Colbourne, G.A. Morris, M. Nilsson, The GNAT: A new tool for processing NMR data, Magn. Reson. Chem. 56 (2018) 546. doi:10.1002/mrc.4717.

[45] G.A. Morris, H. Barjat, T.J. Horne, Reference Deconvolution Methods, Prog. NMR Spectrosc. 31 (1997) 197. doi:10.1016/S0079-6565(97)00011-3.

[46] O. Reynolds, IV. On the theory of lubrication and its application to Mr. Beauchamp Tower's experiments, including an experimental determination of the viscosity of olive oil, Philos. Trans. Royal Soc. 177 (1886) 157. doi:10.1098/rstl.1886.0005.

[47] D.S. Raiford, C.L. Fisk, E.D. Becker, Calibration of methanol and ethylene glycol nuclear magnetic resonance thermometers, Anal. Chem. 51 (1979) 2050. doi:10.1021/ac50048a040.

[48] A.L. Van Geet, Calibration of the methanol and glycol nuclear magnetic resonance thermometers with a static thermistor probe, Anal. Chem. 40 (1968) 2227. doi:10.1021/ac50158a064.

[49] M. Findeisen, T. Brand, S. Berger, A ^{1}H-NMR thermometer suitable for cryoprobes, Magn. Reson. Chem. 45 (2007) 175. doi:10.1002/mrc.1941.

[50] O. Assemat, M.-A. Coutouly, R. Hajjar, M.-A. Delsuc, Validation of molecular mass measurements by means of diffusion-ordered NMR spectroscopy: Application to oligosaccharides, C. R. Chim. 13 (2010) 412. doi:10.1016/j.crci.2009.10.005.

[51] L.G. Longsworth, The mutual diffusion of light and heavy water, J. Phys. Chem. 64 (1960) 1914. doi:10.1021/j100841a027.

[52] M. Holz, H. Weingärtner, Calibration in accurate spin-echo self-diffusion measurements using ^{1}H and less-common nuclei, J. Magn. Reson. 92 (1991) 115. doi: 10.1016/0022-2364(91)90252-O.

[53] M. Holz, S.R. Heil, A. Sacco, Temperature-dependent self-diffusion coefficients of water and six selected molecular liquids for calibration in accurate ^{1}H NMR PFG measurements, Phys. Chem. Chem. Phys. 2 (2000) 4740. doi:10.1039/B005319H.

[54] P. Damberg, J. Jarvet, A. Gräslund, Accurate measurement of translational diffusion coefficients: a practical method to account for nonlinear gradients, J. Magn. Reson. 148 (2001) 343. doi: 10.1006/jmre.2000.2260.

[55] J. Wesfreid, Y. Pomeau, M. Dubois, C. Normand, P. Bergé, Critical effects in Rayleigh-Benard convection, J. Phys. France 39 (1978) 725. doi:10.1051/jphys:01978003907072500.

[56] M. Lappa, Thermal convection: patterns, evolution and stability, John Wiley & Sons, 2009.

[57] A.V. Getling, Rayleigh-Benard Convection: Structures and Dynamics, World Scientific, River Edge, NJ, 1998.

[58] K.C. Chung, H.Y. Yu, S. Ahn, Convection effects on PGSE-NMR self-diffusion measurements at low temperature: Investigation into sources of induced convective flows, Bull. Korean Chem. Soc. 32 (2011) 1970. doi:10.5012/bkcs.2011.32.6.1970.

[59] T.M. Barbosa, R. Rittner, C.F. Tormena, G.A. Morris, M. Nilsson, Convection in liquid-state NMR: expect the unexpected, RSC Adv. 2016;6:95173-6. doi:10.1039/C6RA23427E.

[60] I. Swan, M. Reid, P.W. Howe, M.A. Connell, M. Nilsson, M.A. Moore, G.A. Morris, Sample convection in liquid-state NMR: why it is always with us, and what we can do about it, J. Magn. Reson. 252 (2015) 120. doi:10.1016/j.jmr.2014.12.006.

[61] N. Hedin, T. Yu, I. Furó, Growth of C12E8 micelles with increasing temperature. A convection-compensated PGSE NMR study, Langmuir, 16 (2000) 7548. doi:10.1021/la000595b.

[62] N.M. Loening, J. Keeler, Measurement of convection and temperature profiles in liquid samples, J. Magn. Reson. 139 (1999) 334-41. doi:10.1006/jmre.1999.1777.

[63] T.J. Rottreau, Application of liquid state nuclear magnetic resonance techniques for the study of porous materials, Aston University, 2018.

[64] W.M. Haynes, CRC handbook of chemistry and physics, CRC press, 2014.

[65] L. Rayleigh, LIX. On convection currents in a horizontal layer of fluid, when the higher temperature is on the underside, Phil. Mag. 32 (1916) 529. doi:10.1080/14786441608635602.

[66] A. Jerschow, N. Müller, Suppression of convection artifacts in stimulated-echo diffusion experiments. Double-stimulated-echo experiments, J. Magn. Reson. 125 (1997) 372. doi: 10.1006/jmre.1997.1123.

[67] A. Jerschow, N. Müller, Convection compensation in gradient enhanced nuclear magnetic resonance spectroscopy, J. Magn. Reson. 132 (1998) 13. doi:10.1006/jmre.1998.1400.

[68] J. Anderson, K. Saddington, S80. The use of radioactive isotopes in the study of the diffusion of ions in solution, J. Chem. Soc. (1949) S381. doi:10.1039/JR949000S381.

[69] J.H. Wang, Self-diffusion and structure of liquid water. I. Measurement of self-diffusion of liquid water with deuterium as tracer, J. Am. Chem. Soc. 73 (1951) 510. doi:10.1021/ja01146a002.

[70] J.H. Wang, Self-diffusion and structure of liquid water. II. Measurement of self-diffusion of liquid water with O^{18} as tracer, J. Am. Chem. Soc. 73 (1951) 4181. doi:10.1021/ja01153a039.

[71] J.H. Wang, C.V. Robinson, I.Edelman, Self-diffusion and structure of liquid water. III. Measurement of the self-diffusion of liquid water with H^2, H^3 and O^{18} as Tracers, J. Am. Chem. Soc. 75 (1953) 466. doi:10.1021/ja01098a061.

[72] R. Mills, Self-diffusion in normal and heavy water in the range 1-45°, J. Phys. Chem. . 77 (1973) 685. doi: 10.1021/j100624a025.

[73] A. Poisson, A. Papaud, Diffusion coefficients of major ions in seawater, Mar. Chem. 13 (1983) 265. doi:10.1016/0304-4203(83)90002-6.

[74] P. Debye, Light scattering in solutions, J. Appl. Phys. 15 (1944) 338. doi:10.1063/1.1707436.

[75] P. Doty, R.F. Steiner, Light scattering and spectrophotometry of colloidal solutions, J. Chem. Phys. 18 (1950) 1211. doi:10.1063/1.1747913.

[76] W. Brown, Dynamic light scattering: the method and some applications, Clarendon press, Oxford, 1993.

[77] A. J. Bard, L.R. Faulkner, J. Leddy, G. G. Zoski, Electrochemical methods: fundamentals and applications, Wiley, New York, 1980.

[78] R.G. Compton, M.E. Laing, D.Mason, R.J. Northing, P.R. Unwin, J.S. Rowlinson, Rotating disc electrodes: the theory of chronoamperometry and its use in mechanistic investigations, Proc. Royal Soc. Lond. A 418 (1988) 113. doi:10.1098/rspa.1988.0076.

[79] P.J. Lingane, D.G. Peters, Chronopotentiometry, Crit. Rev. Anal. Chem. 1 (1971) 587. doi:10.1080/1040834nu08542742.

[80] W. Albery, M. Hitchman, J. Ulstrup, Ring-disc electrodes. Part 9.—Application to first-order kinetics, Trans. Faraday Soc. 64 (1968) 2831. doi:10.1039/TF9686402831.

[81] F.G. Cottrell, Der Reststrom bei galvanischer Polarisation, betrachtet als ein Diffusionsproblem, Z. Phys. Chem. 42 (1903) 385. doi:10.1515/zpch-1903-4229.

[82] A. Einstein, Über die von der molekularkinetischen Theorie der Wärme geforderte Bewegung von in ruhenden Flüssigkeiten suspendierten Teilchen, Ann. Phys. 17 (1905) 549. doi:10.1002/andp.19053220806.

[83] W. Sutherland, LXXV. A dynamical theory of diffusion for non-electrolytes and the molecular mass of albumin, Phil. Mag. 9 (1905) 781. doi:10.1080/14786440509463331.

[84] P. Debye, Polar molecules, Chemical Catalog Company, New York, 1929.

[85] C. Wilke, P. Chang, Correlation of diffusion coefficients in dilute solutions, AIChE J. 1 (1955) 264. doi:10.1002/aic.690010222.

[86] C.E. Spiese, Determination of the diffusion constants of dimethylsulfide and dimethylsulfoniopropionate by diffusion-ordered nuclear magnetic resonance spectroscopy, Mar. Chem. 207 (2018) 77. doi:10.1016/j.marchem.2018.10.004.

[87] E. Aliu, A. Hart, J. Wood, Kinetics of Vanillin Hydrodeoxygenation Reaction in an Organic Solvent Using a Pd/C Catalyst, Ind. Eng. Chem. Res. 58 (2019) 15162. doi:10.1021/acs.iecr.9b02907.

[88] J.P. Coelho, R.M. Filipe, M.P. Robalo, R.P. Stateva, Recovering value from organic waste materials: Supercritical fluid extraction of oil from industrial grape seeds, J. Supercrit. Fluids 141 (2018) 68. doi:10.1016/j.supflu.2017.12.008.

[89] D.F. Othmer, M.S. Thakar, Correlating diffusion coefficient in liquids, Ind. Eng. Chem. Res. 45 (1953) 589. doi:10.1021/ie50519a036.

[90] E.G. Scheibel, Correspondence. Liquid Diffusivities. Viscosity of Gases, Ind. Eng. Chem. Res. 46 (1954) 2007. doi:10.1021/ie50537a062.

[91] D.R. Olander, The diffusivity of water in organic solvents, AIChE J. 7 (1961) 175. doi: 10.1002/aic.690070139.

[92] R. Sitaraman, S.H. Ibrahim, N.A. Kuloor, Generalized Equation for Diffusion in Liquids, J. Chem. Eng. Data. 8 (1963) 198. doi:10.1021/je60017a017.

[93] K. Reddy, L. Doraiswamy, Estimating liquid diffusivity, Ind. Eng. Chem. Fundam.. 6 (1967) 77. doi:10.1021/i160021a012.

[94] R. Evans, Z. Deng, A.K. Rogerson, A.S. McLachlan, J.J. Richards, M. Nilsson, G.A. Morris, Quantitative interpretation of diffusion-ordered NMR spectra: can we rationalize small molecule diffusion coefficients? Angew. Chem. Int. Ed. 52 (2013) 3199. doi:10.1002/anie.201207403.

[95] D.P. Valencia, F.J. González, Estimation of diffusion coefficients by using a linear correlation between the diffusion coefficient and molecular weight, J. Electroanal. Chem. 681 (2012) 121. doi:10.1016/j.jelechem.2012.06.013.

[96] D.P. Valencia, F.J. González, Understanding the linear correlation between diffusion coefficient and molecular weight. A model to estimate diffusion coefficients in acetonitrile solutions, Electrochem. Commun. 13 (2011) 129. doi:10.1016/j.elecom.2010.11.032.

[97] F. Perrin, Mouvement Brownien d'un ellipsoide (II). Rotation libre et dépolarisation des fluorescences. Translation et diffusion de molécules ellipsoidales, J. Phys. Radium. 7 (1936) 1. doi:10.1051/jphysrad:01936007010100.

[98] G. Canzi, A. A. Mrse, C. P. Kubiak, Diffusion-Ordered NMR Spectroscopy as a Reliable Alternative to TEM for Determining the Size of Gold Nanoparticles in Organic Solutions, J. Phys. Chem. C 115 (2011) 7972. doi:10.1021/jp2008557.

[99] D. Jeanmaire, J. Laliturai, A. Almalik, P. Carampin, R. d'Arcy, E. Lallana, R. Evans, R. E. P. Winpenny, N. Tirelli, Chemical specificity in REDOX-responsive materials: the diverse effects of different Reactive Oxygen Species (ROS) on polysulfide nanoparticles, Polym. Chem. 5 (2014) 1393. doi:10.1039/C3PY01475D.

[100] P.J. Flory, Principles of Polymer Chemistry , Cornell University Press, Ithaca, 1953.

[101] P.J. Flory, Statistical mechanics of chain molecules, Interscience, New York, 1969.

[102] F. Brochard, P. De Gennes, Dynamical scaling for polymers in theta solvents, Macromolecules 10 (1977) 1157. doi: 10.1021/ma60059a048.

[103] S. Augé, P.O. Schmit, C.A. Crutchfield, M.T. Islam, D.J. Harris, E. Durand, M. Clemancey, A.-A. Quoineaud, J.-M. Lancelin, Y. Prigent, F. Taulelle, M.-A. Delsuc, NMR measure of translational diffusion and fractal dimension. Application to molecular mass measurement, J. Phys. Chem. B 113 (2009) 1914. doi:10.1021/jp8094424.

[104] M.B. Enright, D.M. Leitner, Mass fractal dimension and the compactness of proteins, Phys. Rev. E 71 (2005) 011912. doi:10.1103/PhysRevE.71.011912.

[105] J.A. Jones, D.K. Wilkins, L.J. Smith, C.M. Dobson, Characterisation of protein unfolding by NMR diffusion measurements, J. Biomol. NMR 10 (1997) 199. doi:10.1023/A:1018304117895.

[106] D.K. Wilkins, S.B. Grimshaw, V. Receveur, C.M. Dobson, J.A. Jones, L.J. Smith, Hydrodynamic Radii of Native and Denatured Proteins Measured by Pulse Field Gradient NMR Techniques, Biochemistry, 38 (1999) 16424. doi: 10.1021/bi991765q.

[107] E.F. Dudás, A. Bodor, Quantitative, Diffusion NMR Based Analytical Tool To Distinguish Folded, Disordered, and Denatured Biomolecules, Anal. Chem. 91 (2019) 4929 doi:10.1021/acs.analchem.8b05617.

[108] C.K. Wang, S.E. Northfield, J.E. Swedberg, P.J. Harvey, A.M. Mathiowetz, D.A. Price, S. Liras, D.J. Craik, Translational diffusion of cyclic peptides measured using pulsed-field gradient NMR, J. Phys. Chem. B. 118 (2014) 11129. doi:10.1021/jp506678f.

[109] A. Ambrus, D. Yang, Diffusion-ordered nuclear magnetic resonance spectroscopy for analysis of DNA secondary structural elements, Anal. Biochem. 367 (2007) 56. doi:10.1016/j.ab.2007.04.025.

[110] H. Walderhaug, O. Söderman, D. Topgaard, Self-diffusion in polymer systems studied by magnetic field-gradient spin-echo NMR methods, Prog. Nucl. Magn. Reson. Spectrosc. 56 (2010) 406. doi: 10.1016/j.pnmrs.2010.04.002.

[111] A. Jerschow, N. Müller. Diffusion-separated nuclear magnetic resonance spectroscopy of polymer mixtures, Macromolecules 31 (1998) 6573. doi: 10.1021/ma9801772.

[112] M. Valentini, A. Vaccaro, A. Rehor, A. Napoli, J.A. Hubbell, N. Tirelli, Diffusion NMR Spectroscopy for the Characterization of the Size and Interactions of Colloidal Matter - the case of vesicles and nanoparticles, J. Am. Chem. Soc. 126 (2004) 2142. doi:10.1021/ja037247r.

[113] Y. Bakkour, V. Darcos, S. Li, J. Coudane, Diffusion ordered spectroscopy (DOSY) as a powerful tool for amphiphilic block copolymer characterization and for critical micelle concentration (CMC) determination, Polym. Chem. 3 (2012) 2006. doi:10.1039/C2PY20054F.

[114] G. Robert-Nicoud, R. Evans, C.-D. Vo, C. J. Cadman, N. Tirelli, Synthesis, self-assembly and (absence of) protein interactions of poly(glycerol methacrylate)–silicone macro-amphiphiles, Polym. Chem. 4 (2013) 3458. doi:10.1039/C3PY00273J.

[115] C. Barrère, M. Mazarin, R. Giordanengo, T.N.T. Phan, A. Thevand, S. Viel, L. Charles, Molecular weight determination of block copolymers by pulsed gradient spin echo NMR, Anal. Chem. 81 (2009) 8054. doi:10.1021/ac9018654.

[116] S. Viel, M. Mazarin, R. Giordanengo, T.N.T. Phan, L. Charles, S. Caldarelli, D. Bertin, Improved compositional analysis of block copolymers using Diffusion Ordered NMR Spectroscopy, Anal. Chim. Acta. 65 (2009) 45. doi: 10.1016/j.aca.2009.06.049.

[117] J. Viéville, M. Tanty, M.-A. Delsuc, Polydispersity index of polymers revealed by DOSY NMR, J. Magn. Reson. 212 (2011) 169. doi:10.1016/j.jmr.2011.06.020.

[118] W. Li, H. Chung, C. Daeffler, J. A. Johnson, R. H. Grubbs, Application of ^{1}H DOSY for facile measurement of polymer molecular weights, Macromolecules 45 (2012) 9595. doi: 10.1021/ma301666x.

[119] P. Lewinski, S. Sosnowski, S. Kazmierski, S. Penczek, L-Lactide polymerization studied by ^{1}H NMR with diffusion-ordered spectroscopy (DOSY): a “One NMR Tube Experiment” providing data on monomer conversion, polymer structure, M_n and M_w, Polym. Chem. 6 (2015) 4353. doi:10.1039/C5PY00455A.

[120] C. Chamignon, D. Duret, M.T. Charreyre, A. Favier, ^{1}H DOSY NMR Determination of the Molecular Weight and the Solution Properties of Poly (N-acryloylmorpholine) in Various Solvents, Macromol. Chem. Phys. 217 (2016) 2286. doi:10.1002/macp.201600089.

[121] N. Cherifi, A. Khoukh, A. Benaboura, L. Billon, Diffusion-ordered spectroscopy NMR DOSY: an all-in-one tool to simultaneously follow side reactions, livingness and molar masses of polymethylmethacrylate by nitroxide mediated polymerization, Polym. Chem. 7 (2016) 5249. doi:10.1039/C6PY00927A.

[122] J.G. Rosenboom, J. De Roo, G. Storti, M. Morbidelli, Diffusion (DOSY) ^{1}H NMR as an alternative method for molecular weight determination of poly (ethylene furanoate)(PEF) polyesters, Macromol. Chem. Phys. 218 (2017) 1600436. doi:10.1002/macp.201600436.

[123] K. Gu, J. Onorato, S.S. Xia, C.K. Luscombe, Y.-L. Loo, Determination of the molecular weight of conjugated polymers with diffusion-ordered NMR spectroscopy, Chem. Mater. 30 (2018) 570. doi:10.1021/acs.chemmater.7b05063.

[124] S. Viel, D. Capitani, L. Mannina, A. Segre, Diffusion-ordered NMR spectroscopy: a versatile tool for the molecular weight determination of uncharged polysaccharides, Biomacromolecules 4 (2003) 1843. doi:10.1021/bm0342638.

[125] S. Iqbal, R. Marchetti, A. Aman, A. Silipo, S.A.U. Qader, A. Molinaro, Enzymatic and acidic degradation of high molecular weight dextran into low molecular weight and its characterizations using novel Diffusion-ordered NMR spectroscopy, Int. J. Biol. Macromol. 103 (2017) 744. doi:10.1016/j.ijbiomac.2017.05.073.

[126] N. Kuz'mina, S. Moiseev, V. Krylov, V. Yashkir, V. Merkulov, Determination of the parameters of molecular-weight distribution of hydroxyethyl starches by diffusion-ordered NMR spectroscopy, J. Anal. Chem. 70 (2015) 843. doi:10.1134/S1061934815070060.

[127] R.M. Wenger, T.G. Payne, M.H. Schreier, Cyclosporine: chemistry, structure-activity relationships and mode of action, in Metabolic Control in Diabetes Mellitus Beta Adrenoceptor Blocking Drugs NMR Analysis of Cancer Cells Immunoassay in the Clinical Laboratory Cyclosporine: Springer, Berlin, 1986. pp. 157-91.

[128] A.R. Bogdan, N.L. Davies, K. James, Comparison of diffusion coefficients for matched pairs of macrocyclic and linear molecules over a drug-like molecular weight range, Org. Biomol. Chem. 9 (2011) 7727. doi:10.1039/C1OB05996C.

[129] C.A. Crutchfield, D.J. Harris, Molecular mass estimation by PFG NMR spectroscopy, J. Magn. Reson. 185 (2007) 179. doi:10.1016/j.jmr.2006.12.004.

[130] R. Sacchi, M. Patumi, G. Fontanazza, P. Barone, P. Fiordiponti, L. Mannina, E. Rossi, A.L. Segre, A high-field ^{1}H nuclear magnetic resonance study of the minor components in virgin olive oils, J. Am. Oil Chem. Soc. 73 (1996) 747. doi:10.1007/BF02517951.

[131] C.A. Crutchfield, D.J. Harris, Molecular mass estimation of derivatized compounds: a PFG NMR study, Magn. Reson. Chem. 45 (2007) 463. doi:10.1002/mrc.1991.

[132] M.J. Calandra, Y. Wang, J. Impellizzeri, S. Frank, J.Y. de Saint Laumer, S. Leocata S, A. Chaintreau, Terpene hydroperoxide chemistry in citrus oils; reaction with endogenous aldehydes to form peroxyhemiacetals, Flavour Fragr. J. 31 (2016) 241. doi:10.1002/ffj.3310.

[133] D. Li, I. Keresztes, R. Hopson, P.G. Williard, Characterization of Reactive Intermediates by Multinuclear Diffusion-Ordered NMR Spectroscopy (DOSY), Acc. Chem. Res. 42 (2009) 270. doi: 10.1021/ar800127e.

[134] D. Li, G. Kagan, R. Hopson, P.G. Williard, Formula Weight Prediction by Internal Reference Diffusion-Ordered NMR Spectroscopy (DOSY), J. Am. Chem. Soc. 131 (2009) 5627. doi:10.1021/ja810154u.

[135] D. Li, C. Sun, J. Liu, R. Hopson, W. Li, P.G. Williard, Aggregation studies of complexes containing a chiral lithium amide and n-butyllithium, J. Org. Chem. 73 (2008) 2373. doi:10.1021/jo702655m.

[136] D. Wu, A. Chen, C.S. Johnson Jr, Heteronuclear-detected diffusion-ordered NMR spectroscopy through coherence transfer, J. Magn. Reson., Ser. A, 123 (1996), 215-218 doi:10.1006/jmra.1996.0239.

[137] A. Botana, P.W. Howe, V. Caër, G.A. Morris, M. Nilsson, High resolution ^{13}C DOSY: The DEPTSE experiment, J. Magn. Reson.. 211 (2011) 25. doi:10.1016/j.jmr.2011.03.016.

[138] D. Li, R. Hopson, W. Li, J. Liu, P.G. Williard, ^{13}C INEPT diffusion-ordered NMR spectroscopy (DOSY) with internal references, Org. Lett. 10 (2008) 909. doi:10.1021/ol703039v.

[139] T.L. Rathman, W.F. Bailey, Optimization of Organolithium Reactions, Org. Process Res. Dev. 13 (2009) 144. doi:10.1021/op800246z.

[140] N.D. Barnett, R.E Mulvey, W. Clegg, P.A. O'Neil, Crystal structure of lithium diisopropylamide (LDA): an infinite helical arrangement composed of near-linear nitrogen-lithium-nitrogen units with four units per turn of helix, J. Am. Chem. Soc. 113 (1991) 8187. doi:10.1021/ja00021a066.

[141] P.G. Williard, J.M. Salvino, Synthesis, isolation, and structure of an LDA-THF complex, J. Org. Chem. 58 (1993) 1. doi:10.1021/jo00053a001.

[142] C. Su, R. Hopson, P. G. Williard, Isotopically Enriched ^{13}C Diffusion-Ordered NMR Spectroscopy: Analysis of Methyllithium, J. Org. Chem. 78 (2013) 11733. doi:10.1021/jo401740g.

[143] J. Guang, R. Hopson, P.G. Williard, Diffusion Coefficient-Formula Weight (D-FW) Analysis of 2H Diffusion-Ordered NMR Spectroscopy (DOSY), J. Org. Chem. 80 (2015) 9102. doi:10.1021/acs.joc.5b01457.

[144] J.H. Gilchrist, A.T. Harrison, D.J. Fuller, D.B. Collum, ^{6}Li-^{15}N heteronuclear multiple quantum correlation (HMQC) spectroscopy: Application to the structure determination of lithium 2,2,6,6-tetramethylpiperidide mixed aggregates, Magn. Reson. Chem. 30 (1992) 855. doi:10.1002/mrc.1260300911.

[145] W. Bauer, P.V.R. Schleyer, Two-dimensional ^{6}Li, ^{1}H heteronuclear Overhauser spectroscopy (HOESY) in magnitude and pure absorption representations. Application to a dimer–monomer equilibrium of a 1,4-dilithio compound, Magn. Reson. Chem. 26 (1988) 827-833. doi:10.1002/mrc.1260261005.

[146] G. Kagan, W. Li, R. Hopson, P.G. Williard, ^{6}Li diffusion-ordered NMR spectroscopy (DOSY) and applications to organometallic complexes, Org. Lett. 12 (2010) 520. doi:10.1021/ol902713h.

[147] P. Garca-lvarez, R.E. Mulvey, J.A. Parkinson, "LiZn(TMP)$_3$", a Zincate or a Turbo-Lithium Amide Reagent? DOSY NMR Spectroscopic Evidence, Angew. Chem. Int. Ed. 50 (2011) 9668. doi: 10.1002/anie.201104297.

[148] A.-C. Pöppler, H. Keil, D. Stalke, M. John, ^{7}Li Residual Quadrupolar Couplings as a Powerful Tool To Identify the Degree of Organolithium Aggregation, Angew. Chem. Int. Ed. 51 (2012) 7843. doi:10.1002/anie.201202116.

[149] G. Hamdoun, M. Sebban, V. Tognetti, A. Harrison-Marchand, L. Joubert, J. Maddaluno J, H. Oulyadi, Alkyllithium Mixed Aggregates: Dynamic Behavior and Comprehensive Analysis of NMR ^{2}J(^{7}Li–^{7}Li) Spin–Spin Coupling, Organometallics 34 (2015) 1932. doi:10.1021/acs.organomet.5b00162.

[150] C.-C. Su, M. He, R. Amine, Z. Chen, K. Amine, Internally Referenced DOSY-NMR: A Novel Analytical Method in Revealing the Solution Structure of Lithium-Ion Battery Electrolytes, J. Phys. Chem. Lett. 9 (2018) 3714. doi:10.1021/acs.jpclett.8b01359.

[151] C.-C. Su, M. He, R. Amine, Z. Chen, K. Amine, The Relationship between the Relative Solvating Power of Electrolytes and Shuttling Effect of Lithium Polysulfides in Lithium–Sulfur Batteries, Angew. Chem. Int. Ed. 57 (2018) 12033. doi:10.1002/anie.201807367

[152] C.-C. Su, M. He, R. Amine, T. Rojas, L. Cheng, A.T. Ngo, K. Amine, Solvating power series of electrolyte solvents for lithium batteries, Energy Environ. Sci. 12 (2019) 1249. doi:10.1039/c9ee00141g.

[153] S. Indris, R. Heinzmann, M. Schulz, A. Hofmann, Ionic Liquid Based Electrolytes: Correlating Li Diffusion Coefficients and Battery Performance, J. Electrochem. Soc. 161 (2014) A2036. doi:10.1149/2.0131414jes.

[154] H. Subramanian, C.P. Jasperse, M.P. Sibi, Characterization of Brønsted Acid–Base Complexes by ^{19}F DOSY, Org. Lett. 17 (2015) 1429. doi:10.1021/acs.orglett.5b00297.

[155] J.I. Day, J.D. Weaver, Selective and Scalable Perfluoroarylation of Nitroalkanes, J. Org. Chem. 82 (2017) 6801. doi:10.1021/acs.joc.7b00962.

[156] R. Yousefi, T.J. Struble, J.L. Payne, M. Vishe, N.D. Schley, J.N. Johnston, Catalytic, Enantioselective Synthesis of Cyclic Carbamates from Dialkyl Amines by CO2-Capture: Discovery, Development, and Mechanism, J. Am. Chem. Soc. 141 (2019) 618. doi:10.1021/jacs.8b11793.

[157] J.E. Power, M. Foroozandeh, P. Moutzouri, R.W. Adams, M. Nilsson, S.R Coombes A.R. Phillips, G.A. Morris, Very broadband diffusion-ordered NMR spectroscopy: ^{19}F DOSY, Chem. Commun. 52 (2016) 6892. doi:10.1039/C6CC02917E.

[158] M. Foroozandeh, M. Nilsson, G.A. Morris, Improved ultra-broadband chirp excitation, J. Magn. Reson. 302 (2019) 28. doi:10.1016/j.jmr.2019.03.007.

[159] G. Dal Poggetto, D.C. Favaro, M. Nilsson, G.A. Morris, C.F. Tormena, ^{19}F DOSY NMR analysis for spin systems with $^{n}J_{FF}$ couplings, Magn. Reson. Chem. 52 (2014) 172 doi: 10.1002/mrc.4047.

[160] G. Kagan, W. Li, R. Hopson, P.G. Williard, Internally referenced diffusion coefficient-formula weight (D-FW) analysis of ^{31}P diffusion-ordered NMR spectroscopy (DOSY), Org. Lett. 11 (2009) 4818. doi:10.1021/ol9019106.

[161] W. Li, G. Kagan, H. Yang, C. Cai, R. Hopson, W. Dai, D.A. Sweigart, P.G. Williard, Accurate Formula Weight Determination in Physically Separated Systems by Diffusion Coefficient−Formula Weight Correlation, Organometallics 29 (2010) 1309. doi:10.1021/om901102b.

[162] H.J. Reich, Role of organolithium aggregates and mixed aggregates in organolithium mechanisms, Chem. Rev. 113 (2013) 7130. doi: 10.1021/cr400187u.

[163] I. Keresztes, P.G. Williard, Diffusion-ordered NMR spectroscopy (DOSY) of THF solvated n-butyllithium aggregates, J. Am. Chem. Soc. 122 (2000) 10228. doi:10.1021/ja002278x.

[164] W. Li, G. Kagan, R. Hopson, P.G. Williard, Application of ^{6}Li diffusion-ordered NMR spectroscopy (DOSY) to confirming the solution structure of n-butyllithium, Arkivoc 180 (2011) 187. doi:10.3998/ark.5550190.0012.515.

[165] G. Barozzino-Consiglio, G. Hamdoun, C. Fressigné, A. Harrison-Marchand, J. Maddaluno, H. Oulyadi, A Combined ^{1}H/^{6}Li NMR DOSY Strategy Finally Uncovers the Structure of Isopropyllithium in THF, Chem. Eur. J. 23 (2017) 12475. doi:10.1002/chem.201702990.

[166] K. Zangger, H. Sterk, Homonuclear broadband-decoupled NMR spectra, J. Magn. Reson. 124 (1997) 486. doi:10.1006/jmre.1996.1063.

[167] N.H. Meyer, K. Zangger, Viva la resolución! Enhancing the resolution of ^{1}H NMR spectra by broadband homonuclear decoupling, Synlett. 25 (2014) 920. doi:10.1055/s-0033-1340635.

[168] K. Zangger, Pure shift NMR, Prog. Nucl. Magn. Reson. Spectrosc. 86 (2015) 1. doi:10.1016/j.pnmrs.2015.02.002.

[169] J.A. Aguilar, S. Faulkner, M. Nilsson, G.A. Morris, Pure Shift ^{1}H NMR: A Resolution of the Resolution Problem? Angew. Chem. Int. Ed. 49 (2010) 3901. doi:10.1002/anie.201001107.

[170] M. Nilsson, G.A. Morris, Pure shift proton DOSY: diffusion-ordered ^{1}H spectra without multiplet structure, Chem. Commun. (2007) 933. doi:10.1039/B617761A.

[171] M. Foroozandeh, L. Castañar, L.G. Martins, D. Sinnaeve, G.D. Poggetto, C.F. Tormena, R.W. Adams, G.A. Morris, M. Nilsson, Ultrahigh-Resolution Diffusion-Ordered Spectroscopy, Angew. Chem. Int. Ed. 128 (2016) 15808. doi:10.1002/anie.201609676.

[172] G. Hamdoun, M. Sebban, E. Cossoul, A. Harrison-Marchand, J. Maddaluno, H. Oulyadi H, ^{1}H Pure Shift DOSY: a handy tool to evaluate the aggregation and solvation of organolithium derivatives, Chem. Commun. 50 (2014) 4073. doi:10.1039/C4CC00111G.

[173] D. Li, C. Sun, P.G. Williard, Characterization of a Chiral Enolate Aggregate and Observation of ^{6}Li− ^{1}H Scalar Coupling, J. Am. Chem. Soc. 130 (2008) 11726. doi:10.1021/ja802114j.

[174] G. Kagan, W. Li, C. Sun, R. Hopson, P.G. Williard, Synthesis, Characterization, and Reaction of a Ketone-Derived 1,4-Dienolate Compound, J. Org. Chem. 76 (2010) 65. doi:10.1021/jo1015163.

[175] D.R. Armstrong, P. García-Álvarez, A.R. Kennedy, R.E. Mulvey, S.D. Robertson, Molecular structures of THF-solvated alkali-metal 2,2,6,6-tetramethylpiperidides finally revealed: X-ray crystallographic, DFT, and NMR (including DOSY) spectroscopic studies, Chem. Eur. J. 17 (2011) 6725. doi:10.1002/chem.201100523.

[176] E. Hevia, A.R. Kennedy, R.E. Mulvey, D.L. Ramsay, S.D. Robertson, Concealed Cyclotrimeric Polymorph of Lithium 2,2,6,6-Tetramethylpiperidide Unconcealed: X-Ray Crystallographic and NMR Spectroscopic Studies, Chem. Eur. J. 19 (2013) 14069. doi:10.1002/chem.201302709.

[177] J. Guang, Q. Liu, R. Hopson, G. Kagan, W. Li, T.B. Monroe TB, P.G. Williard, Conformational Polymorphism of Lithium Pinacolone Enolate, J. Am. Chem. Soc. 138 (2016) 15177. doi:10.1021/jacs.6b08177.

[178] J. Guang, R. Duwald, J. Maddaluno, H. Oulyadi, S. Lakhdar, A.-C. Gaumont, A. Harrison-Marchand, Synthesis and identification of aryl and alkyl gem-dilithium phosphido-boranes: A boost to the chemistry of phosphandiides, Chem. Eur. J. 24 (2018) 6717. doi:10.1002/chem.201800742.

[179] G. Kagan, W. Li, D. Li, R. Hopson, P.G. Williard, Characterization of dimeric chiral lithium amide structures derived from N-isopropyl-O-triisopropylsilyl valinol, J. Am. Chem. Soc. 133 (2011) 6596. doi:10.1021/ja109041z.

[180] C. Su, R. Hopson, P.G. Williard, Mixed aggregates of an alkyl lithium reagent and a chiral lithium amide derived from N-ethyl-O-triisopropylsilyl valinol, J. Am. Chem. Soc. 135 (2013) 14367. doi:10.1021/ja406912h.

[181] C. Su, J. Guang, W. Li, K. Wu, R. Hopson, P.G. Williard, Chiral lithium diamides derived from linked N-isopropyl valinol or alaninol, J. Am. Chem. Soc. 136 (2014) 11735. doi:10.1021/ja505179y.

[182] C. Su, R. Hopson, P.G. Williard, Crystal Structure and Solution State Characterization of Lithium (S)-(1-(Bis (2-methoxyethyl) amino)-3-methylbutan-2-yl)(methyl) amide, J. Org. Chem. 78 (2013) 7288. doi:10.1021/jo400839q.

[183] C. Su, R. Hopson, P.G. Williard, Characterization of Hexameric and Octameric sec-Butyllithium/sec-Butoxide Mixed Aggregates, Eur. J. Inorg. Chem. 2013 (2013) 4136. doi:10.1002/ejic.201300749.

[184] B. Lecachey, H. Oulyadi, P. Lameiras, A. Harrison-Marchand, H. Gérard, J. Maddaluno, MeLi + LiCl in THF: One Heterodimer and No Tetramers, J. Org. Chem. 75 (2010) 5976. doi:10.1021/jo101282m.

[185] M. Orchin, The Grignard reagent: Preparation, structure, and some reactions, J. Chem. Educ. 66 (1989) 586. doi:10.1021/ed066p586.

[186] A. Krasovskiy, P. Knochel, A LiCl-Mediated Br/Mg Exchange Reaction for the Preparation of Functionalized Aryl- and Heteroarylmagnesium Compounds from Organic Bromides, Angew. Chem. Int. Ed. 43 (2004) 3333. doi:10.1002/anie.200454084.

[187] D.R. Armstrong, P. García-Álvarez, A.R. Kennedy, R.E. Mulvey, J.A. Parkinson, Diisopropylamide and TMP Turbo-Grignard Reagents: A Structural Rationale for their

Contrasting Reactivities, Angew. Chem. Int. Ed. 122 (2010) 3253. doi:10.1002/ange.201000539.

[188] D.R. Armstrong, A.R. Kennedy, R.E. Mulvey, S.D. Robertson, Opening the black box of mixed-metal TMP metallating reagents: direct cadmation or lithium–cadmium transmetallation? Chem. Sci. 3 (2012) 27007. doi:10.1039/C2SC20392H.

[189] O. Tai, R. Hopson, P.G. Williard, Ligand Binding Constants to Lithium Hexamethyldisilazide Determined by Diffusion-Ordered NMR Spectroscopy, J. Org. Chem. 82 (2017) 6223. doi:10.1021/acs.joc.5b01457.

[190] P.G. Nilsson, B. Lindman, Water self-diffusion in nonionic surfactant solutions. Hydration and obstruction effects, J. Phys. Chem. 87 (1983) 4756. doi:10.1021/j100246a041.

[191] A.B. Chhetri, M.S. Tango, S.M. Budge, K.C. Watts, M.R. Islam, Non-Edible Plant Oils as New Sources for Biodiesel Production, Int. J. Mol. Sci. 9 (2008) 169. doi:10.1177/0144598716630166.

[192] M.G. Kulkarni, A.K. Dalai, Waste Cooking Oil - An Economical Source for Biodiesel: A Review, Ind. Eng. Chem. Res. 45 (2006) 2901. doi:10.1021/ie0510526.

M.C.G. Albuquerque, Y.L. Machado, A.E.B. Torres, D.C.S. Azevedo, C.L. Cavalcante, L.R.

[193] Firmiano, E.J.S. Parente Jr, Properties of biodiesel oils formulated using different biomass sources and their blends, Renew. Energ. 34 (2009) 857. doi:10.1016/j.renene.2008.07.006.

[194] A.F. Lee, J.A. Bennett, J.C. Manayil, K. Wilson, Heterogeneous catalysis for sustainable biodiesel production via esterification and transesterification, Chem. Soc. Rev. 43 (2014) 7887. doi:10.1039/C4CS00189C.

[195] A.M. Socha, G. Kagan, W. Li, R. Hopson, J.K. Sello, P.G. Williard, Diffusion Coefficient−Formula Weight Correlation Analysis via Diffusion-Ordered Nuclear Magnetic

Resonance Spectroscopy (DOSY NMR) To Examine Acylglycerol Mixtures and Biodiesel Production, Energy Fuels 24 (2010) 4518. doi:10.1021/ef100545a.

[196] W. Li, G. Kagan, H. Yang, C. Cai, R. Hopson, D.A. Sweigart, P.G. Williard, Physically Separated References for Diffusion Coefficient-Formula Weight (D-FW) Analysis of Diffusion-Ordered NMR Spectroscopy (DOSY) in Water, Org. Lett. 12 (2010) 2698. doi: 10.1021/ol100686e.

[197] R. Neufeld, D. Stalke, Accurate molecular weight determination of small molecules via DOSY-NMR by using external calibration curves with normalized diffusion coefficients, Chem. Sci. 6 (2015) 3354. doi:10.1039/C5SC00670H.

[198] S. Bachmann, R. Neufeld, M. Dzemski, D. Stalke, New External Calibration Curves (ECCs) for the Estimation of Molecular Weights in Various Common NMR Solvents, Chem. Eur. J. 22 (2016) 8462. doi: 10.1002/chem.201601145.

[199] S. Bachmann, Estimating Molecular Weight of Organometallics in Solution with Diffusion NMR Techniques, George-August-Universität Göttingen, 2017.

[200] J.H. Wang, Theory of the Self-diffusion of Water in Protein Solutions. A New Method for Studying the Hydration and Shape of Protein Molecules, J. Am. Chem. Soc. 76 (1954) 4755. doi: 10.1021/ja01648a001.

[201] A.-K. Kreyenschmidt, S. Bachmann, T. Niklas, D. Stalke, Molecular Weight Estimation of Molecules Incorporating Heavier Elements from van-der-Waals Corrected ECC-DOSY, ChemistrySelect 2 (2017) 6957. doi:10.1002/slct.201701497.

[202] T. Tatic, K. Meindl, J. Henn, S.K. Pandey, D. Stalke, The first asymmetric organolithium tetramers with simple ether donor bases, Chem. Commun. 46 (2010) 4562. doi:10.1039/C002504F.

[203] R. Neufeld, M. John, D. Stalke, The Donor-Base-Free Aggregation of Lithium Diisopropyl Amide in Hydrocarbons Revealed by a DOSY Method, Angew. Chem. Int. Ed. 54 (2015) 6994-6998. doi:10.1002/anie.201502576.

[204] T.J. Kealy, P.L. Pauson, A New Type of Organo-Iron Compound, Nature 168 (1951) 1039. doi:10.1038/1681039b0.

[205] J. Thiele, Ueber Ketonreactionen bei dem Cyclopentadiën, Ber. Dtsch. Chem. Ges. 33 (1900) 666. doi:10.1002/cber.190003301113.

[206] S. Bachmann, B. Gernert, D. Stalke, Solution structures of alkali metal cyclopentadienides in THF estimated by ECC-DOSY NMR-spectroscopy (incl. software), Chem. Commun. 52 (2016) 12861. doi:10.1039/C6CC07273A.

[207] A.I. Ojeda-Amador, A.J. Martínez-Martínez, G.M. Robertson, S.D Robertson, A.R Kennedy, C.T. O'Hara, Exploring the solid state and solution structural chemistry of the utility amide potassium hexamethyldisilazide (KHMDS), Dalton Trans. 46 (2017) 6392. doi: 10.1039/C7DT01118K.

[208] I. Koehne, S. Bachmann, T. Niklas, R. Herbst-Irmer, D. Stalke, A Novel Bulky Heteroaromatic-Substituted Methanide Mimicking NacNac: Bis(4,6-tert-butylbenzoxazol-2-yl)methanide in s-Block Metal Coordination, Chem. Eur. J. 23 (2017) 13141. doi: 10.1002/chem.201702378.

[209] Q. Dufrois, J.-C. Daran, L. Vendier, C. Dinoi, M. Etienne, Triangles and Squares for a Unique Molecular Crystal Structure: Unsupported Two-Coordinate Lithium Cations and CC Agostic Interactions in Cyclopropyllithium Derivatives, Angew. Chem. Int. Ed. 57 (2018) 1786. doi:10.1002/anie.201711426.

[210] C. Schnegelsberg, S. Bachmann, M. Kolter, T. Auth, M. John, D. Stalke, K. Koszinowski, Association and Dissociation of Grignard Reagents RMgCl and Their Turbo Variant RMgCl·LiCl, Chem. Eur. J. 22 (2016) 7752. doi:10.1002/chem.201600699.

[211] R. Neufeld, T.L. Teuteberg, R. Herbst-Irmer, R.A. Mata, D. Stalke, Solution Structures of Hauser Base iPr_2NMgCl and Turbo-Hauser Base $iPr_2NMgCl{\cdot}LiCl$ in THF and the Influence of LiCl on the Schlenk-Equilibrium, J. Am. Chem. Soc. 138 (2016) 4796. doi:10.1021/jacs.6b00345.

[212] R. Neufeld, D. Stalke, Solution Structure of Turbo-Hauser Base TMPMgCl·LiCl in $[D_8]$THF, Chem. Eur. J. 22 (2016) 12624. doi:10.1002/chem.201601494.

[213] M.Á. Fuentes, A. Zabala, A.R. Kennedy, R.E. Mulvey, Structural Diversity in Alkali Metal and Alkali Metal Magnesiate Chemistry of the Bulky 2,6-Diisopropyl-N-(trimethylsilyl)anilino Ligand, Chem. Eur. J. 22 (2016) 14968. doi:10.1002/chem.201602683.

[214] M. De Tullio, A. Hernán-Gómez, Z. Livingstone, W. Clegg, A.R. Kennedy, R.W. Harrington, A. Antiñolo, A. Martínez, F. Carrillo-Hermosilla, E. Hevia, Structural and Mechanistic Insights into s-Block Bimetallic Catalysis: Sodium Magnesiate-Catalyzed Guanylation of Amines, Chem. Eur. J. 22 (2016) 17646. doi: 10.1002/chem.201602906.

[215] S.-C. Roşca, E. Caytan, V. Dorcet, T. Roisnel, J.-F. Carpentier, Y. Sarazin, π Ligands in Alkaline Earth Complexes, Organometallics 36 (2017) 1269. doi:10.1021/acs.organomet.7b00006.

[216] G. Hamdoun, C. Bour, V. Gandon, J.-N. Dumez, Empirical Estimation of the Molecular Weight of Gold Complexes in Solution by Pulsed-Field Gradient NMR, Organometallics 37 (2018) 4692. doi:10.1021/acs.organomet.8b00709.

[217] S.-C. Hunter, S.-J. Chen, C.A. Steren, M.G. Richmond, Z.-L. Xue, Syntheses and Characterization of Tantalum Alkyl Imides and Amide Imides. DFT Studies of Unusual α-$SiMe_3$ Abstraction by an Amide Ligand, Organometallics 34 (2015) 5687. doi: 10.1021/acs.organomet.5b00558.

[218] S. Noel, H. Ren, T. Tu, E. Jeanneau, C. Félix, F. Perret, F. Vocanson, C. Bucherd, G. Royal, I. Bonnamour, U. Darbost, Synthesis and characterization of a stable copper (I)

calix[4]dicyano-diimidazole complex, Tetrahedron Lett. 53 (2012) 4648. doi:10.1016/j.tetlet.2012.06.065.

[219] U.J. Scheele, M. Georgiou, M. John, S. Dechert, F. Meyer, Combining Pyrazolate and N-Heterocyclic Carbene Coordination Motifs: Synthesis and Characterization of a Double-Crowned Silver Complex, Organometallics 27 (2008) 5146. doi: 10.1021/om800487e.

[220] Y. Qiao, W. Ge, L. Jia, X. Hou, Y. Wang, C.M. Pedersen, Glycosylation intermediates studied using low temperature ^{1}H- and ^{19}F-DOSY NMR: new insight into the activation of trichloroacetimidates, Chem. Commun. 53 (2016) 11418. doi:10.1039/C6CC05272J.

[221] Y. Qiao, C.M. Pedersen, D. Huang, W. Ge, M. Wu, C. Chen, S. Jia, Y. Wang, X. Hou, NMR Study of the Hydrolysis and Dehydration of Inulin in Water: Comparison of the Catalytic Effect of Lewis Acid $SnCl_4$ and Brønsted Acid HCl, ACS Sustainable Chem. Eng. 4 (2016) 3327. doi:10.1021/acssuschemeng.6b00377.

[222] J.M. Kieser, Z.J. Kinney, J.R. Gaffen, S. Evariste, A.M. Harrison, A.L. Rheingold, J.D. Protasiewicz, Three Ways Isolable Carbenes Can Modulate Emission of NH-Containing Fluorophores, J. Am. Chem. Soc. 141 (2019) 12055. doi: 10.1021/jacs.9b04864.

[223] L. Wang, W. Amelung, S. Willbold, Diffusion-Ordered Nuclear Magnetic Resonance Spectroscopy (DOSY-NMR): A Novel Tool for Identification of Phosphorus Compounds in Soil Extracts, Environ. Sci. Technol. 51 (2017) 13256. doi:10.1021/acs.est.7b03322.

[224] A. Gierer, K. Wirtz, Molekulare Theorie der Mikroreibung, Z. Naturforsch. 8 (1953) 532. doi:10.1515/zna-1953-0903.

[225] H.C. Chen, S.H. Chen, Diffusion of crown ethers in alcohols, J. Phys. Chem. 88 (1984) 5118. doi:10.1021/j150665a063.

[226] P. Dvořák, M. Šoltésová, J. Lang, Microfriction correction factor to the Stokes–Einstein equation for small molecules determined by NMR diffusion measurements and hydrodynamic modelling, Mol. Phys. 117 (2019) 868. doi:10.1080/00268976.2018.1510144.

[227] M. Lin, M.J. Shapiro, Mixture Analysis in Combinatorial Chemistry. Application of Diffusion-Resolved NMR Spectroscopy, J. Org. Chem. 61 (1996) 7617. doi:10.1021/jo961315t.

[228] H. Barjat, G.A. Morris, A.G. Swanson, A three-dimensional DOSY-HMQC experiment for the high-resolution analysis of complex mixtures, J. Magn. Reson. 131 (1998) 131. doi:10.1006/jmre.1997.1332.

[229] R.E. Hoffman, E. Shabtai, M. Rabinovitz, V.S. Iyer, K. Mullen, A.K. Rai, E. Bayrd, L.T. Scott. Self-diffusion measurements of polycyclic aromatic hydrocarbon alkali metal salts, J. Chem. Soc. Perkin. Trans. 2 (1998) 1659. doi:10.1039/A800382C.

[230] L.H. Lucas, W.H. Otto, C.K. Larive, The 2D-J-DOSY Experiment: Resolving Diffusion Coefficients in Mixtures, J. Magn. Reson. 156 (2002) 138. doi:10.1006/jmre.2002.2536.

[231] B. Antalek, Using pulsed gradient spin echo NMR for chemical mixture analysis: How to obtain optimum results, Concepts Magn. Reson. 14 (2002) 225. doi: 10.1002/cmr.10026.

[232] M. Nilsson, A.M. Gil, I. Delgadillo, G.A. Morris, Improving pulse sequences for 3D diffusion-ordered NMR spectroscopy: 2DJ-IDOSY, Anal. Chem. 76 (2004) 5418. doi:10.1021/ac049174f.

[233] M. Nilsson, A.M. Gil, I. Delgadillo, G.A. Morris, Improving pulse sequences for 3D DOSY: COSY-IDOSY, Chem. Commun. (2005) 1737. doi:10.1039/B415099F.

[234] J. Harmon, C. Coffman, S. Villarrial, S. Chabolla, K.A. Heisel, V.V. Krishnan, Determination of Molecular Self-Diffusion Coefficients Using Pulsed-Field-Gradient NMR: An Experiment for Undergraduate Physical Chemistry Laboratory, J. Chem. Educ. 89 (2012) 780. doi:10.1021/ed200471k.

[235] M.I. Giuffrida, E. Rizzarelli, G.A. Tomaselli, C. Satriano, G. Trusso Sfrazzetto, A novel fully water-soluble Cu(I) probe for fluorescence live cell imaging, Chem. Commun. 50 (2014) 9835. doi:10.1039/C4CC02147A.

[236] A. Poveda, I. Alonso, M.Á. Fernández-Ibáñez, Experimental and computational studies on the mechanism of the Pd-catalyzed C(sp^3)–H γ-arylation of amino acid derivatives assisted by the 2-pyridylsulfonyl group, Chem. Sci. 5 (2014) 3873. doi:10.1039/C4SC00848K.

[237] B.M. Schulze, D.L. Watkins, J. Zhang, I. Ghiviriga, R.K. Castellano, Estimating the shape and size of supramolecular assemblies by variable temperature diffusion ordered spectroscopy, Org. Biomol. Chem. 12 (2014) 7932. doi:10.1039/C4OB01373E.

[238] F.M. Arrabal-Campos, P. Oña-Burgos, I. Fernández, Molecular weight prediction with no dependence on solvent viscosity. A quantitative pulse field gradient diffusion NMR approach, Polym. Chem. 7 (2016) 4326. doi:10.1039/C6PY00691D.

[239] L.Maugeri, J. Asencio-Hernandez, T. Lebl, D.B. Cordes, A.M.Z. Slawin, M.A. Delsuc, D. Philp, Neutral iodotriazoles as scaffolds for stable halogen-bonded assemblies in solution, Chem Sci. 7 (2016) 6422. doi:10.1039/C6SC01974A.

[240] G.H. Sørland, D. Aksnes, Artefacts and pitfalls in diffusion measurements by NMR, Magn. Reson. Chem. 40 (2002) S139. doi: 10.1002/mrc.1112.

[241] R.B. Martin, Comparisons of indefinite self-association models, Chem. Rev. 96 (1996) 3043. doi:10.1021/cr960037v.

[242] S.V. Kolotuchin, P.A. Thiessen, E.E. Fenlon, S.R. Wilson, C.J. Loweth, S.C. Zimmerman, Self-assembly of 1,3,5-benzenetricarboxylic (trimesic) acid and its analogues, Chem. Eur. J. 5 (1999) 2537. doi:10.1002/(SICI)1521-3765(19990903)5:9<2537::AID-CHEM2537>3.0.CO;2-3.

[243] M. Lackinger, S. Griessl, W.A. Heckl, M. Hietschold, G.W. Flynn, Self-assembly of trimesic acid at the liquid-solid interface - a study of solvent-induced polymorphism, Langmuir, 21 (2005) 4984. doi:10.1021/la0467640.

[244] R. Evans, G. Dal Poggetto, M. Nilsson, G.A. Morris, Improving the Interpretation of Small Molecule Diffusion Coefficients, Anal. Chem. 90 (2018) 3987-94. doi:10.1021/acs.analchem.7b05032.

[245] J.M. Álvarez, Á. Raya-Barón, P.M. Nieto, L.E. Cuca, A. Carrasco-Pancorbo, A. Fernández-Gutiérrez, I. Fernández, Flavonoid glycosides from Persea caerulea. Unraveling their interactions with SDS-micelles through matrix-assisted DOSY, PGSE, mass spectrometry, and NOESY, Magn. Reson. Chem. 54 (2016) 718. doi:10.1002/mrc.4434.

[246] A. O'Rourke, S. Kremb, B.M. Duggan, S. Sioud, N. Kharbatia, M. Raji, A.H. Emwas, W.H. Gerwick, C.R. Voolstra, Identification of a 3-Alkylpyridinium Compound from the Red Sea Sponge *Amphimedon chloros* with *In Vitro* Inhibitory Activity against the West Nile Virus NS3 Protease, Molecules 23 (2018) 1472. doi:10.3390/molecules23061472.

[247] J. Parlov Vuković, P. Novak, T. Jednačak, M. Kveštak, D. Kovačević, V. Smrečki, I. Mikulandra, M. Djetelić Ibrahimpašić, S. Glanzer, K. Zangger, Magnetic field influence on asphaltene aggregation monitored by diffusion NMR spectroscopy: Is aggregation reversible at high magnetic fields? J. Dispers. Sci. Technol. (2019) 1. doi:10.1080/01932691.2018.1561302.

[248] V. Abet, R. Evans, F. Guibbal, S. Caldarelli, R. Rodriguez, Modular construction of dynamic nucleodendrimers, Angew. Chem. Int. Ed. 53 (2014) 4862. doi:10.1002/anie.201402400.

[249] O. Parve, I. Reile, J. Parve, S. Kasvandik, M. Kudrjašova, S. Tamp, A. Metsala, L. Villo, T. Pehk, J. Jarvet, L. Vares, An NMR and MD Modeling Insight into Nucleation of

1,2-Alkanediols: Selective Crystallization of Lipase-Catalytically Resolved Enantiomers from the Reaction Mixtures, J. Org. Chem. 78 (2013) 12795. doi:10.1021/jo402189e.

[250] D. Račkauskaitė, K.-E. Bergquist, Q. Shi, A. Sundin, E. Butkus, K. Wärnmark, E. Orentas, A Remarkably Complex Supramolecular Hydrogen-Bonded Decameric Capsule Formed from an Enantiopure C_2-Symmetric Monomer by Solvent-Responsive Aggregation, J. Am. Chem. Soc. 137 (2015) 10536. doi:10.1021/jacs.5b03160.

[251] R. Orłowski, M. Tasior, O. Staszewska-Krajewska, Ł. Dobrzycki, W. Schilf, B. Ventura B, M.K. Cyrański, D.T. Gryko, Hydrogen Bonds Involving Cavity NH Protons Drives Supramolecular Oligomerization of Amido-Corroles, Chem. Eur. J. 23 (2017) 10195. doi:10.1002/chem.201701674.

[252] S.R. Kennedy, A. Miquelot, J.A. Aguilar, J.W. Steed, Trimeric cyclamers: solution aggregation and high Z′ crystals based on guest structure and basicity, Chem. Commun. 52 (2016) 11846. doi:10.1039/C6CC06054D.

[253] A. Busseau, C. Villegas, S. Dabos-Seignon, P. Hudhomme, S. Legoupy, Enhanced Penta(organo)[60]fullerenes by Electroactive Donor Units for Supramolecular Polymers, Eur. J. Org. Chem. 2018 (2018) 4860. doi:10.1002/ejoc.201801042.

[254] M.D. Jones, L. Brady, P. McKeown, A. Buchard, P.M. Schäfer, L.H. Thomas, M.F. Mahon, T.J. Woodman, J. P. Lowe, Metal influence on the iso- and hetero-selectivity of complexes of bipyrrolidine derived salan ligands for the polymerisation of *rac*-lactide, Chem. Sci. 6 (2015) 5034. doi:10.1039/C5SC01819F.

[255] M.M. Kireenko, E.A. Kuchuk, K.V. Zaitsev, V.A. Tafeenko, Y.F. Oprunenko, A.V. Churakov, E.Kh. Lermontova, G.S. Zaitsevaa and S.S. Karlova, Aluminum complexes based on pyridine substituted alcohols: synthesis, structure, and catalytic application in ROP, Dalton Trans. 44 (2015) 11963. doi:10.1039/C5DT01001B.

[256] K.V. Zaitsev, V.S. Cherepakhin, A. Zherebker, A.Kononikhin, E. Nikolaev, A.V. Churakov, Aluminum complexes based on pyridine substituted alcohols: synthesis, structure, and catalytic application in ROP, J. Organomet. Chem. 875 (2018) 11-23. doi:10.1039/C5DT01001B.

[257] T.-P. Lin, J.C. Peters, Boryl–Metal Bonds Facilitate Cobalt/Nickel-Catalyzed Olefin Hydrogenation, J. Am. Chem. Soc. 136 (2014) 13672. doi:10.1021/ja504667f.

[258] M. Trose, F. Nahra, A. Poater, D.B. Cordes, A.M.Z. Slawin, L. Cavallo, C.S.J. Cazin, Investigating the Structure and Reactivity of Azolyl-Based Copper(I)–NHC Complexes: The Role of the Anionic Ligand, ACS Catal. 7 (2017) 8176. doi:10.1021/acscatal.7b02737.

[259] E. Rideau, H. You, M. Sidera, T.D.W. Claridge, S.P. Fletcher, Mechanistic Studies on a Cu-Catalyzed Asymmetric Allylic Alkylation with Cyclic Racemic Starting Materials, J. Am. Chem. Soc. 139 (2017) 5614. doi:10.1021/jacs.7b02440.

[260] D.J. Nelson, F. Nahra, S.R. Patrick, D.B. Cordes, A.M.Z. Slawin, S.P. Nolan, Exploring the Coordination of Cyclic Selenoureas to Gold(I), Organometallics 33 (2014) 3640. doi:10.1021/om500610w.

[261] J.-D. Leng, C.A.P. Goodwin, I.J. Vitorica-Yrezabal, D.P. Mills, Salt metathesis routes to homoleptic near-linear Mg(ii) and Ca(ii) bulky bis(silyl)amide complexes, Dalton Trans. 47 (2018) 12526. doi:10.1039/C8DT00802G.

[262] K.V. Zaitsev, V.S. Cherepakhin, A.V. Churakov, A.S. Peregudov, B.N. Tarasevich, Egorov MP, G. S.Zaitseva, S.S. Karlova, Extending the family of stable heavier carbenes: New tetrylenes based on N,N,O-ligands, Inorganica Chim. Acta 443 (2016) 91. doi:10.1016/j.ica.2015.12.025.

[263] B.J. Truscott, H. Kruger, P.B. Webb, M. Bühl, S.P. Nolan, The Mechanism of CO2 Insertion into Iridium(I) Hydroxide and Alkoxide Bonds: A Kinetics and Computational Study, Chem. Eur. J. 21 (2015) 6930. doi:10.1002/chem.201406509.

[264] T.-P. Lin, J.C. Peters, Boryl–metal bonds facilitate cobalt/nickel-catalyzed olefin hydrogenation, J. Am. Chem. Soc. 136 (2014) 13672. doi:10.1021/ja504667f.

[265] G.M. Borrajo-Calleja, V.Bizet, C. Besnard, C. Mazet. Mechanistic Investigation of the Pd-Catalyzed Intermolecular Carboetherification and Carboamination of 2,3-Dihydrofuran: Similarities, Differences, and Evidence for Unusual Reaction Intermediates, Organometallics 36 (2017) 3553. doi:10.1021/acs.organomet.7b00483.

[266] H.J. Martin, C.R. Pfeiffer, E. Stephen Davies, A.L. Davis, W. Lewis, N.R. Champness, Influence of Hydrogen-Bonding Interactions on Nuclearity and Structure of Palladium Tiara-like Complexes, ACS Omega 3 (2018) 8769. doi:10.1021/acsomega.8b01133.

[267] J. Beament, G. Kociok-Köhn, M.D. Jones, A. Buchard, Bipyrrolidine salan alkoxide complexes of lanthanides: synthesis, characterisation, activity in the polymerisation of lactide and mechanistic investigation by DOSY NMR, Dalton Trans. 47 (2018) 9164. doi:10.1039/C8DT02108B.

[268] F. Nahra, K. Van Hecke, A.R. Kennedy, D.J. Nelson, Coinage metal complexes of selenoureas derived from N-heterocyclic carbenes, Dalton Trans. 47 (2018) 10671. doi:10.1039/C8DT01506F.

[269] O.K. Rasheed, C. Bawn, D. Davies, J. Raftery, I. Vitorica-Yrzebal, R. Pritchard, H. Zhou, P. Quayle, The Synthesis of Group 10 and 11 Metal Complexes of 3, 6, 9-Trithia-1-(2, 6)-pyridinacyclodecaphane and Their Use in A^3-Coupling Reactions, Eur. J. Org. Chem. 2017 (2017) 5252. doi:10.1002/ejoc.201701033.

[270] C.M.A. Farrow, G.R. Akien, N.R. Halcovitch, J.A. Platts, M.P. Coogan, Self-assembly of singlet-emitting double-helical silver dimers: the curious coordination chemistry and fluorescence of bisquinolylpyridone, Dalton Trans. 47 (2018) 3906. doi:10.1039/c7dt04744d.

[271] A.B. Ruiz-Muelle, P. Oña-Burgos, M.A. Ortuño, J.E. Oltra, I. Rodríguez-García, I. Fernández, Unprecedented Spectroscopic and Computational Evidence for Allenyl and

Propargyl Titanocene(IV) Complexes: Electrophilic Quenching of Their Metallotropic Equilibrium, Chem. Eur. J. 22 (2016) 2427. doi:10.1002/chem.201504281.

[272] G. Forte, G. Trusso Sfrazzetto, A. Pappalardo, A DFT study on the recognition of α-amino acid derivatives by chiral uranyl–salen, Comput. Theor. Chem. 1068 (2015) 8. doi:10.1016/j.comptc.2015.06.007.

[273] C.O. Hollfelder, L.N. Jende, H.-M. Dietrich, K. Eichele, C. Maichle-Mössmer, R. Anwander, 1,3-Diene Polymerization Promoted by Half-Sandwich Rare-Earth-Metal Dimethyl Complexes: Active Species Clustering and Cationization/Deactivation Processes, Chem. Eur. J.. 25 (2019) 7298. doi:10.1002/chem.201901269.

[274] A.W.J. Poh, J.A. Aguilar, A.M. Kenwright, K. Mason, D. Parker, Aggregation of Rare Earth Coordination Complexes in Solution Studied by Paramagnetic and DOSY NMR, Chem. Eur. J. 24 (2018) 16170. doi:10.1002/chem.201803766.

[275] R. Puglisi, F.P. Ballistreri, C.M.A. Gangemi, R.M. Toscano, G.A. Tomaselli, Pappalardo A, G. Trusso Sfrazzetto, Chiral Zn–salen complexes: a new class of fluorescent receptors for enantiodiscrimination of chiral amines, New. J. Chem. 41 (2017) 911. doi:10.1039/C6NJ03592B.

[276] R. Puglisi, P.G. Mineo, A. Pappalardo, A. Gulino, G. Trusso Sfrazzetto. Supramolecular Detection of a Nerve Agent Simulant by Fluorescent Zn–Salen Oligomer Receptors, Molecules 24 (2019) 2160. doi:10.3390/molecules24112160.

[277] F. Zaccaria, C. Zuccaccia, R. Cipullo, A. Macchioni, Extraction of Reliable Molecular Information from Diffusion NMR Spectroscopy: Hydrodynamic Volume or Molecular Mass? Chem. Eur. J. 25 (2019) 9930. doi:10.1002/chem.201900812.

[278] S.A.L. Rousseaux, J.Q. Gong, R. Haver , B. Odell, T.D. Claridge, L.M. Herz, H.L.Anderson, Self-assembly of Russian doll concentric porphyrin nanorings, J. Am. Chem. Soc. 137 (2015) 12713. doi:10.1021/jacs.5b07956.

Glossary & Abbreviations

CORE	component-resolved NMR spectroscopy
Cp	cyclopentadienyl
CS	compact spheres
DECRA	direct exponential curve resolution algorithm
DEPT	distortionless enhancement by polarization transfer
DIPA	diisopropylamine
DMSO	dimethylsulfoxide
DOSY	diffusion-ordered spectroscopy
DSE	dissipated spheres and ellipsoids
ECC	external calibration curve
ED	expanded discs
GNAT	general NMR analysis toolbox
HEPES	4-(2-hydroxyethyl)-1-piperazineethanesulfonic acid
HFIP	hexafluoroisopropanol
HMBC	heteronuclear multiple bond correlation spectroscopy
HMPA	hexamethylphosphoramide
HOESY	heteronuclear Overhauser effect spectroscopy
HQ	hydroquinone
HR-DOSY	high-resolution diffusion-ordered spectroscopy
INEPT	insensitive nuclei enhanced by polarization transfer
IPr	1,3-bis(2,6-bis(diisopropyl)imidazol-2-ylidene
*i*PrLi	isopropyllithium
JohnPhos	(2-biphenyl)-di-tert-butylphosphine

LDA	lithium diisopropylamide
LiHMDS	lithium hexamethyldisilazide
LOCODOSY	local covariance order DOSY
LTP	lipoteichoic acid
MES	2-(*N*-morpholino)ethanesulfonic acid
OUTSCORE	optimized unmixing of true spectra for component resolution
P3HT	poly(3-hexylthiophene)
PEF	poly(ethylene furanoate)
PET	poly(ethylene terephthalate)
PFG	pulsed field gradient
PIPES	piperazine-N,N′-bis(2-ethanesulfonic acid)
PS	pure shift
TAI	trichloroacetyl isocynate
TFA	trifluoroacetic acid
THF	tetrahydrofuran
THP	tetrahydropyran
TRIS	tris-(hydroxymethyl)aminomethane
RF	radio frequency
SCORE	speedy component-resolved NMR spectroscopy
SEGWE	Stokes-Einstein-Gierer-Wirtz estimation

Declaration of interests

☒ The authors declare that they have no known competing financial interests or personal relationships that could have appeared to influence the work reported in this paper.

☐The authors declare the following financial interests/personal relationships which may be considered as potential competing interests:

Graphical abstract

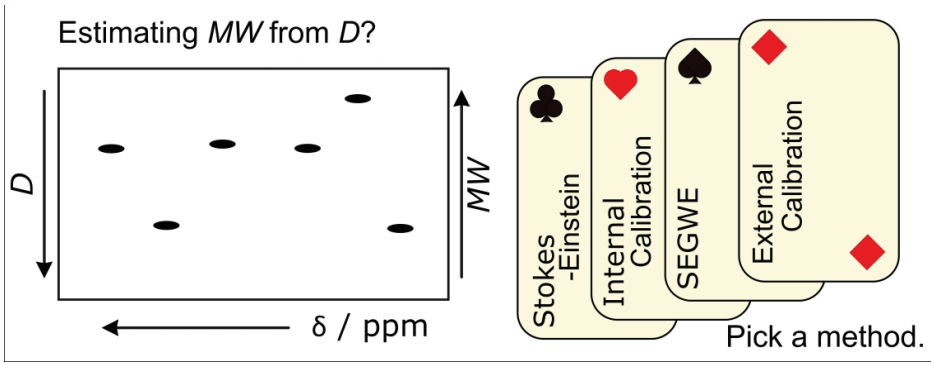

Highlights

- Quantitative interpretation of diffusion coefficients remains a challenge.
- Stokes-Einstein equation poor at estimating small molecule diffusion coefficients.
- Power law methods can be successfully applied to small molecules.
- Power law calibration is either internal to or external from the NMR sample.
- Modification of the Stokes-Einstein equation offers an alternative approach.